Universidade de São Paulo
Instituto de Física

Fenomenologia de Férmions Vectoriais em Física Além do Modelo Padrão

Victor Manuel Peralta Cano

Orientador: Prof. Dr. Gustavo Alberto Burdman

Tese de doutorado apresentada ao Instituto de Física da Universidade de São Paulo, como parte dos requisitos para a obtenção do título de Doutor em Ciências

Banca Examinadora:

Prof. Dr. Gustavo Alberto Burdman (IF/USP)

Prof. Dr. Enrico Bertuzzo - (IF/USP)

Prof. Dr. Oscar José Pinto Éboli - (IF/USP)

Prof. Dr. Ricardo D'Elia Matheus - (IFT/UNESP)

Prof. Dr. Sérgio Ferraz Novaes - (IFT/UNESP)

São Paulo
2017

FICHA CATALOGRÁFICA
Preparada pelo Serviço de Biblioteca e Informação
do Instituto de Física da Universidade de São Paulo

Peralta Cano, Victor Manuel

Fenomenologia de férmions vetoriais em física além do modelo padrão / Phenomenology of vector-like fermions in physics beyond the standard models. São Paulo, 2017.

Tese (Doutorado) – Universidade de São Paulo. Instituto de Física. Depto. de Física Matemática.

Orientador: Prof. Dr. Gustavo Alberto Burdman
Área de Concentração: Física

Unitermos: 1. Partículas elementares; 2. Física de alta energia; 3. Física teórica.

USP/IF/SBI-106/2017

University of São Paulo
Physics Institute

Phenomenology of Vector-like Fermions in Physics Beyond the Standard Model

Victor Manuel Peralta Cano

Supervisor: Prof. Dr. Gustavo Alberto Burdman

Dissertation submitted to the Physics Institute of the University of São Paulo in partial fulfillment of the requirements for the degree of Doctor of Science

Examining Committee:

Prof. Dr. Gustavo Alberto Burdman (IF/USP)

Prof. Dr. Enrico Bertuzzo - (IF/USP)

Prof. Dr. Oscar José Pinto Éboli - (IF/USP)

Prof. Dr. Ricardo D'Elia Matheus - (IFT/UNESP)

Prof. Dr. Sérgio Ferraz Novaes - (IFT/UNESP)

São Paulo
2017

Acknowledgments

First of all, I would like to thank my supervisor, Gustavo Alberto Burdman, for his encouragement and guidance throughout this project. I am deeply indebted to Department of Mathematical Physics at the University of Sao Paulo's Physics Institute. I am also grateful to the elementary particle physics group, for its helpful tips, seminars and enjoyable discussions.

I would like to thank to my thesis committee members, Gustavo Burdman, Enrico Bertuzzo, Oscar José Pinto Éboli, Ricardo D'Elia Matheus and Sérgio Ferraz Novaes for their for their important comments.

In particular, thanks to my friends and colleagues, Leonardo Lima, Lindber Salas, Yuber, Denis, Boris, Gabi, Leila, Leonardo Duarte, Hugo Camacho for great discussions on elementary particle physics.

Thanks too to my undergraduate professors Jorge Abel Espichán Carrillo and Jaime Francisco Vento Flores and Jesús Félix Sánchez Ortiz who encouraged me in the area of physics.

I am very grateful to my parents, Sebastián Peralta, Cirila Cano for their unconditional support all along.

I would like to Acknowledge the financial support of the Committee for the Advancement of Higher Education (CAPES).

Abstract

The Standard model of particle physics provides a successful theory to understand the experimental results of the electroweak and strong interactions. However, it does not have a satisfactory explanation for the hierarchy problem. Many extensions of the Standard Model that solve the hierarchy problem result in new particles. We will study the phenomenology of vector-like fermions resulting in theories where the Higgs boson is typically a pseudo-Nambu-Goldstone boson. In these theories we study the case where a heavy fermion will be heavier than a heavy gluon, and then the channel of a heavy fermion decaying into a color octet is considered. We study this phenomenology at high energy colliders, both the LHC as well as future machines.

Resumo

O modelo padrão de física de partículas fornece uma teoria bem-sucedida para entender os resultados experimentais das interações eletrofracas e fortes. No entanto, não tem uma explicação satisfatória para o problema de hierarquia. Muitas extensões do Modelo Padrão que resolvem o problema hierarquia resultam em novas partículas. Estudaremos a fenomenologia de férmions vetoriais resultando em teorias onde o bóson de Higgs é tipicamente um bóson pseudo-Nambu-Goldstone. Nessas teorias, estudaremos o caso em que um férmion pesado será mais pesado do que um glúon pesado, e então o canal de um férmion pesado decaindo em um octeto de cor é considerado. Estudamos esta fenomenologia em colisores de alta energia, tanto para o LHC quanto as futuras máquinas.

Contents

CHAPTER 1

Introduction

The Standard Model (SM) of elementary particle physics is a quantum field theory that describes the strong, weak and electromagnetic interactions between elementary particles. The gauge sector of the SM is $SU(3)_C \times SU(2)_L \times U(1)_Y$, where $SU(3)_C$ and $SU(2)_L \times U(1)_Y$ indicate the strong and electroweak interactions, respectively. In the SM the electroweak symmetry breaking (EWSB) $SU(2)_L \times U(1)_Y \to U(1)_{EM}$ (here $U(1)_{EM}$ corresponds to the electromagnetic interaction) is due to the Higgs sector. As a result, after the EWSB the weak vector bosons and the fermions obtain masses through the Higgs mechanism. In this mechanism the Higgs scalar field is a doublet of $SU(2)_L$ and it acquires a vacuum expectation value (VEV) such that the symmetry $SU(2)_L \times U(1)_Y$ is spontaneously broken.

The recent discovery of a scalar boson at the Large Hadron Collider (LHC) [1, 2] seems to indicate that it is the SM Higgs boson. If this particle is the Higgs boson of the SM then this discovery confirms that the SM is consistent. As a consequence of the measurements related to the SM [3], we now have direct evidence of all the SM spectrum.

Despite the success of the SM when compared with experiment [3, 4] we have many reasons to believe that the SM is not complete since, to say the least, gravity is not included. The SM does not provide a satisfactory explanation to the hierarchy problem [5, 6]. Here we focus on extensions of the SM that solve the hierarchy problem. In particular, we study quiver theories [7, 8, 9, 10, 11, 12] and their phenomenology. Using quiver theories [5, 13, 14] as well as other similar theories where the Higgs is a pseudo-Nambu-Goldstone boson (pNGB).

We study the fermion excitations in these models by computing their masses and wave functions. Considering both cases left- and right-handed zero mode fermions, we will study the more relevant phenomenology.

To reproduce the phenomenology of these fermion excitations, we compute all their couplings. The one to the Higgs sector will be crucial to do the phenomenology. For instance, the coupling to the first excitations of the gauge bosons will be neglected, but only because we computed first and now we know they will play no role in the pair production.

We study the phenomenology of vector-like quarks at high energy Colliders. Prompted by our results in quiver theories, the vector-like quark can be heavier than the excitedgluons, we study the phenomenology of production and decay of vector-like quark at the LHC and beyond taking into account the decay channel $T \to Gt$, with Q the vector-like quark, G the heavy gluon and q a SM quark.

We start in chapter 2 by presenting the SM, jointly with the motivations to study physics beyond SM. In chapter 3 we briefly study one simple Little Higgs model [15] and introduce the quiver theories, for both gauge bosons and fermions. The Higgs is induced as a pNGB, by considering the quiver theory of EWSB. And then the couplings of fermions excited states were computed. In chapter 4 we study the phenomenology at the LHC of the excited heavy quarks in quiver theories, by using the most relevant couplings computed. In chapter 5 we begin to study the phenomenology of the heavy quarks at a future high energy Collider in a general vector-like theories. Finally we conclude and present the future studies in chapter 6.

CHAPTER 2

The Standard Model

The Standard Model (SM) of elementary particle physics is a quantum field theory that describes the electromagnetic, weak and strong interactions. The theoretical and experimental research in elementary particle physics in the 60s gave evidence of a possible unification of the weak and electromagnetic interactions, due to the fact that both are of vectorial nature and have universal couplings. In other words, they are both described by a gauge theory. Finally, between the years 60 and 70, the SM was first developed by Glashow, Weinberg and Salam, setting the foundations of our modern understanding of elementary particles.

The four basic ingredients necessary to the SM are: quarks, leptons, gauge bosons and the Higgs boson. All the electroweak and strong interactions are explained by gauge theories, namely the SM Lagrangian is invariant under the gauge transformations of $SU(3)_C \times SU(2)_L \times U(1)_Y$, for the strong and electroweak interactions respectively. We can study the strong interactions separately of the electroweak interactions, since both gauge sectors do not mix. The SM has a domain of applicability of at least several hundred of GeV. It is worth mentioning that not only works splendidly in theory, but it has also passed every experiment test so far. In addition, the model presents important symmetries in describing such interactions. In general, the symmetries have a central role in physics, namely, they protect some physical quantity and determine the dynamic structure of the fields. In this chapter, besides a brief introduction to the SM, we will present the gauge hierarchy problem and the problem of the hierarchy of SM fermion masses.

2.1 Quantum Chromodynamics

The sector of strong interactions of the SM better known as QCD is a non-Abelian gauge theory where generators belong to the local symmetry group $SU(3)_C$, and the internal degree of freedom is the named color. One of the properties of QCD is asymptotic freedom, that makes possible to use perturbative methods at very small distances [16]. The Lagrangian of QCD is

$$\mathcal{L} = -\frac{1}{4}F^i_{\mu\nu}F^{\mu\nu i} + \sum_r \ \bar{q}_{r\alpha}\ i\not{D}^\alpha_{\mu\beta}\ q^\beta_r. \tag{2.1}$$

Notice that in (2.1), r is the flavor index of quarks; the index of the adjoint representation is $i = 1, 2, \ldots, 8$ of 8 generators of $SU(3)_C$; $\alpha, \beta = 1, 2, 3$ are the indexes of the fundamental representation, these are the indexes of color, q^β_r is a the quark field and $F^i_{\mu\nu}$ is the gauge field strength tensor which is given by

$$F^i_{\mu\nu} = \partial_\mu G^i_\nu - \partial_\nu G^i_\mu - g_s f_{ijk} G^j_\mu G^k_\nu. \tag{2.2}$$

In (2.2) the fields G^i_μ are the gluons fields and the structure constants f_{ijk} $(i, j, k = 1, 2, \ldots, 8)$ are defined by

$$[\lambda^i, \lambda^j] = 2if_{ijk}\lambda^k. \tag{2.3}$$

The matrices λ^k are the Gell-Mann matrices for $SU(3)$. The covariant derivative is given by

$$D^\alpha_{\mu\beta} = \partial_\mu\ \delta^\alpha_\beta\ +\ \frac{1}{2}ig_s\ G^i_\mu\ \lambda^{\alpha i}_\beta, \tag{2.4}$$

with g_s the gauge coupling constant in $SU(3)_c$ local. We should point out that the mass terms for the quarks fields will appear after the EW symmetry breaking.

2.2 Electroweak Model

The Glashow-Weinberg-Salam theory (GWS) where fermions are chiral is a gauge theory with symmetry $SU(2)_L \times U(1)_Y$, where L and Y represent the left-handed chirality with symmetry of weak isospin, and weak hypercharge, respectively. The left-handed leptons are

$$\mathsf{L}_e = \begin{pmatrix} \nu_e \\ e^- \end{pmatrix}_L \qquad \mathsf{L}_\mu = \begin{pmatrix} \nu_\mu \\ \mu^- \end{pmatrix}_L \qquad \mathsf{L}_\tau = \begin{pmatrix} \nu_\tau \\ \tau^- \end{pmatrix}_L, \tag{2.5}$$

with weak isospin $I_\ell = 1/2$ and hypercharge $Y_{L_\ell} = -1$, and the right-handed leptons are

$$\mathsf{R}_{e,\mu,\tau} = e_R, \mu_R, \tau_R, \tag{2.6}$$

with hypercharge $Y_{R_\ell} = -2$, where the hypercharge is given by the Gell-Mann and Nishijima relation $Q = I_3 + (1/2)Y$. The SM does not include the right-handed

neutrinos because these have no SM gauge quantum numbers. The left-handed quarks are given by

$$\mathsf{L}_q^1 = \begin{pmatrix} u \\ d \end{pmatrix}_L \qquad \mathsf{L}_q^2 = \begin{pmatrix} c \\ s \end{pmatrix}_L \qquad \mathsf{L}_q^3 = \begin{pmatrix} t \\ b \end{pmatrix}_L, \tag{2.7}$$

with weak isospin $I_q = 1/2$ and hypercharge $Y_{L_q} = 1/3$. The right-handed quarks are

$$\mathsf{R}_u^{(1,2,3)} = u_R, c_R, t_R \tag{2.8}$$

and

$$\mathsf{R}_d^{(1,2,3)} = d_R, s_R, b_R \tag{2.9}$$

with $Y_{R_u} = 4/3$ and $Y_{R_d} = -2/3$, respectively.

Now, we write the Lagrangian $\mathcal{L}$ that is invariant under the gauge symmetry $SU(2)_L \times U(1)_Y$ in three parts, as follows

$$\mathcal{L} = \mathcal{L}_G + \mathcal{L}_F + \mathcal{L}_H, \tag{2.10}$$

with

$$\mathcal{L}_G = -\frac{1}{4} W^i_{\mu\nu} W^{\mu\nu i} - \frac{1}{4} B_{\mu\nu} B^{\mu\nu}, \tag{2.11}$$

where the field strength tensor $W^i_{\mu\nu}$ corresponds to the gauge symmetry $SU(2)_L$, with coupling g and is given by

$$W^i_{\mu\nu} = \partial_\nu W^i_\mu - \partial_\mu W^i_\nu + g\varepsilon_{ijk} W^j_\mu W^k_\nu, \tag{2.12}$$

and the field strength tensor $B_{\mu\nu}$ corresponds to the $U(1)_Y$ field with coupling g' and is given by

$$B_{\mu\nu} = \partial_\nu B_\mu - \partial_\mu B_\nu. \tag{2.13}$$

The kinetic term for the fermions is written in two parts

$$\mathcal{L}_F = \mathcal{L}_{\text{leptons}} + \mathcal{L}_{\text{quarks}}, \tag{2.14}$$

that are given by

$$\begin{aligned} \mathcal{L}_{\text{leptons}} = {} & \overline{\mathsf{R}}^n_\ell \; i\gamma^\mu \left(\partial_\mu + i\frac{g'}{2} B_\mu Y \right) \mathsf{R}^n_\ell \\ & + \overline{\mathsf{L}}^n_\ell \; i\gamma^\mu \left(\partial_\mu + i\frac{g'}{2} B_\mu Y + i\frac{g}{2} \vec{\sigma} \cdot \vec{W}_\mu \right) \mathsf{L}^n_\ell, \end{aligned} \tag{2.15}$$

where the index ℓ represents the leptons ($\ell = e, \mu, \tau$); and the second term in (2.14) is

$$\mathcal{L}_{\text{quarks}} = \overline{\mathsf{R}}_u^n \; i\gamma^\mu \left(\partial_\mu + i\frac{g'}{2}B_\mu Y\right) \mathsf{R}_u^n + \overline{\mathsf{R}}_d^n \; i\gamma^\mu \left(\partial_\mu + i\frac{g'}{2}B_\mu Y\right) \mathsf{R}_d^n + \overline{\mathsf{L}}_q^n \; i\gamma^\mu \left(\partial_\mu + i\frac{g'}{2}B_\mu Y + i\frac{g}{2}\vec{\sigma}\cdot\overrightarrow{W}_\mu\right) \mathsf{L}_q^n, \tag{2.16}$$

where the index n is the index of generations ($n = 1, 2, 3$). In (2.15) and (2.16) $\vec{\sigma}$ represents the Pauli matrices:

$$\sigma^1 = \begin{pmatrix} 0 & 1 \\ 1 & 0 \end{pmatrix}, \; \sigma^2 = \begin{pmatrix} 0 & -i \\ i & 0 \end{pmatrix}, \; \sigma^3 = \begin{pmatrix} 0 & -1 \\ 0 & 1 \end{pmatrix}. \tag{2.17}$$

The Lagrangian (2.11) has four massless gauge bosons W_μ^1, W_μ^2, W_μ^3 and B_μ because their mass terms are not invariant under gauge transformations. In addition, the gauge symmetry $SU(2)_L \times U(1)_Y$ prohibits mass terms for fermions, since the left- and right- handed components of the fermionic fields transform in different ways under the $SU(2)_L \times U(1)_Y$ gauge symmetry.

In the SM, the electroweak symmetry is spontaneously broken through the Higgs mechanism. This is done by introducing a scalar that is a doublet of $SU(2)_L$, such that it includes two complex scalar fields as follows

$$\Phi = \begin{pmatrix} \phi^+ \\ \phi^0 \end{pmatrix}, \tag{2.18}$$

and with hypercharge $Y_\Phi = 1$. The Lagrangian for Φ is given by

$$\mathcal{L}_\Phi = (D^\mu\Phi)^\dagger(D_\mu\Phi) - V(\Phi^\dagger\Phi), \tag{2.19}$$

where

$$D_\mu = \partial_\mu + i\frac{g'}{2}B_\mu Y + i\frac{g}{2}\vec{\sigma}\cdot\overrightarrow{W}_\mu \tag{2.20}$$

and the potential in $\mathcal{L}_\Phi$ is

$$V(\Phi^\dagger\Phi) = \mu^2(\Phi^\dagger\Phi) + \lambda(\Phi^\dagger\Phi)^2. \tag{2.21}$$

In the following, we will work with the ground state that minimizes the potential (2.21), considering the case for $\mu^2 < 0$. Then we can write the VEV for Φ as follows:

$$\langle\Phi\rangle_0 = \frac{1}{\sqrt{2}}\begin{pmatrix} 0 \\ v \end{pmatrix}, \tag{2.22}$$

where $v = \sqrt{-\mu^2/\lambda}$. Using the nonlinear sigma model [17], jointly with (2.22), we parameterize the field Φ as

$$\Phi = \exp(\frac{i\xi^j(x)\sigma^j}{2v}) \begin{pmatrix} 0 \\ (v+h(x))/\sqrt{2} \end{pmatrix}, \tag{2.23}$$

where σ^j are Pauli matrices (2.17). But we will work in the unitary gauge, such that the Nambu-Goldstone Bosons (NGB's) ξ^j can be removed by the following gauge transformation:

$$\Phi \to \exp(\frac{-i\xi^j(x)\sigma^j}{2v})\Phi = \frac{1}{\sqrt{2}} \begin{pmatrix} 0 \\ v+h(x) \end{pmatrix}, \tag{2.24}$$

so $\mathcal{L}_\Phi$ in (2.19) can be written in terms of physical fields as

$$\begin{aligned} \mathcal{L}_\Phi = \frac{1}{2}\partial_\mu h \partial^\mu h + \frac{g^2}{4}(v+h)^2 \left[W^+_\mu W^{-\mu} + \frac{1}{2\cos^2\theta_W} Z_\mu Z^\mu \right] \\ - \mu^2 \frac{(v+h)^2}{2} - \lambda \frac{(v+h)^4}{4}, \end{aligned} \tag{2.25}$$

where the Weinberg angle is defined by the relation $\tan\theta_W \equiv g'/g$. We also have defined the mediator fields of the charged weak interactions $W^\pm_\mu$,

$$W^\pm_\mu = (W^1_\mu \mp iW^2_\mu)/\sqrt{2}. \tag{2.26}$$

These physical fields $W^\pm_\mu$ acquire mass equivalent to $M_W = gv/2 = ev/2\sin\theta_W$ and the field that mediates the neutral weak interactions Z_μ,

$$Z_\mu = W^3_\mu \cos\theta_W - B_\mu \sin\theta_W, \tag{2.27}$$

acquires a mass $M_Z = \sqrt{g^2+g'^2}v/2 = M_W/\cos\theta_W$. The photon field is written as the orthogonal neutral combination

$$A_\mu = B_\mu \cos\theta_W + W^3_\mu \sin\theta_W, \tag{2.28}$$

and its mass is $M_A = 0$, leaving the $U(1)_{EM}$ unbroken. There are also Yukawa interactions between the Higgs doublet Φ with the quarks and leptons, that can be written as

$$\mathcal{L}_{\Phi F} = \mathcal{L}_{\text{Y(quarks)}} + \mathcal{L}_{\text{Y(leptons)}}, \tag{2.29}$$

where

$$\mathcal{L}_{\text{Y(quarks)}} = -\sum_{i,j=1}^{3} \left[G^u_{ij}\ \overline{\mathsf{R}}^i_u \left(\tilde{\Phi}^\dagger \mathsf{L}^j_q \right) + G^d_{ij}\ \overline{\mathsf{R}}^i_d \left(\Phi^\dagger \mathsf{L}^j_q \right) + \text{h.c.} \right], \tag{2.30}$$

and

$$\mathcal{L}_{\mathrm{Y(leptons)}} = -\sum_{i,j=1}^{3}\left[G^{\ell}_{i,j}(\overline{\mathsf{L}}^{i}_{\ell}\Phi)\mathsf{R}^{j}_{\ell} + \mathrm{h.c.}\right], \tag{2.31}$$

where G^{u}_{ij}, G^{d}_{ij} and $G^{\ell}_{i,j}$ are the Yukawa couplings, these are not diagonal in the generation indexes nor real, and $\tilde{\Phi} \equiv i\sigma_2\Phi^*$. We note that all these terms are also gauge invariant under $SU(2)_L$ and have zero net hypercharge Y.

In the following we will consider $\mathcal{L}_{\mathrm{Y(quarks)}}$ in (2.30), and after replacing ϕ (2.24) in (2.30), we can identify

$$-\bar{u}_R^{\,i}\; M^{u}_{ij}\; u_L^{j} \;+\; \mathrm{h.c.}, \tag{2.32}$$

where u_L^j is the left-handed up-type quark of the doublet L^j_q (2.7) and $\bar{u}^i_R = \{\bar{u}_R, \bar{c}_R, \bar{t}_R\}$.

To the down-type quarks we have also

$$-\bar{d}_R^{\,i}\; M^{d}_{ij}\; d_L^{j} \;+\; \mathrm{h.c.}, \tag{2.33}$$

where d_L^j is the left-handed down-type quark of the doublet L^j_q (2.7) and $\bar{d}^i_R = \{\bar{d}_R, \bar{s}_R, \bar{b}_R\}$.

The matrices M^u and M^d, which are generally not diagonal, are given by $M^{u(d)}_{ij} = G^{u(d)}_{ij} v/\sqrt{2}$. To diagonalize these mass matrices, the unitary matrices $U(D)_{L,R}$ are defined such as:

$$u^i_L = U^{ij}_L\; u'^{\,j}_L, \qquad d^i_L = D^{ij}_L\; d'^{\,j}_L, \tag{2.34}$$

$$u^i_R = U^{ij}_R\; u'^{\,j}_R, \qquad d^i_R = D^{ij}_R\; d'^{\,j}_R, \tag{2.35}$$

Note that the gauge eigenstates (q) are linear combinations of the mass eigenstates (q'), so we have to do the basis changes given by (2.34) and (2.35) to diagonalize M^U and M^D, as follows

$$M^{U}_{\mathrm{diag}} \;\equiv\; U^{\dagger}_R\; M^U\; U_L \;=\; \begin{pmatrix} m_u & 0 & 0 \\ 0 & m_c & 0 \\ 0 & 0 & m_t \end{pmatrix}, \tag{2.36}$$

$$M^{D}_{\mathrm{diag}} \;\equiv\; D^{\dagger}_R\; M^D\; D_L \;=\; \begin{pmatrix} m_d & 0 & 0 \\ 0 & m_s & 0 \\ 0 & 0 & m_b \end{pmatrix}. \tag{2.37}$$

Considering the quark sector in (2.29) after the EW symmetry breaking, we need to go to the mass basis to diagonalize the Yukawa terms in (2.30). This is done with the $U_{L,R}$, $D_{L,R}$ unitary transformations.

For the case of charged current $J^{+}_{\mu\ W}$, we have that it must be proportional to

$$\left(\begin{array}{ccc} \bar{u}' & \bar{c}' & \bar{t}' \end{array} \right)_L U_L^\dagger \, \gamma_\mu \, D_L \left(\begin{array}{c} d' \\ s' \\ b' \end{array} \right)_L . \tag{2.38}$$

That is, the charged current coupling will not be diagonal anymore, since $U_L^\dagger D_L \neq \mathbf{1}_3$. This unitary matrix that express the mixing between the quarks is known as Cabibbo-Kobayashi-Maskawa (CKM) matrix

$$\mathsf{V}_{\rm CKM} \equiv U_L^\dagger D_L = \left(\begin{array}{ccc} V_{ud} & V_{us} & V_{ub} \\ V_{cd} & V_{cs} & V_{cb} \\ V_{td} & V_{ts} & V_{tb} \end{array} \right). \tag{2.39}$$

In the case of neutral current $J_{\mu\ Z}$, considering up-type SM quarks, it must be proportional to

$$\left(\begin{array}{ccc} \bar{u}' & \bar{c}' & \bar{t}' \end{array} \right)_{L,R} U_{L,R}^\dagger \, \gamma_\mu \, U_{L,R} \left(\begin{array}{c} u' \\ c' \\ t' \end{array} \right)_{L,R} = \left(\begin{array}{ccc} \bar{u}' & \bar{c}' & \bar{t}' \end{array} \right)_{L,R} \gamma_\mu \left(\begin{array}{c} u' \\ c' \\ t' \end{array} \right)_{L,R} \tag{2.40}$$

So there is no mixing of the quarks in the sector of neutral currents, due to the fact that U_L and U_R are unitary, namely, the couplings are diagonal. Thus, in the Standard Model there are no interactions that change flavor in neutral currents, at least at tree level.

Now we will consider $\mathcal{L}_{\rm Y(leptons)}$, jointly with ϕ in (2.24), we can obtain mass terms

$$-\bar{e}_L^{\ i} \, M^\ell_{i,j} \, e_R^{\ j} + \text{ h.c.}, \tag{2.41}$$

where $e^i_{L,R} = \{e_{L,R}, \mu_{L,R}, \tau_{L,R}\}$ and we identify from (2.31) that the charged lepton mass matrix is given by $M^\ell_{i,j} = G^\ell_{i,j} v/\sqrt{2}$.

To diagonalize $M^\ell_{i,j}$, the matrices U_ℓ and W_ℓ are defined as

$$e^i_L = U^{ij}_\ell \ e'^{\ j}_L, \qquad e^i_R = W^{ij}_\ell \ e'^{\ j}_R. \tag{2.42}$$

Then these basis changes yield the diagonal lepton mass matrix

$$M^\ell_{\rm diag} \equiv D_R^\dagger \, M^D \, D_L = \left(\begin{array}{ccc} m_e & 0 & 0 \\ 0 & m_\mu & 0 \\ 0 & 0 & m_\tau \end{array} \right). \tag{2.43}$$

With this procedure it is possible to obtain the masses terms to the leptons. However, the value of M_ℓ is not predicted by the theory since the Yukawa couplings $G^\ell_{i,j}$ were introduced arbitrarily to reproduce the masses of the observed leptons. Just as in the quark case, the theory does not provide the values of $M^{u(d)}_{ij}$. That

is, the Yukawa couplings $G_{ij}^{u(d)}$ were arbitrarily introduced to correctly give the masses of the fermions observed, once they are diagonalized.

2.3 Motivation of Physics Beyond the SM

In the previous sections we saw that the SM of elementary particles offers a theoretical explanation for the interactions of all elementary particles we know of today. It is extremely successful when compared with the experimental data we have nowadays. As examples, we have the detection of neutral currents in the decade of 70s, the predictions made to the bosons mass $W_{\mu}^{\pm}$ and Z_{μ}, experiments made in LEPI, LEPII and the Tevatron [18, 19] with high precision ($\lesssim 1\%$).

The model needs a scalar particle remaining form the process of spontaneous symmetry breaking in the electroweak sector, the Higgs boson that couples with the other particles of the SM and that recently has been discovered at the LHC [1, 2].

Despite the success of the SM, it has deficiencies in how to explain the hierarchy problem and the hierarchy of the SM fermion masses among many others. The hierarchy problem is related to the quantum instability of the vacuum that sets the electroweak scale around $m_{EW} \sim 250GeV$. In addition, the SM does not include the interaction with gravity, which is non-renormalizable and can be ignored up to scales of order of Planck mass.

2.3.1 The Gauge Hierarchy Problem

Despite the success of the SM when compared with experiment [3, 4] we have quite important reasons to believe that the SM is not complete, besides the fact that gravity is not included. Among all these, the one that requires new physics not too far above the TeV scale is the hierarchy problem. The SM does not provide a satisfactory explanation to the hierarchy problem [5, 6]. This problem can be understood when we calculate the quantum corrections to the Higgs mass. For instance, the largest of these corrections comes from the virtual top pair contribution up to 1 loop to the Higgs propagator as in Figure (2.1). This contribution is given by

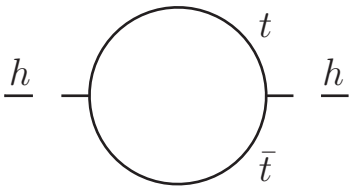

Figure 2.1. Quantum contribution to the Higgs boson propagator from the top quark loop in the SM.

$$
\begin{aligned}
-i\delta m_h^2 &= -N_c \left(\frac{\lambda_t}{\sqrt{2}}\right)^2 \int \frac{d^4p}{(2\pi)^4} \mathrm{Tr}\left[\left(\frac{\not{p} + m_t}{p^2 - m_t^2}\right) \left(\frac{\not{p} + m_t}{p^2 - m_t^2}\right) \right] \\
&= -2N_c\lambda_t^2 \int \frac{d^4p}{(2\pi)^4} \frac{p^2 + m_t^2}{(p^2 - m_t^2)^2}.
\end{aligned} \tag{2.44}
$$

Using a Wick rotation, i.e., $p_0 \to ip_4$, $p^2 \to -p_E^2$, jointly with the angular integration, we obtain

$$
\begin{aligned}
\delta m_h^2 &= -\frac{N_c\lambda_t^2}{8\pi^2} \int_0^{\Lambda_{UV}^2} dp_E^2 \frac{p_E^2(p_E^2 - m_t^2)}{(p_E^2 + m_t^2)^2} \\
&= -\frac{N_c\lambda_t^2}{8\pi^2} \left[\Lambda_{UV}^2 + ... \right],
\end{aligned} \tag{2.45}
$$

where $N_c = 3$, and Λ_{UV} is the highest energy where we believe the SM can be used for this computation. For instance, if we consider $\Lambda_{UV} = M_{Planck}$, the scale where gravity becomes strong and needs to be included,

$$
M_{Planck} = \left(\frac{\hbar c}{G_{\mathrm{Newton}}}\right)^{1/2} \simeq \ 1.2 \times 10^{19} \ \mathrm{GeV}, \tag{2.46}
$$

where in this scale the quantum gravitational effects will become important. On the other hand, the recent discovery of a new particle at the Large Hadron Collider (LHC) [1, 2] confirms that this particle is like the Higgs boson of the SM with mass $m_h \approx 125$ GeV, when the electroweak symmetry is broken by the VEV of scalar Higgs.

So, as shown in (2.45) this correction to the Higgs mass squared has quadratic sensitivity to the cutoff of the theory, and then, if the SM is valid until the Planck scale, we will need a large fine tuning to obtain the observed Higgs mass in the electroweak scale. This fine tunning is not natural and needs new physics beyond the SM to restore naturalness [5]. That is not the case for the masses associated to other SM elementary particles, for instance, considering a light fermion or a

gauge boson as can be found in Ref. [20], as we see below.

Let us consider the quantum corrections to the self-energy of the electron as an example, as shown in Figure (2.2). We will compute this correction at zero external momentum, considering the one-loop diagram of the electron propagator that comes from the γ boson contribution, this result in a contribution given by

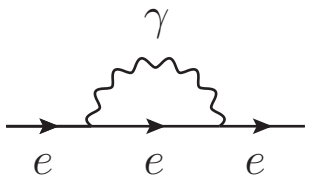

Figure 2.2. Electron self energy.

$$\begin{aligned}\delta m_{e\gamma} =& m_e e^2 \frac{1}{2\pi^2} \int_0^{\Lambda} dp_E \frac{p_E^3}{(p_E^2)\,(p_E^2 + m_e^2)} \\ =& m_e e^2 \frac{1}{4\pi^2} \ln\left(\frac{\Lambda^2 + m_e^2}{m_e^2}\right).\end{aligned} \tag{2.47}$$

Consequently, from the loop considered to determine δm_e, we can see that this is divergent but only logarithmically sensitive to the cutoff of the theory. If, for instance, we use $\Lambda_{UV} = M_{Planck}$ we have

$$\delta m_e = 0.3 m_e, \tag{2.48}$$

which is not that large. It is also a multiplicative shift, a reflection of chiral symmetry.

Similarly to the previous calculations, we illustrate the quantum correction at one-loop of the W self energy, at external zero momentum. For instance, considering the contributions as indicated in Figure (2.3).

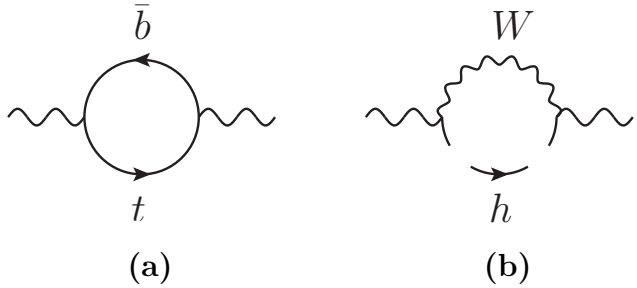

Figure 2.3. EW quantum corrections at one-loop for the W boson self energy involving: (a) t and b, (b) W and h.

The corresponding contribution to the δm_W^2 after a Wick rotation and the angular integration associated with the first diagram in Figure (2.3) is given by

$$\begin{aligned}\delta m_{Wa}^2 &= N_c g^2 m_t m_b \frac{1}{8\pi^2}\int_0^{\Lambda} dp_E \frac{p_E^3}{(p_E^2+m_t^2)(p_E^2+m_b^2)} \\ &= \frac{N_c g^2 m_t m_b}{16\pi^2(m_t^2-m_b^2)}\left[m_t^2\,\ln\left(\frac{\Lambda^2+m_t^2}{m_t^2}\right) - m_b^2\,\ln\left(\frac{\Lambda^2+m_b^2}{m_b^2}\right)\right], \end{aligned} \tag{2.49}$$

where $N_c = 3$ due that we deal with three colors of quarks.

Now, from the diagram in Figure (2.2b) gives a contribution to the δm_W^2 given by

$$\begin{aligned}\delta m_{Wb}^2 &= g^2 m_W^2 \frac{1}{8\pi^2}\int_0^{\Lambda} dp_E \frac{p_E^3}{(p_E^2+m_W^2)(p_E^2+m_h^2)} \\ &= \frac{g^2 m_W^2}{16\pi^2(m_W^2-m_h^2)}\left[m_W^2\,\ln\left(\frac{\Lambda^2+m_W^2}{m_W^2}\right) - m_h^2\,\ln\left(\frac{\Lambda^2+m_h^2}{m_h^2}\right)\right] \end{aligned} \tag{2.50}$$

Notice that according to (2.49) and (2.50) for the contributions considered to the δm_W^2, these contributions are also divergent but have logarithmic divergence to the cutoff. And it is possible to write these contributions as proportional to m_W^2. Consequently, in the massless limit of fermions as well as gauge bosons we will have the mass parameters quantum corrections go to zero and recover a chiral and EW gauge symmetry, respectively.

We conclude that the quadratically divergence takes place in the Higgs mass squared as indicated in (2.45), and its quantum correction is unnatural, it is due that in the SM there is no symmetry that protects the Higgs mass.

2.3.2 Problem of Fermion Mass Hierarchy

When we review in Section 2.2 the electroweak sector of the SM, especially when through Higgs mechanism the Φ acquired an VEV, we obtained mass terms. That is as a consequence of the Yukawa interactions given by (2.31) and (2.30), these mass terms can be identified as

$$M_f = \frac{G_f v}{\sqrt{2}}, \tag{2.51}$$

where G_f are Yukawa couplings of the fermions, and are extremely varied. For instance, we have that the coupling for the electron and the top are $G_e \sim 10^{-6}$ and $G_t \sim 1$, respectively. This is a problem, since the SM does not explain why the fermions can have masses so different, after the electroweak symmetry breaking through the Higgs mechanism.

Thus, to explain the fact that these couplings are so different it is necessary to introduce physics beyond the Standard Model. There are many other problems with the SM. The strong CP problem, origin of baryon asymmetry, dark matter, among others. We will focus on theories that address the hierarchy problem, and in particular in which the Higgs mass is protected by a symmetry similar to that protecting the pion mass in QCD, i.e, the Higgs will be a pNGB.

The hierarchy problem (and maybe the problem of the fermion mass hierarchy) seem to be a good guides to construct theories Beyond the SM. Let us consider theories that solve these hierarchy problems generating large hierarchy of scales.

CHAPTER 3

New Fermions in BSM Theories

As was pointed out in the previous chapter, the SM does not provide a satisfactory explanation for the hierarchy problem. Extensions of the SM that solve the hierarchy problem without supersymmetry [21] require the presence of new states partners of the SM fields under some symmetry. In particular there will be partners of fermions, especially of the top quark, of gauge bosons, etc. We will focus here on the Vector-like quarks that are partners of the SM fermions. Several theories have been suggested in the literature, for instance Little Higgs models [15, 22], composite Higgs models [23, 24, 25] and quiver theories [8, 10].

As a first example, we will study how the hierarchy problem is addressed in a Little Higgs model [15, 26]. Firstly, we consider two independent $SU(3)$ global symmetries, with two nonlinear sigma fields that parametrize the spontaneous symmetry breaking associated with the coset $[SU(3)/SU(2)]^2$ and are given by

$$\phi_1 = \exp\left\{\frac{i}{f}\begin{pmatrix} 0 & 0 & k_1 \\ 0 & 0 & k_2 \\ k_1^* & k_2^* & 0 \end{pmatrix}\right\} \exp\left\{\frac{i}{f}\begin{pmatrix} 0 & 0 & H_1 \\ 0 & 0 & H_2 \\ H_1^* & H_2^* & 0 \end{pmatrix}\right\} \begin{pmatrix} 0 \\ 0 \\ f \end{pmatrix}, \quad (3.1)$$

$$\phi_2 = \exp\left\{\frac{i}{f}\begin{pmatrix} 0 & 0 & k_1 \\ 0 & 0 & k_2 \\ k_1^* & k_2^* & 0 \end{pmatrix}\right\} \exp\left\{-\frac{i}{f}\begin{pmatrix} 0 & 0 & H_1 \\ 0 & 0 & H_2 \\ H_1^* & H_2^* & 0 \end{pmatrix}\right\} \begin{pmatrix} 0 \\ 0 \\ f \end{pmatrix}, \quad (3.2)$$

where H_1, H_2, k_1 and K_2 are complex fields, with the same symmetry breaking scale given by f. The symmetry breaking pattern is the coset $[SU(3)/SU(2)]^2$, therefore, after the breaking symmetry of the two $SU(3)$ we will identify 10 spontaneously broken generators, resulting in 10 NGBs. Notice that two singlet

fields of $SU(2)$ were ignored for simplicity in the parametrization of both scalar fields ϕ_1 and ϕ_2. Then, we add the interaction between the scalar fields and gauge bosons associated with the $SU(3)$ through the covariant derivatives acting on ϕ_1 and ϕ_2. We write the Lagrangian $\mathcal{L}$ associated with these fields as follows

$$\mathcal{L} = (D^\mu \phi_1)^\dagger (D_\mu \phi_1) + (D^\mu \phi_2)^\dagger (D_\mu \phi_2), \tag{3.3}$$

where

$$D_\mu = \partial_\mu - ig A^a_\mu T^a, \tag{3.4}$$

such that T^a are the $SU(3)$ generators with $a = 1, 2, \ldots, 8$. We can identify the interactions between the scalar fields and the gauge bosons by expanding the kinetic terms in (3.3),

$$\begin{aligned}(D_\mu \phi_i)^\dagger (D^\mu \phi_i) = (\partial_\mu \phi_j)^\dagger (\partial^\mu \phi_j) + g \left[i \phi_i^\dagger A^a_\mu T^a \partial^\mu \phi_i + \text{h.c.} \right] \\ + g^2 \left[\phi_i^\dagger A^a_\mu A^{\mu b} T^b T^a \phi_i \right].\end{aligned} \tag{3.5}$$

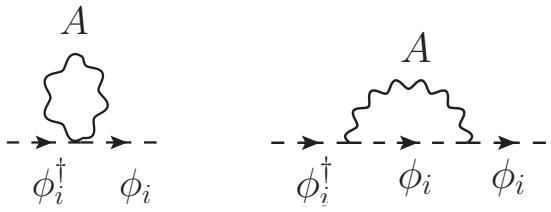

Figure 3.1. Quantum corrections at one-loop for two-point function of the scalar fields ϕ_i due to the $SU(3)$ gauge interaction.

In the calculation of the quantum contribution from Figure (3.1**a**) the Feynman gauge will be used. This gives

$$\begin{aligned} i\Sigma_{(\mathbf{a})} &= \int \frac{d^4k}{(2\pi)^4} \left[ig^2 g^{\mu\nu} \left(T^r_{ij} T^s_{jm} + T^s_{ij} T^r_{jm} \right) \right] \left(\frac{-i g_{\mu\nu} \delta^{rs}}{k^2} \right), \\ &= -8ig^2 \left(T^r_{ij} T^r_{jm} \right) \frac{1}{16\pi^2} \Lambda^2. \end{aligned} \tag{3.6}$$

from Figure (3.1**b**), we also have

$$\begin{aligned} i\Sigma_{(\mathbf{b})} &= \int \frac{d^4k}{(2\pi)^4} \left(igk^\mu T^r_{ij} \right) \left(\frac{i\delta^{jl}}{k^2} \right) \left(igk^\nu T^s_{lm} \right) \left(\frac{-i g_{\mu\nu} \delta^{rs}}{k^2} \right), \\ &= ig^2 \left(T^r_{ij} T^r_{jm} \right) \frac{1}{16\pi^2} \Lambda^2. \end{aligned} \tag{3.7}$$

So the contributions potential

$$\propto \frac{g^4}{16\pi^2}\ \Lambda^2 \left(\phi_1^\dagger \phi_1 + \phi_2^\dagger \phi_2\right), \tag{3.8}$$

and then substituting (3.1), (3.2) in (3.8) we will obtain a constant term that that does not contribute to the potential for H, since (3.8) does not depend on the Higgs.

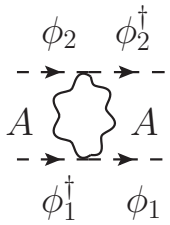

Figure 3.2. Quantum correction at one-loop from the interaction terms of two gauge boson and two scalars included in (3.3).

Now, we consider the quantum correction from Figure (3.2) we can write the Feynman integral by considering a power counting

$$i\Sigma_4 \propto \int \frac{d^4k}{(2\pi)^4} \times \left(\frac{g^2}{k^2}\right)\left(\frac{g^2}{k^2}\right), \tag{3.9}$$

which results in

$$= \frac{g^4}{16\pi^2}\ \ln\left(\frac{\Lambda^2}{\mu^2}\right), \tag{3.10}$$

the following operator that does not have a quadratic divergence

$$\frac{g^4}{16\pi^2}\ \ln\left(\frac{\Lambda^2}{\mu^2}\right) |\phi_1^\dagger \phi_2|^2. \tag{3.11}$$

To identify the coefficient of $H^\dagger H$, i.e., its mass squared we will substitute the parameterizations (3.1), (3.2) in (3.11), for this purpose we compute

$$\phi_1^\dagger \phi_2 = \begin{pmatrix} 0 & f \end{pmatrix} \exp\left\{-\frac{2i}{f}\begin{pmatrix} 0 & H \\ H^\dagger & 0 \end{pmatrix}\right\}\begin{pmatrix} 0 \\ f \end{pmatrix} \tag{3.12}$$

after expanding the exponential matrix up to order of $\left(\frac{1}{f^2}\right)$ we have

$$\begin{aligned}\phi_1^\dagger\phi_2 = \begin{pmatrix} 0 & f \end{pmatrix} \Bigg[\begin{pmatrix} 1 & 0 \\ 0 & 1 \end{pmatrix} - \frac{2i}{f} \begin{pmatrix} 0 & H \\ H^\dagger & 0 \end{pmatrix} \\ -\frac{2}{f^2} \begin{pmatrix} HH^\dagger & 0 \\ 0 & H^\dagger H \end{pmatrix} + \mathcal{O}\left(\frac{1}{f^3}\right) \Bigg] \begin{pmatrix} 0 \\ f \end{pmatrix} \\ = f^2 - 2H^\dagger H + \cdots \end{aligned} \tag{3.13}$$

we can substitute this result in (3.11), obtaining a mass term

$$-\frac{g^4 f^2}{4\pi^2} \ln\left(\frac{\Lambda^2}{\mu^2}\right) H^\dagger H. \tag{3.14}$$

Thus we have a theory that does not have quadratic divergence at one-loop for the mass of H, and it is the pseudo-Nambu Goldstone Boson associated with two scalar fields that break separately each $SU(3)$ to $SU(2)$. The fact that to generate a genuine contribution to the Higgs potential we need the contributions of both ϕ_1 and ϕ_2 is an example of the so-called collective breaking. Notice that the term given in (3.11) explicitly breaks both $SU(3)$ to the diagonal.

There is a similar mechanism for the Yukawa contributions to the potential. The ϕ_1 and ϕ_2 Yukawas are

$$\mathcal{L} = -\lambda_1 \bar{t}_{1R} \phi_1^\dagger \Psi_L - \lambda_2 \bar{t}_{2R} \phi_2^\dagger \Psi_L + \text{h.c.}, \tag{3.15}$$

where Ψ_L is a $SU(3)$ triplet given by

$$\Psi_L = \begin{pmatrix} t \\ b \\ T \end{pmatrix}_L, \tag{3.16}$$

and taking into account the $SU(2)$ doublet

$$Q_L = \begin{pmatrix} t \\ b \end{pmatrix}_L, \tag{3.17}$$

jointly with

$$H = \begin{pmatrix} H_1 \\ H_2 \end{pmatrix}. \tag{3.18}$$

Now, we can substitute (3.1), (3.2) in (3.15) and using the rotation where k_1 and k_2 are removed, i.e., in unitary gauge for $SU(3)$ jointly with (3.17), we have

$$\begin{aligned}
&-\lambda_1 \bar{t}_{1R} \left[\exp\left\{ \frac{i}{f} \begin{pmatrix} 0 & H \\ H^\dagger & 0 \end{pmatrix} \right\} \begin{pmatrix} 0 \\ f \end{pmatrix} \right]^\dagger \begin{pmatrix} Q \\ T \end{pmatrix}_L \\
&-\lambda_2 \bar{t}_{2R} \left[\exp\left\{ \frac{-i}{f} \begin{pmatrix} 0 & H \\ H^\dagger & 0 \end{pmatrix} \right\} \begin{pmatrix} 0 \\ f \end{pmatrix} \right]^\dagger \begin{pmatrix} Q \\ T \end{pmatrix}_L ,
\end{aligned} \tag{3.19}$$

expanding the exponential matrix functions up to order of $\left(\frac{1}{f^2}\right)$

$$\begin{aligned}
&-\lambda_1 \bar{t}_{1R} \begin{pmatrix} 0 & f \end{pmatrix} \left[1 - \frac{i}{f} \begin{pmatrix} 0 & H \\ H^\dagger & 0 \end{pmatrix} - \frac{1}{2f^2} \begin{pmatrix} HH^\dagger & 0 \\ 0 & H^\dagger H \end{pmatrix} \right] \begin{pmatrix} Q \\ T \end{pmatrix}_L \\
&-\lambda_2 \bar{t}_{2R} \begin{pmatrix} 0 & f \end{pmatrix} \left[1 + \frac{i}{f} \begin{pmatrix} 0 & H \\ H^\dagger & 0 \end{pmatrix} - \frac{1}{2f^2} \begin{pmatrix} HH^\dagger & 0 \\ 0 & H^\dagger H \end{pmatrix} \right] \begin{pmatrix} Q \\ T \end{pmatrix}_L ,
\end{aligned} \tag{3.20}$$

and considering

$$\lambda_1 = \lambda_2 = \frac{\lambda}{\sqrt{2}}, \tag{3.21}$$

the terms given in (3.20) are simplified to

$$-\frac{\lambda}{\sqrt{2}} \left[f\left(\bar{t}_{1R} + \bar{t}_{2R}\right) T_L + i\left(\bar{t}_{2R} - \bar{t}_{1R}\right) H^\dagger Q_L - \frac{1}{2f}\left(\bar{t}_{2R} + \bar{t}_{1R}\right) H^\dagger H T_L + ... + \text{h.c.} \right], \tag{3.22}$$

now, writing the following combinations

$$T_R = \bar{t}_{1R} + \bar{t}_{2R} \tag{3.23}$$

$$\bar{t}_R = \frac{i}{\sqrt{2}}\left(\bar{t}_{2R} - \bar{t}_{1R}\right), \tag{3.24}$$

substituting these combinations, we rewrite (3.22) as

$$-\lambda \left[f \overline{T}_R T_L + \bar{t}_R H^\dagger Q_L - \frac{1}{2f} \overline{T}_R H^\dagger H T_L + ... + \text{h.c.} \right], \tag{3.25}$$

where as in Ref. [26], here H can be identified as

$$H = \frac{1}{\sqrt{2}} \begin{pmatrix} h - i\varphi_3 \\ -\sqrt{2}\varphi^- \end{pmatrix}, \tag{3.26}$$

expanding about the symmetric point, $\langle h \rangle = 0$, we identify from (3.25) the following terms

$$-\lambda f \overline{T}_R T_L - \frac{\lambda}{\sqrt{2}} \bar{t}_R t_L h + \frac{\lambda}{4f} \overline{T}_R T_L h^2 + ... + \text{h.c.}. \tag{3.27}$$

From these, we can compute the corrections to the Higgs mass squared up to 1 loop, these quantum corrections to the Higgs propagator are shown in Figure (3.3).

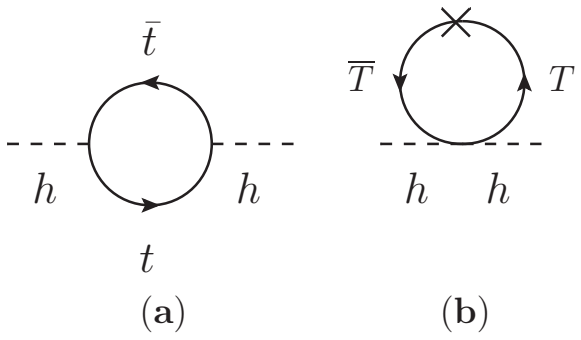

Figure 3.3. Quantum contributions to the Higgs propagator from the top and T at one loop according to the interactions given in (3.27).

The contribution to the Higgs mass squared from Figure (3.3a) is given by

$$\begin{aligned} \delta m^2_{h(\mathbf{a})} &= -N_c \lambda^2 \frac{1}{4\pi^2} \int_0^{\Lambda} dp_E \frac{p_E^3}{p_E^2} \\ &= -\frac{N_c}{8\pi^2} \lambda^2 \Lambda^2, \end{aligned} \tag{3.28}$$

and from Figure (3.3b), we also have

$$\begin{aligned} \delta m^2_{h(\mathbf{b})} &= N_c \lambda^2 \frac{1}{4\pi^2} \int_0^{\Lambda} dp_E \frac{p_E^3}{p_E^2} \\ &= \frac{N_c}{8\pi^2} \lambda^2 \Lambda^2. \end{aligned} \tag{3.29}$$

Thus the quadratic divergent contributions to the Higgs mass (3.28) and (3.29) are canceled by the addition of the quantum corrections at one-loop from the top and T. And also we saw that the model involves three scales Λ, f and $M_{weak} \sim$ such that its squared is given by the mass term in (3.14), where $\Lambda \lesssim 4\pi f$ as in Ref. [15], this could be obtained by doing a naive dimensional analysis after expanding the kinetic term of the scalar fields (3.1), (3.2). The size of f is of order to the TeV scale if g is equal to the $SU(2)$ gauge coupling. Thus, it is important to study theories where we will have fermion masses that are in the TeV scale to solve the hierarchy problem through to the cancellation of the quadratic divergence as above. This was an example of theories where a Vector-like quark must be present to solve the hierarchy problem. In the next sections we will introduce another example where the fermion masses can be in the TeV scale.

3.1 Quiver Theories

This section has attempted to provide a brief summary of the literature relating to quiver theories [7, 8, 10], because these are another possibility to address the hierarchy problem and the fermion mass hierarchies, in similar way to AdS_5 theories [5, 13, 14]. To study the more important phenomenology associated with the excited SM particles as studied in Ref. [10], we need to compute the couplings involved by obtaining their wave functions as we will see below.

In the quiver theories approach we consider a four dimensional (4D) gauge theory associated with a product gauge group

$$G = G_0 \times G_1 \times \ldots \times G_{N-1} \times G_N. \tag{3.30}$$

Here, we will consider that $G_j = SU(n)_j$ is a gauge symmetry, where $j = 0, 1, \ldots, N$. In addition to this framework, we include a set of scalar link fields Φ_j, with $j = 1, \ldots, N$, such that Φ_j transforms under the bi-fundamental representation of groups $G_{j-1} \times G_j$, as follows:

$$\Phi_j \to U_{j-1} \Phi_j U_j^{\dagger}. \tag{3.31}$$

The action with the considerations mentioned above is given by

$$S = \int d^4x \left\{ \sum_{j=0}^{N} -\frac{1}{2} \mathrm{Tr}\left[F^j_{\mu\nu}\, F^{j\mu\nu}\right] + \sum_{j=1}^{N} \mathrm{Tr}\left[(D_\mu \Phi_j)^{\dagger} (D^\mu \Phi_j)\right] - V(\Phi_j) \right\}, \tag{3.32}$$

where $F^j_{\mu\nu} = F^{j\ a}_{\mu\nu} T^a_j$ is the gauge field strength tensor. Here T^a_j are the generators of the symmetry group $SU(n)_j$ and $F^{j\ a}_{\mu\nu}$ is more explicitly given by

$$F^{j\ a}_{\mu\nu} = \partial_\mu A^{j\ a}_\nu - \partial_\nu A^{j\ a}_\mu + g_j\ f^{j\ abc}\ A^{j\ b}_\mu\ A^{j\ c}_\nu, \tag{3.33}$$

where $f^{j\ abc}$ are related through the commutation relations $[T^a_j, T^b_j] = i f^{j\ abc} T^c_j$. The covariant derivative $D_\mu \Phi_j$ is given by

$$D_\mu \Phi_j = \partial_\mu\ \Phi_j + i g_{j-1}\ A^a_{\mu,j-1}\ T^a_{j-1}\ \Phi_j - i g_j\ \Phi_j\ A^a_{\mu,j}\ T^a_j. \tag{3.34}$$

In addition, we assume that the Φ_j's develop a diagonal VEV, such that $SU(n)_{j-1} \times SU(n)_j$ is broken down to the diagonal group. This means that for each VEV we have to have $n^2 - 1$ Nambu-Goldstone Bosons (NGBs) and we can use the parameterization of the non-linear sigma models for the Φ_j's given by

$$\Phi_j = v_j e^{i\pi^a_j \hat{T}^a_j / v_j}, \tag{3.35}$$

where the broken generators are $\hat{T}^a_j$'s, the NGBs are π^a_j and the Φ_j's VEVs v_j are related with the breaking of $SU(n)_{j-1} \times SU(n)_j$. The model can be schematically represented by Figure (3.4). We choose to parametrize the v_j's as

$$v_j = v q^j, \tag{3.36}$$

with $0 < q < 1$, such that v is the UV mass scale and then we have that the v_j's decrease as follow $v_1 ... > v_j ... > v_N$. These choices have been studied in [7, 8, 9, 10]. In this example we can consider that each gauge coupling satisfies

$$g_0 = g_1 = ... g_N = g, \tag{3.37}$$

and as we have indicated that all gauge groups are identical $T^a_j = T^a_{j-1} = T^a$, with $j = 1, \ldots, N$. The action (3.32) can be represented by the bosonic quiver diagram of Figure (3.4), where the circles represent the gauge group's G_j, $j = 0, 1, \ldots, N$. Here j is identified with the index of the site in the quiver diagram, henceforth we will call j as site index. To expand the kinetic term of the Φ_j's in (3.32), we need to use (3.35). we obtain

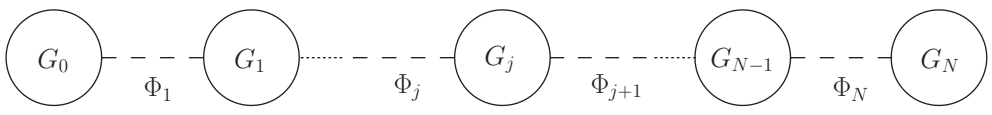

Figure 3.4: Quiver diagram associated with the theory in (3.32).

$$\begin{aligned}\mathrm{Tr}\left[(D_\mu\Phi_j)^\dagger(D^\mu\Phi_j)\right] &= \mathrm{Tr}\left[(\partial_\mu\Phi_j)^\dagger(\partial^\mu\Phi_j)\right] + g\mathrm{Tr}\left[i(\partial_\mu\Phi_j)^\dagger(A^\mu_{j-1}\Phi_j - \Phi_j A^\mu_j) + \text{h.c.}\right] \\ &\quad + v_j^2 g^2 \mathrm{Tr}\left[A_{\mu,j-1}A^\mu_{j-1}\right] - 2g^2\mathrm{Tr}\left[\Phi_j^\dagger A_{\mu,j-1}\Phi_j A^\mu_j\right] \\ &\quad + v_j^2 g^2 \mathrm{Tr}\left[A_{\mu,j}A^\mu_j\right]. \end{aligned} \tag{3.38}$$

After that, we replace (3.35) in (3.38), using the normalization $\mathrm{Tr}\left[T^a T^b\right] = \frac{1}{2}\delta^{ab}$, such that we consider only quadratic terms in the fields π^a_j and $A^a_{\mu,j}$. Thus we have

$$\begin{aligned}\sum_{j=1}^{N}\mathrm{Tr}\left[(D_\mu\Phi_j)^\dagger(D^\mu\Phi_j)\right] &= \sum_{j=1}^{N}\left[\frac{1}{2}(\partial_\mu\pi^a_j)^2 - v_j g\ \partial_\mu\pi^a_j(A^{\mu\ a}_j - A^{\mu\ a}_{j-1}) + \frac{1}{2}v_j^2 g^2 (A^a_{\mu,j-1})^2\right. \\ &\quad \left. - v_j^2 g^2 A^a_{\mu,j-1}A^{\mu\ a}_j + \frac{1}{2}v_j^2 g^2 (A^a_{\mu,j-1})^2\right] \\ &= \sum_{j=1}^{N}\frac{1}{2}[\partial_\mu\pi^a_j - v_j g(A^{\mu\ a}_j - A^{\mu\ a}_{j-1})]^2. \end{aligned} \tag{3.39}$$

As we can see, (3.39) includes the cross term mixing the NGBs with the gauge bosons in (3.32). To cancel these quadratic terms of the form $\partial_\mu\pi^a_j(A^{\mu\ a}_j - A^{\mu\ a}_{j-1})$, we chose to introduce the gauge-fixing term

$$\mathcal{L}_{GF} = -\frac{1}{2\xi}\sum_{j=0}^{N}[\partial_\mu A^{\mu\ a}_j + \xi g(v_j\pi^a_j - v_{j+1}\pi^a_{j+1})]^2, \tag{3.40}$$

where ξ is the gauge parameter, and we considered that ξ is the same site for all sites. Then (3.40) can be written as

$$\begin{aligned}\mathcal{L}_{GF} &= -\frac{1}{2\xi}\sum_{j=0}^{N}(\partial_\mu A^{\mu\ a}_j)^2 + \sum_{j=0}^{N} g A^{\mu\ a}_j(v_j\partial_\mu\pi^a_j - v_{j+1}\partial_\mu\pi^a_{j+1}) \\ &\quad - \frac{1}{2}\sum_{j=0}^{N}\xi[g(v_j\pi^a_j - v_{j+1}\pi^a_{j+1})]^2, \end{aligned} \tag{3.41}$$

where the second term was integrated by parts. This can be rewritten as follows

$$\begin{aligned}\mathcal{L}_{GF} &= -\frac{1}{2\xi}\sum_{j=0}^{N}(\partial_\mu A^{\mu\ a}_j)^2 + \sum_{j=1}^{N} g v_j\partial_\mu\pi^a_j(A^{\mu\ a}_j - A^{\mu\ a}_{j-1}) \\ &\quad - \frac{1}{2}\sum_{j=0}^{N}\xi[g(v_j\pi^a_j - v_{j+1}\pi^a_{j+1})]^2. \end{aligned} \tag{3.42}$$

Thus the action (3.32), using (3.39), with the inclusion of the gauge-fixing term in the form of (3.42) is given by

$$\begin{aligned} S = \int d^4x \Bigg\{ & -\sum_{j=0}^{N} \left[\frac{1}{4} (F_{\mu\nu}^{j\ a})^2 + \frac{1}{2\xi} (\partial_\mu A_j^{\mu\ a})^2 \right] + \frac{1}{2} \sum_{j=1}^{N} (\partial_\mu \pi_j^a)^2 \\ & - \frac{1}{2} \sum_{j=1}^{N-1} \xi [g(v_j \pi_j^a - v_{j+1} \pi_{j+1}^a)]^2 - \frac{1}{2} \xi g^2 v_1^2 (\pi_1^a)^2 - \frac{1}{2} \xi g^2 v_N^2 (\pi_N^a)^2 \\ & + \frac{1}{2} \sum_{j=1}^{N} v_j^2 g^2 (A_j^{\mu\ a} - A_{j-1}^{\mu\ a})^2 \Bigg\}. \end{aligned} \tag{3.43}$$

Notice that this action includes the mass terms of NGBs and gauge bosons. The mass term for the NGBs in the Lagrangian associated with the action (3.43) is given by

$$\mathcal{L}_{M_\pi} = -\frac{1}{2} \sum_{j=1}^{N-1} \xi [g(v_j \pi_j^a - v_{j+1} \pi_{j+1}^a)]^2 - \frac{1}{2} \xi g^2 v_1^2 (\pi_1^a)^2 - \frac{1}{2} \xi g^2 v_N^2 (\pi_N^a)^2 \equiv -\frac{1}{2} \pi^{aT} M_\pi^2 \pi^a, \tag{3.44}$$

where π^{aT} was written in the basis $\pi^{aT} = (\pi_1^a, \pi_2^a, \ldots, \pi_N^a)$. To write the mass matrix M_π^2 for the NGBs, we used the parametrization (3.36), obtaining

$$M_\pi^2 = g^2 v^2 \xi \begin{pmatrix} 2q^2 & -q^3 & 0 & \ldots & 0 & 0 \\ -q^3 & 2q^4 & -q^5 & \ldots & 0 & 0 \\ 0 & -q^5 & 2q^6 & \ldots & 0 & 0 \\ \vdots & \vdots & \vdots & \ddots & \vdots & \vdots \\ 0 & 0 & 0 & \ldots & 2q^{2(N-1)} & -q^{2N} \\ 0 & 0 & 0 & \ldots & -q^{2N} & 2q^{2N} \end{pmatrix}. \tag{3.45}$$

The determinant of M_π^2 is given by

$$\mathrm{Det}[M_\pi^2] = (g^2 v^2 \xi)^N (N+1) q^{N(N+1)}. \tag{3.46}$$

We can see that it is different from zero. In other words, the NGBs have no zero mode in their mass eigenstate basis, such that these NGB masses are proportional to $\sqrt{\xi}$, so by taking the limit $\xi \to \infty$, it corresponds to the unitary gauge. In this limit the NGBs disappear from the theory. We will use this gauge, and we say that the NGBs are eaten by the gauge bosons which become massive. We will see later that it is possible to extend one of the NGBs to be the Higgs by choosing differently the boundary conditions.

To determine the spectrum of the massive gauge bosons, we consider the mass term for the gauge bosons in the Lagrangian associated with the action (3.43) that is given by

$$\mathcal{L}_{M_A} = \frac{1}{2}\sum_{j=1}^{N} v_j^2 g^2 (A_j^{\mu\ a} - A_{j-1}^{\mu\ a})^2 \equiv -\frac{1}{2}(A_\mu^a)^T M_A^2 A^{\mu\ a}. \tag{3.47}$$

Analogously to the case of the NGBs, $(A_\mu^a)^T$ was written in the basis $(A_\mu^a)^T = (A_{\mu,0}, A_{\mu,1}, \ldots, A_{\mu,N})$, and using the parametrization (3.36), M_A^2 can be written as follows

$$M_A^2 = g^2 v^2 \begin{pmatrix} q^2 & -q^2 & 0 & 0 & \ldots & 0 & 0 \\ -q^2 & q^2+q^4 & -q^4 & 0 & \ldots & 0 & 0 \\ 0 & -q^4 & q^4+q^6 & -q^6 & \ldots & 0 & 0 \\ \vdots & \vdots & \vdots & \vdots & \ddots & \vdots & \vdots \\ 0 & 0 & 0 & 0 & \ldots & q^{2(N-1)}+q^{2N} & -q^{2N} \\ 0 & 0 & 0 & 0 & \ldots & -q^{2N} & q^{2N} \end{pmatrix}. \tag{3.48}$$

The spectrum of masses can be obtained by diagonalizing this matrix. For this purpose, we will define the orthonormal rotation

$$A_{\mu,j}^a = \sum_{n=0}^{N} f^{j,n} A_\mu^{a\ (n)}, \tag{3.49}$$

where the $A_\mu^{a\ (n)}$ are the mass eigenstates, such that in this basis $\mathcal{L}_{M_A}$ can be written as

$$\mathcal{L}_{M_A} = \frac{1}{2}\sum_{n=0}^{N} m_n^2 (A_\mu^{a\ (n)})^2. \tag{3.50}$$

Here we perform a numerical calculation of $f^{j,n}$ for hypothetical gauge bosons, following our previous formulation. Considering $v \lesssim M_P = 10^{19}$ GeV and $v_N \cong \mathcal{O}(1)$ TeV, We show their wave-functions in Figures (3.5) and (3.6) for $N = 4$ and $N = 15$, respectively. In both cases, the zero mode of gauge bosons will be flat as in AdS_5 theories with fields in the bulk [13, 27].

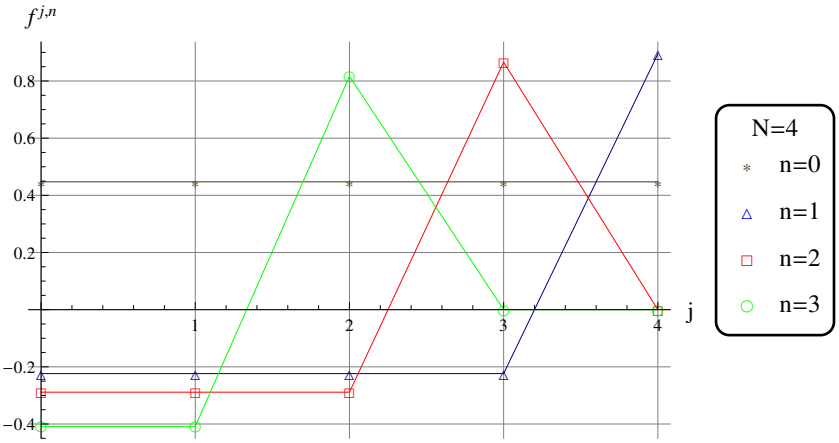

Figure 3.5. Gauge boson wave functions, where j is a index of site and n is a index of Kaluza-Klein mode. In this case $N = 4$ and some allowed n are shown. For the visualization, we choose by the opposite signs of $f^{j,0}$ and $f^{j,2}$.

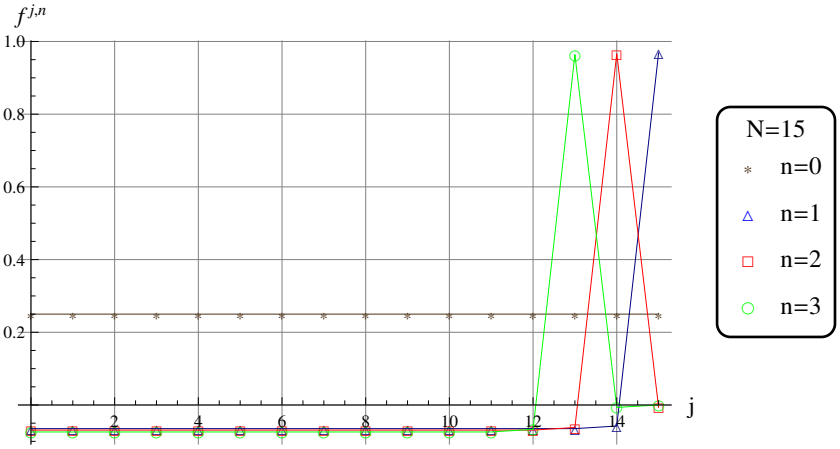

Figure 3.6. Gauge boson wave functions, where j is a index of site and n is a index of Kaluza-Klein mode. In this case $N = 15$ and some allowed n are shown. For the visualization, we choose by the opposite signs of $f^{j,2}$ and $f^{j,3}$.

In order to understand better the behavior of the gauge boson wave functions, we now look at the equations they satisfy.

The coefficients $f^{j,n}$ can be obtained from the equations of motion for the fields A_j^μ by using the Lagrangian given for

$$\mathcal{L}_A = \sum_{j=0}^{N} \left\{ -\frac{1}{4} F_{\mu\nu,j} \; F_j^{\mu\nu} + \frac{g^2}{2} [v_j (A_{\mu,j-1} - A_{\mu,j})]^2 \right\}, \tag{3.51}$$

where for simplicity, the abelian case was supposed. and then we can use the Euler-Lagrange equations

$$\frac{\partial \mathcal{L}}{\partial A_{\nu,j}} - \partial_\mu \left(\frac{\partial \mathcal{L}}{\partial(\partial_\mu A_{\nu,j})} \right) = 0, \tag{3.52}$$

we obtain the following equation

$$(\partial^2 A_j^\nu - \partial^\nu \partial_\mu A_j^\mu) \;+\; g^2 v_j^2 \,(A_j^\nu - A_{j-1}^\nu) \;+\; g^2 v_{j+1}^2 \,(A_j^\nu - A_{j+1}^\nu) = 0. \tag{3.53}$$

Now, we will use Lorentz gauge $\partial_\mu A_j^\mu = 0$ and substituting (3.49) in (3.53) we obtain

$$f^{j,n}\partial^2 A^{\nu,(n)} \;+\; g^2 v^2 q^{2j}[(1+q^2)f^{j,n} \;-\; f^{j-1,n} \;-\; q^2 f^{j+1,n}]A^{\nu,(n)} \;=\; 0. \tag{3.54}$$

Imposing that $A^{\nu,(n)}$ satisfies the Proca equation, that is

$$\partial^2 A_{\nu,n} = -m_n^2 A_{\nu,n}, \tag{3.55}$$

thus, we substitute (3.55) and using the definition $x_n^2 \equiv m_n^2/g^2v^2$ in (3.54), it happens that we obtain

$$[q + q^{-1} - q^{-1}(x_n q^{-j})^2]f^{j,n} - qf^{j+1,n} - q^{-1}f^{j-1,n} = 0, \tag{3.56}$$

jointly with the discrete Neumann boundary conditions

$$f^{0,n} = f^{-1,n}, \quad f^{N,n} = f^{N+1,n}, \tag{3.57}$$

with the normalization condition

$$\sum_{j=0}^{N} (f^{j,n})^2 = 1. \tag{3.58}$$

We will now concentrate in the zero mode, $n = 0$ and $m_0 = 0$.

The equation (3.56) for the zero mode is

$$[q + q^{-1}]f^{j,0} - qf^{j+1,0} - q^{-1}f^{j-1,0} = 0, \tag{3.59}$$

such that for $j = 0$ in (3.56), we have

$$[q + q^{-1}]f^{0,0} - qf^{1,0} - q^{-1}f^{-1,0} = 0,$$

and using (3.57) we obtain

$$f^{0,0} = f^{1,0}, \tag{3.60}$$

iterating to the others $j's$ we have

$$f^{0,0} = f^{1,0} = f^{2,0} = ... = f^{N,0}, \tag{3.61}$$

and by using the normalization condition (3.58), we obtain

$$f_{j,0} = \frac{1}{\sqrt{N+1}}. \tag{3.62}$$

This means that the components of zero mode are equal in all sites. It is analogous to what happens in AdS_5 theory, where the zero modes of the gauge bosons are delocalized, as can be seen in Figures (3.5) and (3.6) for $n = 0$. For massive modes the equation (3.56) has solution as shown in Ref. [28]. For this purpose we define the following variables

$$t[j] = x_n q^{-j}, \tag{3.63}$$

$$F(t[j]) = q^j f^{j,n}, \tag{3.64}$$

and we substitute (3.63) and (3.64) in the equation of q-differences (3.56) we obtain

$$(q + q^{-1} - q^{-1}t^2)F(t) - F(tq^{-1}) - F(tq) = 0. \tag{3.65}$$

The equation (3.65) is a special case of Hahn-Exton equation [28, 29] with solutions that are called q-Bessel functions. More general solutions can be written as

$$F(t) = AJ_1(t; q^2) + BY_1(t; q^2), \tag{3.66}$$

where in general $J_\nu(t; q^2)$ and $Y_1(t; q^2)$ are the q-Bessel and q-Neumann functions respectively. It is interesting to examine the continuum limit $q \to 1^-$ and $N \to \infty$, as we will in the next section, we obtain the continuous ordinary functions of Bessel and Neumann [28],

$$J_\nu(t; q) = t^\nu \frac{(q^{\nu+1}; q)_\infty}{(q; q)_\infty} \sum_{i=0}^{\infty} \frac{(-1)^i q^{i(i+1)/2}}{(q^{\nu+1}; q)_i (q; q)_i} t^{2i}, \tag{3.67}$$

with the factors $(y; q)_i$ are defined as

$$(y; q)_k = \begin{cases} 1 & \text{se } k = 0 \\ \prod_{n=0}^{k-1}(1 - yq^n) & \text{se } k \geq 1 \end{cases} \tag{3.68}$$

for $y \in \mathbb{C}$, $i \in \mathbb{Z}_+ = \{0, 1, 2, \ldots\}$ and $(y; q)_\infty \equiv \lim_{i\to\infty}(y; q)_i$. Meanwhile

$$Y_\nu(t; q) = \frac{\Gamma_q(\nu)\Gamma_q(1-\nu)}{\pi} q^{-\nu^2/2}[\cos(\pi\nu)q^{\nu/2}J_\nu(t; q) - J_{-\nu}(tq^{-\nu/2}; q)], \tag{3.69}$$

where the function $\Gamma_q(\nu)$ is defined for

$$\Gamma_q(\nu) = \frac{(q;q)_\infty}{(q^\nu;q)_\infty}(1-q)^{1-\nu}. \tag{3.70}$$

Using (3.64), (3.65) and the boundary conditions (3.57), it is possible to find the coefficients $f^{j,n}$ to within a constant N_n that can be obtained from the normalization condition (3.58) as follow

$$f^{j,n} = N_n q^{-j}[Y_0(x_n;q^2)J_1(x_n q^{-j};q^2) - J_0(x_n;q^2)Y_1(x_n q^{-j};q^2)]. \tag{3.71}$$

Additionally, the spectrum of masses is obtained from the equation

$$J_0(x_n;q^2)Y_0(q^{-(N+1)}x_n;q^2) \;-\; Y_0(x_n;q^2)J_0(q^{-(N+1)};q^2) = 0. \tag{3.72}$$

In the continuum limit, when $q \to 1^-$, these coefficients (3.71) coincide to the wave functions of the excited gauge bosons in AdS_5 theory. Thus with the deconstruction of a 5-dimensional gauge theory it is possible to produce a correspondent quiver theory in four dimensions.

3.1.1 Relation to AdS_5

We know that the AdS_5 theories solve the gauge hierarchy problem, as well as the hierarchy of fermion masses. However, these theories are non renormalizable, so it is interesting to obtain a higher universe of theories that solve large hierarchies. We will start considering a continuous 5-dimensional gauge action in the Abelian case. The extension to the non-Abelian case is straightforward. Working with AdS_5 theories, where the extra dimension is compactified on the orbifold S_1/Z_2 with $-L \leq y \leq L$ and the metrics is given by

$$ds^2 = e^{-2k|y|}\eta_{\mu\nu}dx^\mu dx^\nu - dy^2, \tag{3.73}$$

where k is the AdS_5 curvature. The action for gauge bosons is given by

$$S_A = \int d^5x\sqrt{g}\left[-\frac{1}{4g_5^2}F_{MN}F^{MN}\right], \tag{3.74}$$

where g_5 is the gauge coupling in 5 dimensions, and $F_{MN} = \partial_M A_N - \partial_N A_M$ with $M = 0, 1, 2, 3$ and 5 (y).

The action (3.74) can be simplified to

$$
\begin{aligned}
S_5^A &= \int d^5x\sqrt{g}\,\left[-\frac{1}{4g_5^2}g^{MO}g^{NP}F_{MN}F_{OP}\right], \\
&= \int d^4x\int_0^L dy\sqrt{g}\,\left[-\frac{1}{4g_5^2}e^{4ky}F_{\mu\nu}F^{\mu\nu}+\frac{1}{2g_5^2}e^{2ky}\left(F_{5\mu}\right)^2\right], \\
&= \int d^4x\int_0^L dy\,\left[-\frac{1}{4g_5^2}F_{\mu\nu}F^{\mu\nu}+\frac{1}{2g_5^2}e^{-2ky}\left(\partial_5 A_\mu-\partial_\mu A_5\right)^2\right]. \qquad (3.75)
\end{aligned}
$$

We will discretize the compact dimension, with spacing ℓ. So the action (3.75) will now be

$$
\begin{aligned}
S_5^A = \ell\int d^4x\,\Bigg[&\sum_{j=0}^{N}-\frac{1}{4g_5^2}(F^j_{\mu\nu}F^{j\mu\nu}) \\
&+\sum_{j=1}^{N}\frac{1}{2g_5^2}e^{-2k\ell j}\left(\frac{A^j_\mu-A^{j-1}_\mu}{\ell}-\partial_\mu A^j_5\right)^2\Bigg], \qquad (3.76)
\end{aligned}
$$

where the derivatives with respect to y taken to be discretized. This action can be compared to the action from the quiver theory, To make this clear we will rescale the gauge fields as

$$
\begin{aligned}
S_4^A = \int d^4x\,\Bigg[&-\sum_{j=0}^{N}\frac{1}{4g^2}(F_{\mu\nu,j}\;F_j^{\mu\nu}) \\
&+\frac{1}{2}\sum_{j=1}^{N}[\partial_\mu\pi_j+v_j(A_{\mu,j-1}-A_{\mu,j})]^2\Bigg]. \qquad (3.77)
\end{aligned}
$$

We can see the equivalence of both theories setting the dictionary between discretized five-dimensional gauge theory with the purely four-dimensional gauge theory (3.77) as shown in Ref. [7]. The dictionary identifying both theories is shown in Table (3.1). In this way, we identify the sites zero and N as branes UV and IR respectively.

We know that AdS_5 theories solve the hierarchy problem of particle physics for $kL \approx 37$ [13, 30, 31, 32]. The continuous theory (AdS_5) is obtained from a quiver theory when $N \to \infty$, such that $N\ell = L$, where L is the size of the extra dimension and ℓ is the network spacing. So we have

$$
kN\ell \sim 37. \qquad (3.78)
$$

Now, we will see that happens by using (3.36), the matching in Table (3.1), jointly

Theory with 4 dimensions		Theory with 5 dimensions
$\frac{1}{g^2}$	$\leftrightarrow$	$\frac{\ell}{g_5^2}$
v	$\leftrightarrow$	$\frac{1}{\sqrt{\ell} g_5}$
q	$\leftrightarrow$	$e^{-k\ell}$

Table 3.1. Dictionary between a quiver theory and a gauge theory with 5 dimensional discretized with a curve extra dimension.

with $v \lesssim M_P = 10^{19}$ GeV and $v_N \cong \mathcal{O}(1)$ TeV,

$$e^{-kN\ell} = \frac{v_N}{v} \simeq 10^{-16}, \tag{3.79}$$

and then

$$q \simeq 10^{-16/N}. \tag{3.80}$$

In the continuum limit we have that (3.79) corresponds to the expression in AdS_5 theories with metric given by (3.73). So we see that the deconstruction of AdS_5 can be seen as a way to obtain four-dimensional theories that solve the hierarchy problem. This will be the case as long as (3.80) is satisfied. However, for large values of N the four-dimensional theory is very similar to AdS_5. In order to obtain a very different theory from deconstruction, N must be small.

From (3.80) we can infer the following relation

$$k\ell \sim \frac{37}{N}, \tag{3.81}$$

identifying two cases, the first one is if $N > 37$, this meas that $k\ell < 1$ or $k < \Lambda_{UV}$, we still have an AdS_5 theory. But if $N < 37$, then $k\ell > 1$ or $k > \Lambda_{UV}$, then $N < 37$, we will have a pure four-dimensional theory different from AdS_5, since no continuum limit possible since curvature is larger than M_{Planck}.

3.1.2 Higgs in Quiver Theories

In the SM, the Higgs boson is required in order to trigger EWSB. However we do not know how the Higgs sector was obtained in low energies. One possibility to consider is the Higgs as a pNGB as shown in Refs. [23, 33, 34, 35]. The discovery of the Higgs boson of the SM [1, 2], suggests that we need to focus not only on gauge bosons and fermions, as we will see in the next subsection, but on the Higgs sector of quiver theories as recently considered in Refs. [8, 9, 10, 12, 36]. In this section we include the Higgs as a pNGB. This is achieved by switching on the gauge fields associated to G_j, with $j = 1, ..., N-1$, and reducing the gauge groups G_0 to H_0 and G_N to H_N so that some of the NGBs are not eaten by gauge bosons. Here H_0 and H_N are subgroups of G_0 and G_N respectively. Consequently, to consider the Higgs as a pNGB, the gauge structure given in Figure (3.4) needs to be modified.

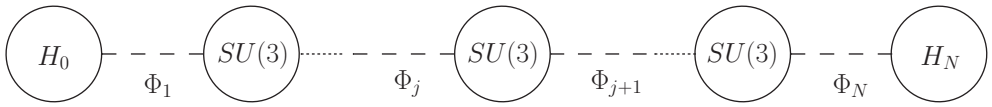

Figure 3.7: Quiver diagram associated with a quiver theory considering the Higgs as a pNGB, where $G_j = SU(3)$, $0 < j < N$ and $H_0 = H_N = SU(2) \times U(1)$ will be gauged.

Here, we would have four degrees of freedom that will be identified with the degrees of freedom of the Higgs doublet, after the breaking of the quiver symmetry. In particular, we will switch on the gauge fields associated to $SU(3)_j$ for $1 < j < N-1$ and $H_0 = H_N = SU(2) \times U(1)$, the gauge structure in this case is given by the quiver diagram in Figure (3.7). In this way, in the 0 and N sites, the symmetry $SU(2) \times U(1)$ not include the generators associated to $SU(3)/SU(2) \times U(1)$, where the matrices in the fundamental representation of $SU(3)$ are given by the eight Gell-Mann matrices

$$T^a = \frac{\lambda^a}{2}. \tag{3.82}$$

These matrices are given by

$$\lambda^1 = \begin{pmatrix} 0 & 1 & 0 \\ 1 & 0 & 0 \\ 0 & 0 & 0 \end{pmatrix}, \ \lambda^2 = \begin{pmatrix} 0 & -i & 0 \\ i & 0 & 0 \\ 0 & 0 & 0 \end{pmatrix}, \ \lambda^3 = \begin{pmatrix} 0 & -1 & 0 \\ 0 & 1 & 0 \\ 0 & 0 & 0 \end{pmatrix},$$
$$\lambda^4 = \begin{pmatrix} 0 & 0 & 1 \\ 0 & 0 & 0 \\ 1 & 0 & 0 \end{pmatrix}, \ \lambda^5 = \begin{pmatrix} 0 & 0 & -i \\ 0 & 0 & 0 \\ i & 0 & 0 \end{pmatrix}, \ \lambda^6 = \begin{pmatrix} 0 & 0 & 0 \\ 0 & 0 & 1 \\ 0 & 1 & 0 \end{pmatrix},$$
$$\lambda^7 = \begin{pmatrix} 0 & 0 & 0 \\ 0 & 0 & -i \\ 0 & i & 0 \end{pmatrix}, \ \lambda^8 = \frac{1}{\sqrt{3}} \begin{pmatrix} 1 & 0 & 0 \\ 0 & 1 & 0 \\ 0 & 0 & -2 \end{pmatrix}. \tag{3.83}$$

We define the matrices

$$Y^a \equiv \{T^1, T^2, T^3, T^8\} \tag{3.84}$$

and

$$X^\alpha \equiv \{T^4, T^5, T^6, T^7\}, \tag{3.85}$$

are the generators associated to $SU(2) \times U(1)$ and $SU(3)/SU(2) \times U(1)$ respectively. We use the convention that Latin and Greek indices take values of 1, 2, 3, 8 and 4, 5, 6, 7, respectively. Notice that the generators X^α will be associated with the degrees of freedom of the Higgs doublet. Now, we will expand the kinetic term of the Φ_j's, such that we will consider only quadratic terms in the NGBs and gauge fields associated to the generators X^α

$$\frac{1}{2}[\partial_\mu \pi_1^\alpha - v_1 g A_{\mu 1}^\alpha]^2 + \sum_{j=2}^{N-1} \frac{1}{2}[\partial_\mu \pi_j^\alpha - v_j g (A_{\mu j}^\alpha - A_{\mu, j-1}^\alpha)]^2$$
$$+ \frac{1}{2}[\partial_\mu \pi_N^\alpha + v_N g A_{\mu N}^\alpha]^2. \tag{3.86}$$

The cross terms mixing the NGB's with the gauge bosons associated to X^α can be canceled by introducing the gauge-fixing term

$$\mathcal{L}_G = -\sum_{j=1}^{N-1} \frac{1}{2\xi}[\partial_\mu A_j^{\mu\alpha} - \xi g (v_j \pi_j^\alpha - v_{j+1} \pi_{j+1}^\alpha)]^2. \tag{3.87}$$

After adding this gauge-fixing term to expansion in (3.86), we obtain

$$\frac{1}{2}\sum_{j=1}^{N}(\partial_\mu \pi_j^a)^2 - \sum_{j=1}^{N-1}\frac{1}{2\xi}(\partial_\mu A_j^{\mu\ \alpha})^2 - \frac{1}{2}\sum_{j=1}^{N-1}\xi[g(v_j\pi_j^a - v_{j+1}\pi_{j+1}^a)]^2$$
$$+\frac{1}{2}\sum_{j=2}^{N-1}v_j^2 g^2(A_j^{\mu\ \alpha} - A_{j-1}^{\mu\ \alpha})^2 - \frac{1}{2}g^2v_1^2(A_1^{\mu\ \alpha})^2 - \frac{1}{2}g^2v_N^2(A_{N-1}^{\mu\ \alpha})^2. \tag{3.88}$$

Here, we identify the mass matrix $M_{A^\alpha}^2$ for the gauge bosons associated to X^α, this is given by

$$M_{A^\alpha}^2 = g^2v^2\begin{pmatrix} q^2+q^4 & -q^4 & 0 & 0 & \cdots & 0 & 0 \\ -q^4 & q^4+q^6 & -q^6 & 0 & \cdots & 0 & 0 \\ \vdots & \vdots & \vdots & \vdots & \ddots & \vdots & \vdots \\ 0 & 0 & 0 & 0 & \cdots & -q^{2N} & q^{2(N-1)}+q^{2N} \end{pmatrix}, \tag{3.89}$$

where we used the parametrization (3.36). We also identify the mass matrix M_π^2 for the NGBs associated to X^α as follow

$$M_{\pi^\alpha}^2 = g^2v^2\xi\begin{pmatrix} q^2 & -q^3 & 0 & 0 & \cdots & 0 & 0 \\ -q^3 & 2q^4 & -q^5 & 0 & \cdots & 0 & 0 \\ 0 & -q^5 & 2q^6 & -q^7 & \cdots & 0 & 0 \\ \vdots & \vdots & \vdots & \vdots & \ddots & \vdots & \vdots \\ 0 & 0 & 0 & 0 & \cdots & 2q^{2(N-1)} & -q^{2N-1} \\ 0 & 0 & 0 & 0 & \cdots & -q^{2N-1} & q^{2N} \end{pmatrix}. \tag{3.90}$$

But now, unlike in the case of (3.45), the determinant vanishes:

$$\mathrm{Det}[M_{\pi^\alpha}^2] = 0. \tag{3.91}$$

This indicates that the NGBs associated to X^α have a zero mode in their mass eigenstate basis. This mode is a physical state due the fact that, in the unitary gauge, that is, $\xi \to \infty$, this state will not disappear from the theory.
Now, we will define the orthonormal rotation that diagonalizes $M_{\pi^\alpha}^2$

$$\pi_j^\alpha = \sum_{n=1}^{N} b^{j,n}\pi^{\alpha\ (n)}, \tag{3.92}$$

where the index n indicates the eigenmode. Since we are interested in the zero mode, we focus on $b^{j,0}$, henceforth we will denote it as b^j. It is possible to show

(using the eigenvalue equation associated to $M^2_{\pi^\alpha}$ for the zero eigenvalue) that,

$$b^j = \frac{q^{N-j}}{\sqrt{\sum_{j=1}^{N} q^{2(j-1)}}}, \tag{3.93}$$

where we used the normalization condition

$$\sum_{j=1}^{N} |b^j|^2 = 1. \tag{3.94}$$

Then, by using (3.92) and (3.93), we obtain

$$\pi^{\alpha\ (0)} = \sum_{j=1}^{N} \frac{q^{N-j}}{\sqrt{\sum_{j=1}^{N} q^{2(j-1)}}} \pi_j^\alpha. \tag{3.95}$$

The expression (3.93) indicates that the Higgs is always localized close the N-th site. This fact will be used in Subsection 3.1.5.

Also, we notice that the combination $\pi_j^\alpha X^\alpha$ gives

$$\pi_j^\alpha X^\alpha = \frac{1}{2} \begin{pmatrix} 0 & 0 & \pi_j^4 - i\pi_j^5 \\ 0 & 0 & \pi_j^6 - i\pi_j^7 \\ \pi_j^4 + i\pi_j^5 & \pi_j^6 + i\pi_j^7 & 0 \end{pmatrix}, \tag{3.96}$$

where the Higgs doublet H, as shown in Ref. [10], is identified as $(h_1\ h_2)^T$, where h_1 and h_2 are given by $\frac{1}{\sqrt{2}}(\pi_j^4 - i\pi_j^5)$ and $\frac{1}{\sqrt{2}}(\pi_j^6 - i\pi_j^7)$ respectively.

In this way, we have obtained a Higgs out of the breaking of the (partially gauged) global symmetry $H_0 \times G_1 \times \ldots \times G_{N-1} \times H_N$. Is this global symmetry that protects the Higgs mass.

3.1.3 Fermions in Quiver Theories

We will study the spectrum of Vector-like quarks in quiver theories and their couplings to gauge bosons and the Higgs as can be found in Ref. [10]. Then the phenomenology will be done in the following chapter.

The fermions are included in the quiver theories by the following action:

$$S_\psi = \int d^4x \Bigg\{ \sum_{j=0}^{N} \left[\bar{\psi}_{L,j} i \not{D}_j \psi_{L,j} + \bar{\psi}_{R,j} i \not{D}_j \psi_{R,j} - (\mu_j \bar{\psi}_{L,j} \psi_{R,j} + \text{h.c.}) \right] - \sum_{j=1}^{N} \lambda \, (\bar{\psi}_{R,j-1} \Phi_j \psi_{L,j} + \text{h.c.}) \Bigg\}, \tag{3.97}$$

where the fermions ψ_j are vector-like, transform in the fundamental representation of $SU(n)_j$, λ are Yukawa couplings, and μ_j is the mass term in the interaction eigenstates.

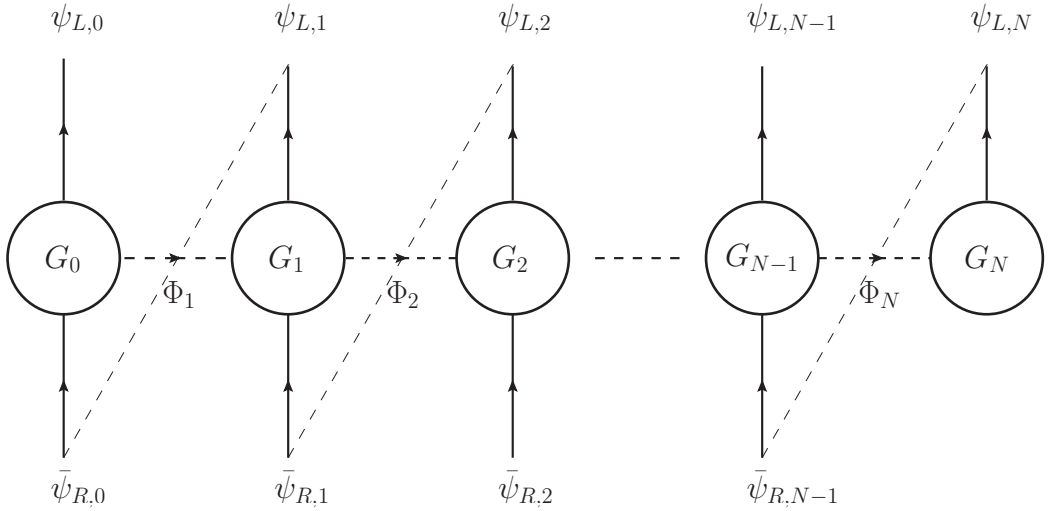

Figure 3.8: Quiver diagram including the fermions in the action in (3.97), with the condition that the spectrum includes a fermion with left-handed zero mode.

Using the link fields in terms of their VEVs (3.36), as shown in Refs. [7, 8, 12, 10]. In addition, we need to consider the next relations that were shown in Ref.[7]

$$\mu_j = -gvq^{c+j+1/2}, \qquad \lambda = g, \tag{3.98}$$

where c is the localization parameter for fermions associated to AdS_5 theories for fermions in the Bulk. Now, we can identify the mass term for the fermions in the Lagrangian associated with the action (3.97) as

$$\mathcal{L}_{M_\psi} = -\sum_{j=0}^{N} (\mu_j \bar{\psi}_{L,j} \psi_{R,j} + \text{h.c.}) - \sum_{j=1}^{N} \lambda v_j \, (\bar{\psi}_{R,j-1} \psi_{L,j} + \text{h.c.}) \equiv -\overline{\Psi}_L M_\psi^T \Psi_R + \text{h.c.}, \tag{3.99}$$

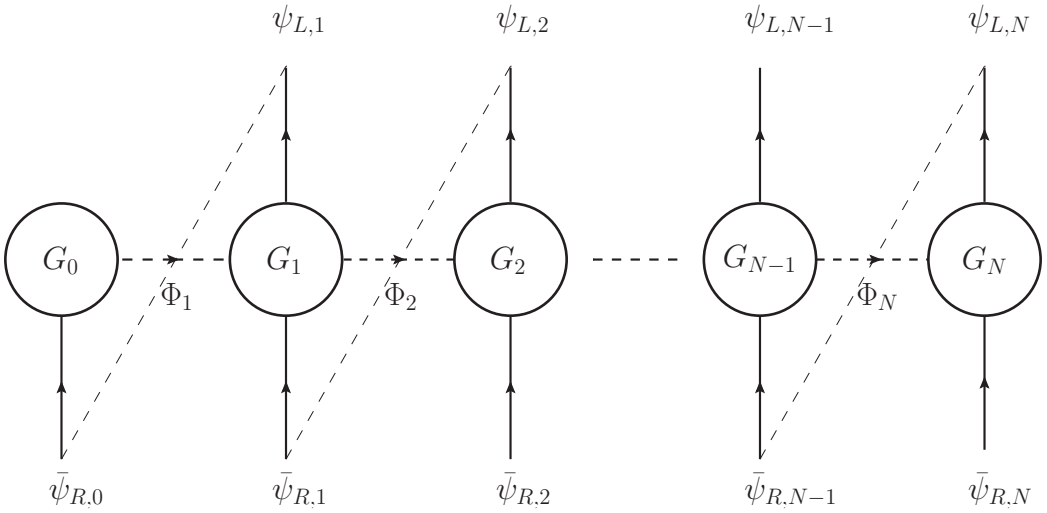

Figure 3.9: Quiver diagram including the fermions in the action in (3.97), with the condition that the spectrum includes a fermion with right-handed zero mode.

where $\Psi_{L/R}^T$ was written in the basis $\Psi_{L/R}^T = (\psi_{L/R,0}, \psi_{L/R,1}, \ldots, \psi_{L/R,N})$, we can change from this basis to the mass eigenstate basis as follow

$$\psi_{L/R,j} = \sum_{n=0}^{N} h_{L/R}^{j,n} \chi_{L/R}^{(n)}, \tag{3.100}$$

where $\chi_{L/R}^{(n)}$ are the mass eigenstate. Thus, to find $\psi_{L,j}$ as a linear combination of $\chi_L^{(n)}$, we can obtain it by diagonalizing the matrix

$$M_\psi^T M_\psi = \begin{pmatrix} \mu_0^2 & \lambda\mu_0 v_1 & 0 & \cdots & 0 & 0 \\ \lambda\mu_0 v_1 & \lambda^2 v_1^2 + \mu_1^2 & \lambda\mu_1 v_2 & \cdots & 0 & 0 \\ 0 & \lambda\mu_1 v_2 & \lambda^2 v_2^2 + \mu_2^2 & \cdots & 0 & 0 \\ \vdots & \vdots & \vdots & \ddots & \vdots & \vdots \\ 0 & 0 & 0 & \cdots & \lambda^2 v_{N-1}^2 + \mu_{N-1}^2 & \lambda\,\mu_{N-1}\,v_N \\ 0 & 0 & 0 & \cdots & \lambda\mu_{N-1}\,v_N & \lambda^2 v_N^2 + \mu_N^2 \end{pmatrix}.$$

Analogously we diagonalize the matrix $M_\psi M_\psi^T$ to obtain $\psi_{R,j}$ as a linear combination of $\chi_R^{(n)}$. Now, we need to indicate if the action (3.97) belongs to a fermion with left- or right- handed zero mode. Thus, the case where we will have a fermion with left-handed zero mode is achieved by taking $\mu_N = 0$, it corresponds to the

quiver diagram of Figure (3.8), in this case the linear combination

$$\psi_{L,j} = \sum_{n=0}^{N} h_L^{j,n}(c_L)\chi_L^{(n)} \tag{3.101}$$

is found by diagonalizing the matrix

$$M_\psi^T M_\psi = g^2 v^2 \begin{pmatrix} q^{2c_L+1} & -q^{c_L+\frac{3}{2}} & \dots & 0 & 0 \\ -q^{c_L+\frac{3}{2}} & q^{2c_L+3}+q^2 & \dots & 0 & 0 \\ 0 & -q^{c_L+\frac{7}{2}} & \dots & 0 & 0 \\ \vdots & \vdots & \ddots & \vdots & \vdots \\ 0 & 0 & \dots & q^{2c_L+2N-1}+q^{2(N-1)} & -q^{c_L+\frac{1}{2}(4N-1)} \\ 0 & 0 & \dots & -q^{c_L+\frac{1}{2}(4N-1)} & q^{2N} \end{pmatrix}. \tag{3.102}$$

To write this matrix explicitly, the parametrizations (3.36) and (3.98) were used.

On the other hand, if we take $\mu_0 = 0$, we will have a fermion with right-handed zero mode, for this case the quiver diagram corresponds to Figure (3.9), such that the linear combination

$$\psi_{R,j} = \sum_{n=0}^{N} h_R^{j,n}(c_R)\chi_R^{(n)} \tag{3.103}$$

can be found by diagonalizing the matrix

$$M_\psi M_\psi^T = g^2 v^2 \begin{pmatrix} q^{2} & -q^{c_R+\frac{5}{2}} & \dots & 0 & 0 \\ -q^{c_R+\frac{5}{2}} & q^{4}+q^{2c_R+3} & \dots & 0 & 0 \\ 0 & -q^{c_R+\frac{9}{2}} & \dots & 0 & 0 \\ \vdots & \vdots & \ddots & \vdots & \vdots \\ 0 & 0 & \dots & q^{2c_R+2N-5}+q^{2(N-2)} & -q^{c_R+\frac{1}{2}(4N-7)} \\ 0 & 0 & \dots & -q^{c_R+\frac{1}{2}(4N-7)} & q^{2c_R+2N-3} \end{pmatrix}, \tag{3.104}$$

where we used the parametrizations (3.36) and (3.98). Notice that the values of $c_{L,R}$ for fermions zero mode of the SM were found in Ref. [8]

3.1.3.1 Equation of Motion for $\psi_{L,j}$ and $\psi_{R,j}$

We saw that $\chi_L^{(n)}$ and $\chi_R^{(n)}$ are the mass eigenstates. We will impose that they satisfy the Dirac equation

$$i\partial\!\!\!/\chi_L^{(n)} - m_n\chi_R^{(n)} = 0, \tag{3.105}$$
$$i\partial\!\!\!/\chi_R^{(n)} - m_n\chi_L^{(n)} = 0. \tag{3.106}$$

On the other hand the equations of motion can be obtained from (3.97). Expressing the link fields in terms of their VEVs, we obtain

$$\text{for } \bar{\psi}_{R,j}: \quad i\,\partial\!\!\!/\,\psi_{R,j} + \lambda v_{j+1}\,\psi_{L,j+1} + \mu_j\,\psi_{L,j} = 0, \tag{3.107}$$
$$\text{for } \bar{\psi}_{L,j}: \quad i\,\partial\!\!\!/\,\psi_{L,j} + \lambda v_j\,\psi_{R,j-1} + \mu_j\,\psi_{R,j} = 0. \tag{3.108}$$

Using (3.100), (3.107) and (3.108) we obtain

$$m_n\,h_R^{j,n} + \mu_j\,h_L^{j,n} + \lambda v_{j+1}\,h_L^{j+1,n} = 0, \tag{3.109}$$
$$m_n\,h_L^{j,n} + \mu_j\,h_R^{j,n} + \lambda v_j\,h_R^{j-1,n} = 0, \tag{3.110}$$

where the equations (3.109) and (3.110) are coupled. After decoupling these we obtain

$$\left(\mu_j^2 + \lambda^2 v_j^2 - m_n^2\right) h_L^{j,n} + \lambda\mu_j v_{j+1} h_L^{j+1,n} + \lambda\mu_{j-1} v_j h_L^{j-1,n} = 0, \tag{3.111}$$

$$\left(\mu_j^2 + \lambda^2 v_{j+1}^2 - m_n^2\right) h_R^{j,n} + \lambda\mu_{j+1} v_{j+1} h_R^{j+1,n} + \lambda\mu_j v_j h_R^{j-1,n} = 0. \tag{3.112}$$

In the next subsection we will obtain the analytical zero mode wave functions by imposing conditions to have a left-handed zero mode or a right-handed zero mode.

Zero Mode Wave-Function

To obtain the SM fermion spectrum as the zero modes, we can impose as boundary condition $h_R^{N,n} = 0$, that is $\psi_{R,N} = 0$ to obtain a left-handed zero mode, or we can impose $h_L^{0,n} = 0$, that corresponds to $\psi_{L,0} = 0$ to obtain a right-handed zero mode.

In the case of a left-handed zero mode, we use (3.109) to obtain

$$\mu_j\,h_L^{j,0} + \lambda v_{j+1} h_L^{j+1,0} = 0,$$

which is equivalent to

$$\frac{h_L^{j+1,0}}{h_L^{j,0}} = q^{c_L - 1/2}. \tag{3.113}$$

Since $0 < q < 1$, for $c_L > 1/2$ the left-handed zero mode wave function will be "localized" close to the zero site corresponding to the left side of quiver diagram in Figure (3.8), and for $c_L < 1/2$ it will be localized close to the N site, that corresponds to the right side of the quiver diagram in Figure (3.9). The 0 site corresponds to the UV scale because v_1 is largest and the N site corresponds to the IR scale because v_N is the smallest VEV. Nothing to do with fermion localization.

Alternatively, if we consider a right-handed zero mode, we use (3.110) to obtain

$$\mu_j \; h_R^{j,0} + \lambda v_j h_R^{j-1,0} = 0,$$

and then

$$\frac{h_R^{j,0}}{h_R^{j-1,0}} = q^{-(c_R + 1/2)}. \tag{3.114}$$

So for $c_R > -1/2$ the right-handed zero mode wave function is localized in the N site (IR), on the other hand for $c_R < -1/2$ it will be localized closer to the zero site (UV).

To obtain an analytical expression for the zero mode wave functions for the fermions, we write

$$h_{L,R}^{j,0} = z_{L,R}^{j} h_{L,R}^{0,0}, \tag{3.115}$$

where we have considered the definitions $z_L \equiv q^{c_L - 1/2}$ and $z_R \equiv q^{-(c_R + 1/2)}$, such that the normalization conditions for the zero mode wave functions can be written as follows

$$\sum_{j=0}^{N} |h_{L,R}^{j,0}|^2 = |h_{L,R}^{0,0}|^2 \sum_{j=0}^{N} z_{L,R}^{2j} = 1, \tag{3.116}$$

and then we obtain

$$h_{L,R}^{0,0} = \sqrt{\frac{1 - z_{L,R}^2}{1 - z_{L,R}^{2(N+1)}}}. \tag{3.117}$$

So if the zero mode wave function of a fermion is closer to the N site associated to the scale (IR), this has more coupling with the Higgs. In analogous way, if the zero mode wave function of a fermion is localized closer to the zero site, such that it is associated to the scale UV, it has less coupling with the Higgs [8], given that the Higgs is localized close to the N-th site.

The quiver theories will have characteristics similar to AdS_5 theories, but from this point of view we can say that they have different phenomenology, in important aspects of the theory. We mention that the AdS_5 theories are a particular case of quiver theories in the continuum limit.

Spectrum of Excited States

To understand the phenomenology, such as the production or decay of the excited fermions in quiver theories, we need to compute the spectrum of these excited states. Based on Subsection 3.1.3, we computed the masses of the excited fermions ($n > 0$) by diagonalizing the fermion mass matrices (3.102) or (3.104) to have left- and right-handed zero modes, respectively. Once we have fixed N jointly with $v = M_P = 10^{19}$ GeV and v_N =1 TeV, then these matrices will depend on the localization parameters.

Thus the masses for the first excited states of fermions with left-handed zero modes are shown in Figure (3.10), for $c_L > 0.5$, i.e., in which their left-handed zero modes wave functions are localized in the UV sites; the masses will be of order v_N, differently, for $c_L < 0.5$, the masses will be exponentially heavier.
The case when there are right-handed zero modes, the masses for the first excited states of fermions are shown in Figure (3.11). We see that for $c_R > -0.5$, i.e., the case in which their right-handed zero modes wave functions are localized in the IR sites; similarly to the previous case, the masses will be of order v_N and be exponentially heavier for $c_R < -0.5$.

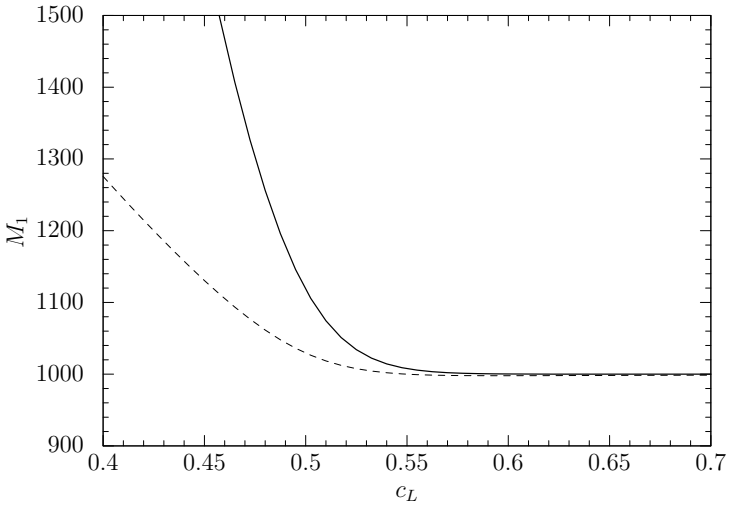

Figure 3.10. Masses of the first excited states of the fermions that belong to their tower with left-handed zero mode, the solid and dashed lines correspond to N=4, 15, respectively.

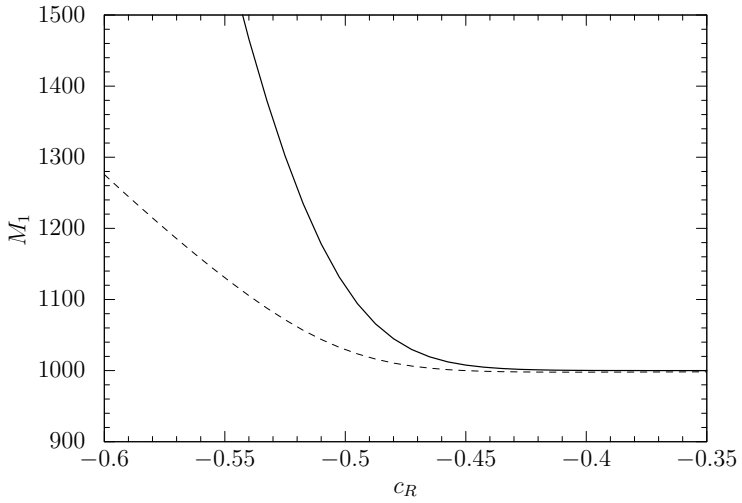

Figure 3.11. Masses of the first excited states of the fermions that belong to their tower with right-handed zero mode, the solid and dashed lines correspond to N=4, 15, respectively.

Having computed the wave functions and mass spectrum for the fermion excitations, their couplings will be computed below.

3.1.4 Couplings of Fermionic Excited States

Based in the approach of [10, 11, 12] we can now compute the couplings of the excited fermions to the gauge bosons and the Higgs sector in the frame of quiver theories. The rest of this subsection is organized as follows: First, we show how to compute the couplings of the excited fermions to gauge boson excitations, for both cases left- and right-handed fermion zero modes. We will concentrate in computing the couplings of the zero-mode fermions, for the cases of the first and third generations of quarks, to the first excited state of a gluon. In addition, the couplings of the excited fermions to their zero mode and the first excited gauge bosons. Afterwards we shall focus on obtaining the couplings of the fermions considered in the previous subsection to the Higgs sector. The relevant wave functions showing in Appendix A will be used below.

3.1.4.1 Couplings to Gauge Bosons

We will obtain the coupling of the excited fermions to gauge boson excitations in the quiver theories. These couplings are included in the kinetic terms in (3.97). We first consider the case where the spectrum includes a fermion with a left-

handed zero mode, as follows

$$\mathcal{L}_{\Psi_L A} = \sum_{j=0}^{N} \widetilde{g}_j \bar{\psi}_{L,j} \ \gamma^\mu A_{\mu,j} \psi_{L,j}, \tag{3.118}$$

where $\widetilde{g}_j$ is the gauge coupling associated with the $SU(n)_j$ gauge group, $\psi_{L,j}$ and $A_{\mu,j}$ are interaction eigenstates associated to the site j, such that $j = 0, 1, \ldots, N$.

Now, We can write the fields included in (3.118) by using their mass eigenstates basis (3.49) and (3.101). Note also in this case that $h_L^{j,n}$ is given in (3.100) and obtained by diagonalizing the matrix $M_\psi^T M_\psi$ (3.102) by taking $\mu_N = 0$, such that (3.118) can be written as

$$\mathcal{L}_{\Psi_L A} = \sum_{j,n,m,p=0}^{N} \left[\widetilde{g} (h_L^{j,n})^* f^{j,m} h_L^{j,p}\right] \bar{\chi}_L^{(n)} \ \gamma^\mu A_\mu^{(m)} \chi_L^{(p)}, \tag{3.119}$$

where we have used the expansion given in (3.49), $A_\mu^{(m)} = A_\mu^{a\ (m)} T^a$ and $\widetilde{g}_j$ was assumed to be equal to $\widetilde{g}$. We also define the effective coupling of the n and p fermion excitations to the m gauge boson excitation as

$$g_L^{n,m,p} \equiv \widetilde{g} \sum_{j=0}^{N} \left[(h_L^{j,n})^* f^{j,m} h_L^{j,p}\right]. \tag{3.120}$$

Notice that in (3.120), for a given number of sites in this model, this $g_L^{n,m,p}$ depends on the value of c_L according to (3.101). In addition, it allows the mixing between different modes of a left-handed fermion to a gauge boson excitation.

Now, to establish the relation between $\widetilde{g}$ and the SM couplings, $g_L^{n,m,p}$ in (3.120), we impose that for $n = m = p = 0$

$$g_L^{0,0,0} = \widetilde{g} \sum_{j=0}^{N} \left[(h_L^{j,0})^* f^{j,0} h_L^{j,0}\right], \tag{3.121}$$

we obtain the corresponding SM gauge coupling of the zero modes. We can use (3.62) and the fact the $h_L^{j,0}$ satisfies the normalization condition for a given value of c_L. The coupling $g_L^{0,0,0}$ in (3.121) may be written in the form

$$g_L^{0,0,0} = \frac{\widetilde{g}}{\sqrt{N+1}} \sum_{j=0}^{N} \left[(h_L^{j,0})^* h_L^{j,0}\right], \tag{3.122}$$

from which we obtain

$$g_L^{0,0,0} = g = \frac{\widetilde{g}}{\sqrt{N+1}}, \tag{3.123}$$

where g is the gauge coupling of the SM, so (3.124) yields

$$\widetilde{g} = g\sqrt{N+1}, \tag{3.124}$$

and then substituting (3.124) into (3.120). We find then that

$$g_L^{n,m,p} = g\sqrt{N+1}\sum_{j=0}^{N}\left[(h_L^{j,n})^* f^{j,m} h_L^{j,p}\right]. \tag{3.125}$$

On the other hand, in the case of a fermion with right-handed zero mode, we proceed in a similar way, analogously to the previous case. We have

$$\mathcal{L}_{\Psi_L A} = \sum_{j=0}^{N} \widetilde{g}_j \bar{\psi}_{R,j}\ \gamma^\mu A_{\mu,j}\psi_{R,j}. \tag{3.126}$$

Thus, considering this type of spectrum we can write

$$g_R^{n,m,p} = g\sqrt{N+1}\sum_{j=0}^{N}\left[(h_R^{j,n})^* f^{j,m} h_R^{j,p}\right], \tag{3.127}$$

where for a fixed number of sites, $g_R^{n,m,p}$ will depend on the value of c_R, since in this case $h_R^{j,n}$ is obtained diagonalizing the matrix $M_\psi M_\psi^T$ (3.104) by taking $\mu_0 = 0$. In subsections (3.1.4.1) and (3.1.4.1) we will show some results, for couplings that involve a first excited state of a gauge boson to excited fermions.

Zero Mode

Here we perform a numerical calculation, first to obtain the couplings of the left-handed zero mode to a first excited state of a gauge boson, i.e. $g_L^{0,1,0}(c_L)$. Using (3.125), we obtain this coupling as a function of the localization parameter c_L, for specific quiver theories with five and sixteen sites, i.e. $N = 4$ and $N = 15$ respectively. As shown in Figure (3.12), that agrees with the analytical calculation obtained in the previous Refs. [8, 9, 11]. In this plot there are two plateaus: the upper plateau, for $c_L < 0.5$ corresponds to left-handed fermions whose zero modes are localized close to the N-th site, that is, in the IR region. And the lower plateau, for $c_L > 0.5$, where the left-handed fermions have their zero modes localized close to the zeroth site, that is, in the UV region.

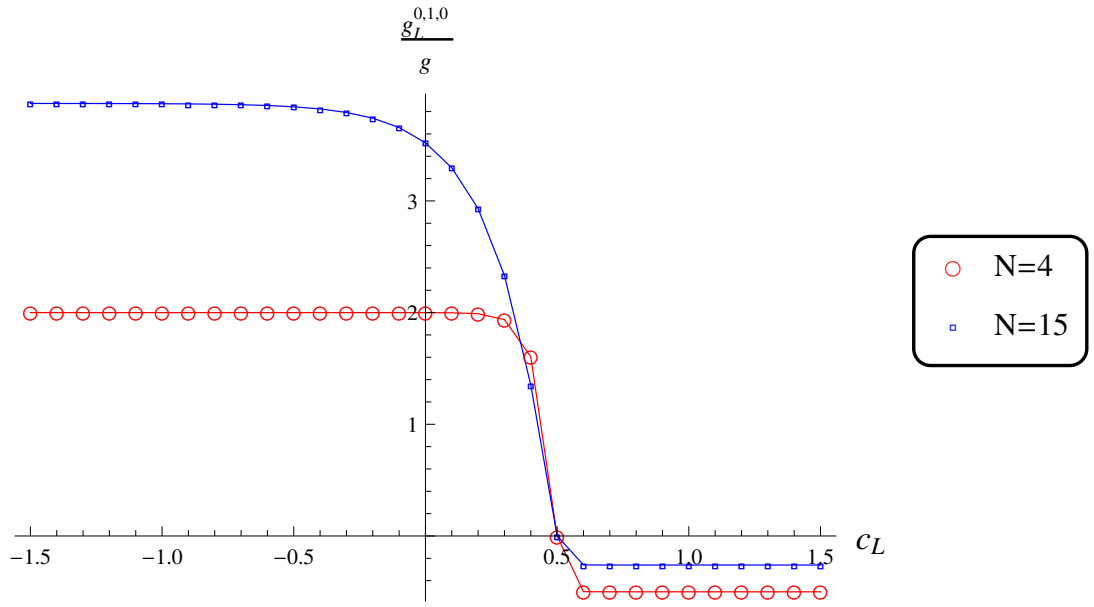

Figure 3.12. Couplings of the left-handed zero mode to a first excited state of a gauge boson, in units of the SM gauge boson coupling, as a function of the localization parameter. For N=4, N=15.

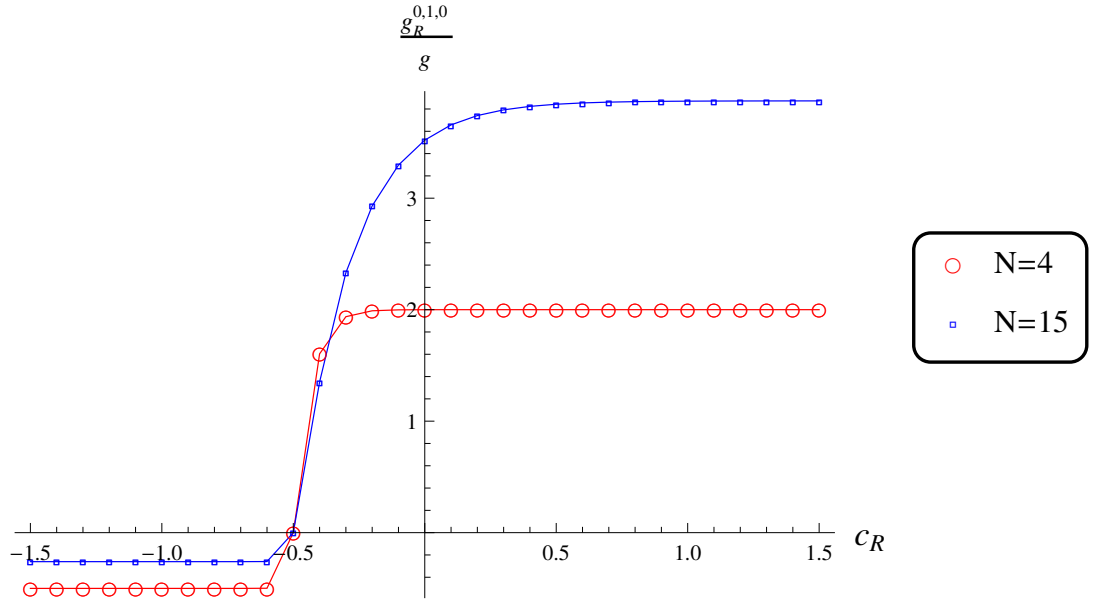

Figure 3.13. Couplings of the fermions with right-handed zero mode to a first excited state of gauge boson, in units of the SM gauge boson coupling, as a function of the localization parameter. For N=4, N=15.

We also obtain the couplings of the fermions with a right-handed zero-mode

to a first excited state of gauge boson, i.e. $g_R^{0,1,0}(c_R)$, as a function of the localization parameter c_R, for specific quiver theories with five and sixteen sites, i.e. $N = 4$ and $N = 15$ respectively, (3.125) was used.

The Figure (3.13) shows this calculation, which is in agreement with the analytical calculation obtained in the previous Refs. [8, 9, 11]. In this plot there are also two plateaus: the lower plateau, for $c_R < -0.5$, corresponds to right-handed zero-mode fermions localized close to the zeroth site, that is, in the UV region. And the upper plateau, for $c_R > -0.5$, corresponds to right-handed zero-modes localized close to the N-th site, that is, in the IR region.

Off Diagonal Couplings

We will compute the off diagonal couplings involving the first excited fermion, a zero-mode fermion and a first excitation of gauge boson. This will be later used to study the phenomenology of the excited fermions. A similar procedure was followed to obtain the values of the couplings of the first excited fermions to their zero mode and the first excited of a gauge boson. We use (3.120) and (3.127) with n=0, and m=p=1, then we can substitute these values to obtain

$$g_L^{0,1,1} = g\sqrt{N+1}\sum_{j=0}^{N}\left[(h_L^{j,0})^* f^{j,1} h_L^{j,1}\right], \tag{3.128}$$

where $h_L^{j,0}$, $h_L^{j,1}$ and $f^{j,1}$ are obtained through rotation to the mass eigenstates (3.49) and (3.101). Analogously we can obtain using (3.49) and (3.103)

$$g_R^{0,1,1} = g\sqrt{N+1}\sum_{j=0}^{N}\left[(h_R^{j,0})^* f^{j,1} h_R^{j,1}\right]. \tag{3.129}$$

As we have already mentioned, $g_L^{0,1,1}$ and $g_R^{0,1,1}$ depend on the values of c_L and c_R. These couplings appear in the effective Lagrangian as

$$g_L^{0,1,1}\bar{\chi}_L^{(0)}\ \gamma^\mu A_\mu^{(1)}\chi_L^{(1)} + \text{h.c.} \tag{3.130}$$

and

$$g_R^{0,1,1}\bar{\chi}_R^{(0)}\ \gamma^\mu A_\mu^{(1)}\chi_R^{(1)} + \text{h.c.} \tag{3.131}$$

To calculate the couplings in (3.128) and (3.129), the localization parameters $c_{L,R}$ that are found in Refs. [8, 11] were used. This choice corresponds to a solution that gives the correct quark masses as well as the correct CKM matrix. In addition, we considered the values of $c_{L,R}$ for the first and third generation of SM quarks. These localization parameters are $c_{u_R} = -0.73$, $c_{u_L} = 0.62$, $c_{d_R} = -0.96$

and $c_{t_R} = -0.12$, $c_{t_L} = 0.51$, $c_{b_R} = -0.61$ for the first and third generation respectively.

The results are displayed in Table (3.2), as shown in Ref. [10]. The column labeled '$u^{(1)}$' gives the values of the couplings between the first excited state of the up quark from the first-generation of the SM to their zero mode, i.e., the up quark and the first excited state of a gauge boson $A^{(1)}$ in units of the zero-mode SM gauge coupling obtained by using the values of localization parameters c_{u_L} and c_{u_R}, for left and right handed chiralities, and for quiver theories with $N = 4$ or $N = 15$.

Analogously, the column labeled '$d^{(1)}$' contains the values of the couplings between the first excited state of the down quark from the first-generation of the SM to their zero mode, i.e., the down quark and the first excited state of a gauge boson $A^{(1)}$ in units of the zero-mode SM gauge coupling. In this case we used the values of localization parameters c_{u_L} and c_{d_R}. On the other hand the columns labeled respectively '$t^{(1)}$' and '$b^{(1)}$', were obtained by using the values of the localization parameters c_{t_R}, c_{t_L} and c_{b_R}, for left and right handed chiralities, and for quiver theories with $N = 4$ or $N = 15$. As can be seen, just the largest couplings are found in the third generation, particularly the right-handed top sector for a quiver theory with $N = 15$. This is in agreement with the overlap of the wave-functions that were shown in Figures (3.5) and (3.6) for the gauge boson and top fermion with right-handed zero mode and localization parameter c_R for a quiver theory with $N = 15$.

N		$u^{(1)}$	$d^{(1)}$	$t^{(1)}$	$b^{(1)}$
4	L	0.028	0.028	0.85	0.85
	R	5.2×10^{-4}	1.1×10^{-7}	0.075	0.04
15	L	0.033	0.033	0.83	0.83
	R	7.1×10^{-4}	1.7×10^{-7}	1.49	0.046

Table 3.2. The couplings of the first excited fermions to their zero mode and the first excited gauge boson, in units of the zero-mode SM gauge coupling, for N=4, N=15

3.1.5 Couplings to the Higgs Boson

Based on Subsection 3.1.3, where it was studied how treat the wave-functions associated to fermions in quiver theories, we now consider the couplings of the excited fermions to the Higgs sector. We will follow the approach from Ref. [10]. Then to obtain these couplings, we need to consider the general form of the fermion couplings to the link fields that contain the Higgs doublet. As we have seen in (3.97), it will involve fermions of the same tower $\psi_{L,j}$ and $\psi_{R,j}$ with a

common zero mode, that is, after the application of the boundary condition to have left- or right- handed zero mode.

Moreover, we consider another type of Yukawa terms involving fermions of different towers, as follow

$$\bar{\psi}_{R,j-1}\Phi_j\xi_{L,j}, \tag{3.132}$$

where $\xi_{L,j}$ is associated to a tower with a zero mode, and $\psi_{R,j-1}$ is associated to a tower with a zero mode different from $\xi_{L,j}$. Notice that this term is gauge invariant due also to the transformation (3.31), so is allowed by the theory.

Here the term given in (3.132) is related to the quiver diagram of Figure (3.14). In contrast to the Yukawa terms included in (3.97), where these can be obtained from the deconstruction of AdS_5 theory with fermions as shown in Ref. [7] and then these have analog in the continuum limit, the term in (3.132) does not have analog in the continuum limit.

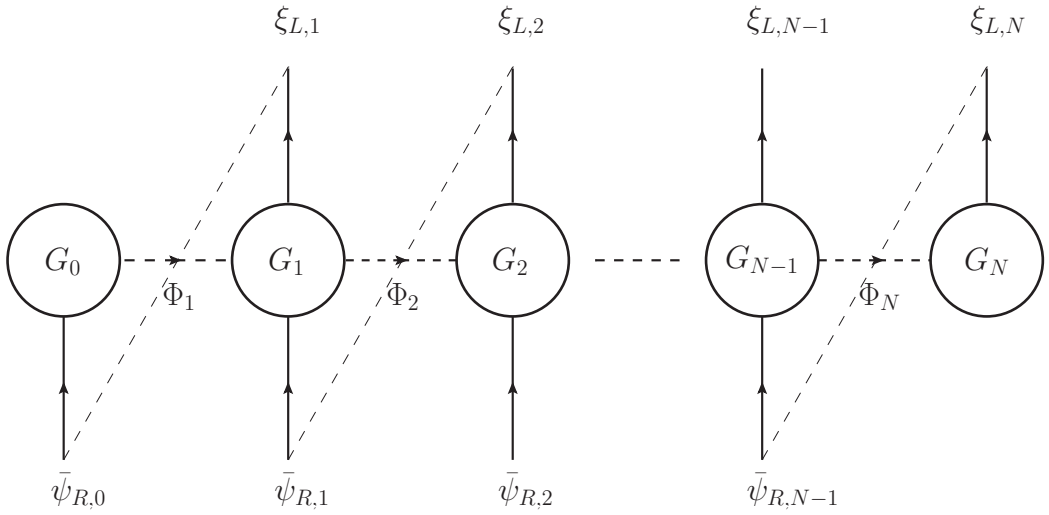

Figure 3.14. Quiver diagram including the interaction between fermions of different towers associated to (3.132).

The Higgs is a pNGB extracted from the link fields Φ_j in the manner explained in Subsection 3.1.2.

The coupling in (3.132) can be written as

$$-\sum_{j=1}^{N} y_j\bar{\psi}_{R,j-1}\Phi_j\xi_{L,j} + \text{h.c.}, \tag{3.133}$$

where the Yukawa couplings y_j in (3.133) are assumed to be $\mathcal{O}(1)$, and the fermion fields $\xi_{L,j}$ and $\psi_{R,j-1}$ correspond to different zero modes, characterized by the localization parameters c_L or c_R, with appropriate quantum numbers. The Higgs doublet is given by

$$H = \frac{1}{\sqrt{2}} \begin{pmatrix} \sqrt{2}\varphi^+ \\ v + H^0 + i\varphi_3 \end{pmatrix}. \tag{3.134}$$

Then, to obtain the couplings of the excited fermions to the Higgs sector, the rotations (3.101) and (3.103) were substituted into (3.133), and the Higgs doublet couplings in (3.133) are rewritten as follows

$$-\sum_{j=1}^{N}\sum_{n,m=0}^{N} y_j (h_R^{j-1,n})^* h_L^{j,m} b^j \bar{q}_R^{(n)} H Q_L^{(m)} + \text{h.c.}, \tag{3.135}$$

where b^j is given by (3.93).

Notice that after the quiver symmetry breaking, we still have terms in the theory invariant under $SU(2) \times U(1)$, as mentioned above, and then we consider terms that are invariant under $SU(2)$ and have zero net hypercharge Y. Thus, considering mixing of the excited states of quarks belonging to the same family, we can write

$$\begin{aligned} \mathcal{L} \supset & -\sum_{n,m=0}^{N}\sum_{j=1}^{N} y_{uj} (h_R^{j-1,n}(c_{\mathsf{R}_u}))^* h_L^{j,m}(c_{\mathsf{L}_q}) b^j \overline{\mathsf{R}}_u^{(n)} \widetilde{H}^\dagger \mathsf{L}_q^{(m)} \\ & -\sum_{n,m=0}^{N}\sum_{j=1}^{N} y_{dj} (h_R^{j-1,n}(c_{\mathsf{R}_d}))^* h_L^{j,m}(c_{\mathsf{L}_q}) b^j \overline{\mathsf{R}}_d^{(n)} H^\dagger \mathsf{L}_q^{(m)} + \text{h.c.}, \end{aligned} \tag{3.136}$$

where $\widetilde{H} = i\sigma_2 H^*$.

Here $\mathsf{R}_u^{(n)}$ and $\mathsf{R}_d^{(n)}$ are the excited states of the right-handed up- and right-handed down-type quarks fields, respectively with different right-handed zero modes. Also in (3.136) $\mathsf{L}_q^{(m)}$ contains the excited states of the left-handed quarks. After that, we select the coupling between the first excited state of the right-handed up-type quark to the Higgs doublet and the left-handed doublet of SM quarks from the same family as follow

$$-\sum_{j=1}^{N} y_{uj} (h_R^{j-1,1}(c_{\mathsf{R}_u}))^* h_L^{j,0}(c_{\mathsf{L}_q}) b^j \overline{\mathsf{R}}_u^{(1)} \widetilde{H}^\dagger \mathsf{L}_q^{(0)} + \text{h.c.}, \tag{3.137}$$

The results are shown in Table (3.3). For instance, considering the third gener-

ation of SM quarks, i.e., using (3.137), with the localization parameters c_{t_R}, c_{t_L} and (3.93), we obtained the couplings displayed in the column labeled '$t_R^{(1)}\, t_L^{(0)}$, for quiver theories with $N = 4$ or $N = 15$. On the other hand the column labeled '$u_R^{(1)}\, u_L^{(0)}$' were obtained by using the values of the localization parameters c_{u_R}, c_{u_L} (corresponding to the first generation of SM quarks).

We also considered the coupling between the right-handed up-type SM quark to the Higgs doublet and the first excited state of the left-handed doublet of quarks associated to the same family as follow

$$-\sum_{j=1}^{N} y_{uj}(h_R^{j-1,0}(c_{\mathsf{R}_u}))^* h_L^{j,1}(c_{\mathsf{L}_q}) b^j \overline{\mathsf{R}}_u^{(0)} \widetilde{H}^\dagger \mathsf{L}_q^{(1)} + \text{h.c.}, \tag{3.138}$$

The results are also shown in Table (3.3). For instance, considering the third generation of SM quarks, i.e., using (3.138), with the localization parameters c_{t_R}, c_{t_L} and (3.93), for the Higgs wave function, we obtained the couplings displayed in the column labeled '$t_L^{(1)}\, t_R^{(0)}$' for quiver theories with $N = 4$ or $N = 5$. Similarly, the values of the couplings in the column labeled '$u_L^{(1)}\, u_R^{(0)}$' was obtained by using the values of the localization parameters c_{u_R}, c_{u_L} (corresponding to the first generation of SM quarks). The next selection of couplings, that we have considered is between the right-handed down-type SM quark to the Higgs doublet and the first excited state of the left-handed doublet of quarks associated to the same family

$$-\sum_{j=1}^{N} y_{dj}(h_R^{j-1,0}(c_{\mathsf{R}_d}))^* h_L^{j,1}(c_{\mathsf{L}_q}) b^j \overline{\mathsf{R}}_d^{(0)} H^\dagger \mathsf{L}_q^{(1)} + \text{h.c.}. \tag{3.139}$$

The evaluation for this couplings are also shown in Table (3.3). For instance, considering the third generation of SM quarks, i.e., using (3.139), with the localization parameters c_{t_R}, c_{t_L} and (3.93), we obtained the couplings displayed in the column labeled '$t_L^{(1)}\, b_R^{(0)}$' for quiver theories with $N = 4$ or $N = 15$. Similarly, by considering the first generation and showed in the column labeled '$u_L^{(1)}\, d_R^{(0)}$', where the localization parameters c_{d_R}, c_{u_L} were used.

Finally, we also considered the coupling between the first excited state right-handed down-type quark to the Higgs doublet and the left-handed doublet of SM quarks associated to the third generation of SM quarks. This coupling was calculated by using

$$-\sum_{j=1}^{N} y_{dj}(h_R^{j-1,1}(c_{\mathsf{R}_d}))^* h_L^{j,0}(c_{\mathsf{L}_q}) b^j \overline{\mathsf{R}}_d^{(1)} H^\dagger \mathsf{L}_q^{(0)} + \text{h.c.}, \tag{3.140}$$

and the results are shown in the column labeled '$b_R^{(1)}\, t_L^{(0)}$' in Table (3.3).

As can be seen in Table (3.3), the larger couplings are found in the third generation. Once again, this agrees with the overlap of the wave-functions associated with the localization parameters (c_{t_L}, c_{t_R} and c_{b_R}, the wave-functions associated with these localization parameters were obtained in Appendix (A)) and with the (3.93).

N	$t_R^{(1)}\, t_L^{(0)}$	$t_L^{(1)}\, t_R^{(0)}$	$u_R^{(1)}\, u_L^{(0)}$	$u_L^{(1)}\, u_R^{(0)}$	$t_L^{(1)}\, b_R^{(0)}$	$u_L^{(1)}\, d_R^{(0)}$	$b_R^{(1)}\, t_L^{(0)}$
4	0.365	0.028	4.1×10^{-9}	0.00173	0.041	3.02×10^{-6}	2.64×10^{-4}
15	0.179	0.352	3.4×10^{-5}	3.02×10^{-4}	0.0143	1.28×10^{-7}	0.001

Table 3.3. Couplings of fermions from different towers to the Higgs doublet, for allowed modes 0 and 1.

Now that we have calculated the couplings in this section, we will study in the next chapter the phenomenology of the excited fermions.

3.2 General Effective Theory for New Fermions

Our aim is to provide alternatives to the study of the phenomenology involving new heavy fermions that, besides quiver theories there are also many others Vector-like quarks theories. So it is of interest to study Vector-like quark phenomenology in a general model-independent way. Generically, we can consider vector-like quarks as being multiplets of $SU(2)_L$ as shown in Refs. [37, 38, 39], such that these new fermions will be coupled to SM fermions and gauge bosons through the Yukawa terms and kinetic terms, respectively. Our procedure will be according to Ref. [38], where these new fermions couple to the third generations of SM quarks. In this section, the cases of a singlet vector-like up-type and SM doublet will be studied. For the first case, we will use the bound associated to the tbW coupling [40] and for the second one, the constraint associated to the decay $Z \to b\bar{b}$ [41] will be used. It is due to after the EWSB the mixing between the vector-like quarks and the third generation of the SM quarks induce deviations on the couplings associated with these measurements. In addition to these cases, for each one the interaction with a heavy gluon will be included.

3.2.1 Vector-like quark SU(2)-singlet up-type, T

Let us consider a vector-like up-type fermion T', a singlet of $SU(2)_L$ with hypercharge equal to 2/3. It couples to the SM quarks through the Yukawa couplings as follows

$$\mathcal{L}_{\mathrm{Y(VLT)}} = -Y^u_{i\beta}\ \overline{q}'_{Li}\tilde{\Phi}u'_{R\beta} - Y^d_{ij}\ \overline{q}'_{Li}\Phi d'_{Rj} + \mathrm{h.c.}, \tag{3.141}$$

where $i, j = 1, 2, 3$ correspond to indexes of generations in the SM (q'_{Li} and u'_{Ri} are $SU(2)_L$-doublet and -singlet, respectively) and the index $\beta = 1, 2, 3, 4$, such that $u'_4 = T'$. To indicate that the fermions are not in their mass eigenstate primes are used. In addition, there is a vector-like term of the form

$$\mathcal{L}_{\mathrm{M(VLT)}} = -M\ \overline{T}'_L T'_R + \mathrm{h.c.}. \tag{3.142}$$

The Higgs doublet is given by

$$\Phi = \frac{1}{\sqrt{2}}\begin{pmatrix} 0 \\ v + H \end{pmatrix}. \tag{3.143}$$

We substitute (3.143) in (3.141) and considering the mixing between T' and the third generation, we can identify the mass term that is written as follows

$$\mathcal{L}_{Mass} = -\begin{pmatrix} \bar{t}'_L & \overline{T}'_L \end{pmatrix} \mathbf{M_{t'T'}} \begin{pmatrix} t'_R \\ T'_R \end{pmatrix} + \mathrm{h.c.}, \tag{3.144}$$

where

$$\mathbf{M_{t'T'}} = \begin{pmatrix} \frac{v}{\sqrt{2}}Y^u_{33} & \frac{v}{\sqrt{2}}Y^u_{34} \\ 0 & M \end{pmatrix}. \tag{3.145}$$

We have that the masses in the mass eigenstate are given by

$$m_t^2 = \frac{M^2 + \frac{v^2}{2}\left(|Y^u_{33}|^2 + |Y^u_{34}|^2\right) - \sqrt{\left(M^2 + \frac{v^2}{2}\left(|Y^u_{33}|^2 + |Y^u_{34}|^2\right)\right)^2 - 2v^2M^2|Y^u_{33}|^2}}{2} \tag{3.146}$$

$$m_T^2 = \frac{M^2 + \frac{v^2}{2}\left(|Y^u_{33}|^2 + |Y^u_{34}|^2\right) + \sqrt{\left(M^2 + \frac{v^2}{2}\left(|Y^u_{33}|^2 + |Y^u_{34}|^2\right)\right)^2 - 2v^2M^2|Y^u_{33}|^2}}{2}, \tag{3.147}$$

by using (3.146), (3.147), jointly with $v^2 \ll M^2$, we can expand the square roots in powers of $\left(\frac{v}{M}\right)^2$ as follow

$$m_t^2 = \frac{M^2 + \frac{v^2}{2}\left(|Y_{33}^u|^2 + |Y_{34}^u|^2\right) - M^2\left[1 + \frac{1}{2}\left(\frac{v}{M}\right)^2\left(|Y_{34}^u|^2 - |Y_{33}^u|^2\right) + \mathcal{O}\left(\frac{v}{M}\right)^4\right]}{2} \tag{3.148}$$

$$m_T^2 = \frac{M^2 + \frac{v^2}{2}\left(|Y_{33}^u|^2 + |Y_{34}^u|^2\right) + M^2\left[1 + \frac{1}{2}\left(\frac{v}{M}\right)^2\left(|Y_{34}^u|^2 - |Y_{33}^u|^2\right) + \mathcal{O}\left(\frac{v}{M}\right)^4\right]}{2}, \tag{3.149}$$

and then m_t^2 and m_T^2 go as $\left(\frac{v}{\sqrt{2}}Y_{33}^u\right)^2$ and $M^2 + \left(\frac{v}{\sqrt{2}}Y_{34}^u\right)^2$, respectively. Therefore, this means that m_T is greater than the unphysical vector-like mass. Also, using (3.146) and (3.147), we can deduce the relation

$$m_T^2 = M^2\left(1 + \frac{\frac{v^2}{2}|Y_{34}^u|^2}{M^2 - m_t^2}\right). \tag{3.150}$$

This relation is shown in Figure (3.15). We see that the differences between m_T and M decrease for large M, whereas for small M, theses differences increase.

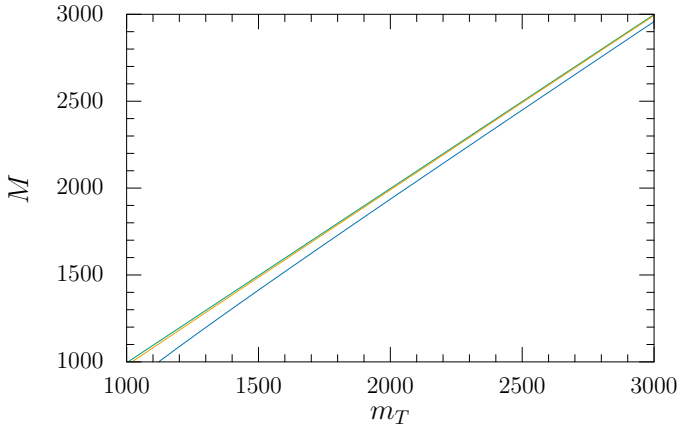

Figure 3.15. Correlation between the mass vector-like and m_T, for $\frac{v}{\sqrt{2}}|Y_{34}^u| = 100$, 200 and 500 from left to right.

Now, we write $\mathbf{M_{t'T'}}$ as factorized as follows

$$\mathbf{M_{t'T'}} = V_L^\dagger \begin{pmatrix} m_t & 0 \\ 0 & m_T \end{pmatrix} V_R, \tag{3.151}$$

where $V_{L,R}$ are given by

$$V_{L,R} = \begin{pmatrix} \cos\theta_u^{L,R} & \sin\theta_u^{L,R} \\ -\sin\theta_u^{L,R} & \cos\theta_u^{L,R} \end{pmatrix}, \tag{3.152}$$

in such a way that the next relations are obtained by using (3.152), (3.151) and (3.145)

$$\begin{aligned}
&\frac{v}{\sqrt{2}}Y_{33}^u \cos\theta_u^L \cos\theta_u^R - \frac{v}{\sqrt{2}}Y_{34}^u \cos\theta_u^L \sin\theta_u^R + M \sin\theta_u^L \sin\theta_u^R = m_t, \\
&\frac{v}{\sqrt{2}}Y_{33}^u \sin\theta_u^L \cos\theta_u^R - \frac{v}{\sqrt{2}}Y_{34}^u \sin\theta_u^L \sin\theta_u^R - M \cos\theta_u^L \sin\theta_u^R = 0, \\
&\frac{v}{\sqrt{2}}Y_{33}^u \cos\theta_u^L \sin\theta_u^R - \frac{v}{\sqrt{2}}Y_{34}^u \cos\theta_u^L \cos\theta_u^R - M \sin\theta_u^L \cos\theta_u^R = 0, \\
&\frac{v}{\sqrt{2}}Y_{33}^u \sin\theta_u^L \sin\theta_u^R - \frac{v}{\sqrt{2}}Y_{34}^u \sin\theta_u^L \cos\theta_u^R + M \cos\theta_u^L \cos\theta_u^R = m_T,
\end{aligned} \tag{3.153}$$

where, assuming real Yukawa couplings, we have

$$\sin\theta_u^L = \frac{vM}{\sqrt{2}} \frac{Y_{34}^u}{\sqrt{(M^2 - m_t^2)^2 + \dfrac{v^2 M^2 |Y_{34}^u|^2}{2}}} \tag{3.154}$$

and

$$\sin\theta_u^R = \frac{m_t}{M} \sin\theta_u^L. \tag{3.155}$$

To obtain the couplings between T to the SM third generations and the EW gauge bosons we first write the fermion-gauge boson interaction in the EW basis

$$\begin{aligned}
&\begin{pmatrix} \bar{t}'_L & \bar{b}'_L \end{pmatrix} i\gamma^\mu \left(-igA_\mu^a \tau^a - ig' B_\mu Y\right) \begin{pmatrix} t'_L \\ b'_L \end{pmatrix} \\
&+ \bar{t}'_R \, i\gamma^\mu \left(-ig' B_\mu Y\right) t'_R + \bar{b}'_R \, i\gamma^\mu \left(-ig' B_\mu Y\right) b'_R \\
&+ \overline{T}'_{L,R} \, i\gamma^\mu \left(-ig' B_\mu Y\right) T'_{L,R},
\end{aligned} \tag{3.156}$$

where A_μ^a and B_μ are the gauge bosons of $SU(2)_L$ and $U(1)_Y$ respectively. In the

following we use the vector mass eigenstates jointly with the rotations defined by (3.152) and, furthermore we will neglect the prime in b'_L, because we have considered the mixing between the up sector of the SM third generation and T' according to (3.141) where the down-type quarks are not affected by the mixing. After these substitutions in (3.156), we obtain in the mass eigenstates

$$\begin{aligned}
&\left(\cos\theta_u^L \frac{g}{\sqrt{2}} \bar{t}_L \not{W}^+ b_L + \text{h.c.}\right) \\
&+ \frac{g}{2c_W} \bar{t} \not{Z} \left(\cos^2\theta_u^L P_L - \frac{4}{3} s_W^2\right) t \\
&+ \frac{g}{2c_W} \bar{b} \not{Z} \left(-P_L + \frac{2}{3} s_W^2\right) b \\
&+ \frac{g}{2c_W} \bar{T} \not{Z} \left(\sin^2\theta_u^L P_L - \frac{4}{3} s_W^2\right) T \\
&+ \left(\sin\theta_u^L \frac{g}{\sqrt{2}} \overline{T}_L \not{W}^+ b_L + \text{h.c.}\right) \\
&+ \left(\cos\theta_u^L \sin\theta_u^L \frac{g}{2c_W} \bar{t} \not{Z} P_L T + \text{h.c.}\right) \\
&+ \frac{2g s_W}{3} \left(\bar{t} \not{A} t + \bar{T} \not{A} T\right) - \frac{g s_W}{3} \left(\bar{b} \not{A} b\right),
\end{aligned} \tag{3.157}$$

while the Higgs interaction involving T and the SM third generation comes from the Yukawa couplings (3.141), by using (3.152), as follows

$$\begin{aligned}
&- \frac{g m_T}{2 m_W} \sin^2\theta_u^L \overline{T} T H \\
&- \frac{g m_T}{2 m_W} \overline{T} \left(\frac{m_t}{m_T} \cos\theta_u^L \sin\theta_u^L P_R + \cos\theta_u^L \sin\theta_u^L P_L\right) t H + \text{h.c.} \\
&- \frac{g m_t}{2 m_W} \cos^2\theta_u^L \bar{t} t H - \frac{g m_b}{2 m_W} \cos^2\theta_u^L \bar{b} b H.
\end{aligned} \tag{3.158}$$

We can use a CMS measurement of single top cross sections at 7 TeV [40], that is the V_{tb} (tbW coupling), such that $|V_{tb}| > 0.92$, which results in the constraint

$$|\sin\theta_u^L| < 0.4. \tag{3.159}$$

We point out that $\sin^2\theta_u^L$ is always further suppressed by $\frac{v}{M}$. The QCD interaction of the Vector-like quark is just as in the SM: T, the interaction following is

considered

$$\mathcal{L}_{gTT} = g_s \bar{T} \gamma_\mu \mathsf{T}^a g^{\mu,a} T. \tag{3.160}$$

Finally, we also allow for the interaction of the Vector-like quark with a heavy gluon G, given by

$$\mathcal{L}_{GTt} = g_s \left(f_L \bar{t}_L \gamma_\mu \mathsf{T}^a G^{\mu,a} T_L + f_R \bar{t}_R \gamma_\mu \mathsf{T}^a G^{\mu,a} T_R + \text{h.c.} \right), \tag{3.161}$$

where $g_s f_L$ and $g_s f_R$ are left- and right-handed couplings between t, T and G.

3.2.2 Vector-like quark SM SU(2)-doublet

Considering a vector-like SM $\begin{pmatrix} T' & B' \end{pmatrix}^{\mathbf{T}}$, where it is a doublet of $SU(2)_L$ and has hypercharge $1/6$, this couples to the SM quarks in the weak eigenstate through the Yukawa couplings as follow

$$\mathcal{L}_{\text{Y(VLT)}} = -Y^u_{\alpha i}\, \overline{q}'_{L\alpha} \tilde{\Phi} u'_{Ri} - Y^d_{\alpha j}\, \overline{q}'_{L\alpha} \Phi d'_{Rj} + \text{h.c.}, \tag{3.162}$$

where $i, j = 1, 2, 3$ correspond to indexes of generations in the SM (q'_{Li} is a doublet of $SU(2)_L$ and u'_{Ri} is a singlet of $SU(2)_L$) and the index $\alpha = 1, 2, 3, 4$, such that $q'_{L,R4} = \begin{pmatrix} T'_{L,R} & B'_{L,R} \end{pmatrix}^{\mathbf{T}}$, to indicate that the fermions are not in their mass eigenstate primes are used, jointly with the mass vector-like term

$$\mathcal{L}_{\text{M(VLT)}} = -M \overline{q}'_{L4} q_{R4} + \text{h.c.}. \tag{3.163}$$

Thus we substitute (3.143) in (3.162) and considering the mixing between T', B' and the SM third generation, we can identify the mass term that is written as follows

$$\mathcal{L}_{Mass} = \begin{pmatrix} \bar{t}'_L & \overline{T}'_L \end{pmatrix} \mathbf{M^u} \begin{pmatrix} t'_R \\ T'_R \end{pmatrix} + \begin{pmatrix} \bar{b}'_L & \overline{B}'_L \end{pmatrix} \mathbf{M^d} \begin{pmatrix} b'_R \\ B'_R \end{pmatrix} + \text{h.c.}, \tag{3.164}$$

Now, we write $\mathbf{M^{u,d}}$ as factorized as follows

$$\mathbf{M^{u,d}} = V_L^{u,d\dagger} \begin{pmatrix} m_{t,b} & 0 \\ 0 & m_{T,B} \end{pmatrix} V_R^{u,d} + \text{h.c.}, \tag{3.165}$$

where $V_{L,R}^{u,d}$ are given by

$$V_{L,R}^{u,d} = \begin{pmatrix} \cos\theta_{u,d}^{L,R} & \sin\theta_{u,d}^{L,R} \\ -\sin\theta_{u,d}^{L,R} & \cos\theta_{u,d}^{L,R} \end{pmatrix}. \tag{3.166}$$

we also have the relations

$$M_{T,B}^2 = M^2 \left(1 + \frac{\frac{v^2}{2}|Y_{34}^{u,d}|^2}{M^2 - m_{t,b}^2} \right). \tag{3.167}$$

Here the next relations are obtained by using (3.166), (3.165) and (3.164)

$$\begin{aligned}
&\frac{v}{\sqrt{2}} Y_{33}^{u,d} \cos\theta_{u,d}^L \cos\theta_{u,d}^R - \frac{v}{\sqrt{2}} Y_{34}^{u,d} \cos\theta_u^L \sin\theta_{u,d}^R + M \sin\theta_{u,d}^L \sin\theta_{u,d}^R = m_{t,b}, \\
&\frac{v}{\sqrt{2}} Y_{33}^{u,d} \sin\theta_{u,d}^L \cos\theta_{u,d}^R - \frac{v}{\sqrt{2}} Y_{34}^{u,d} \sin\theta_{u,d}^L \sin\theta_{u,d}^R - M \cos\theta_{u,d}^L \sin\theta_{u,d}^R = 0, \\
&\frac{v}{\sqrt{2}} Y_{33}^{u,d} \cos\theta_{u,d}^L \sin\theta_{u,d}^R - \frac{v}{\sqrt{2}} Y_{34}^{u,d} \cos\theta_{u,d}^L \cos\theta_{u,d}^R - M \sin\theta_{u,d}^L \cos\theta_{u,d}^R = 0, \\
&\frac{v}{\sqrt{2}} Y_{33}^{u,d} \sin\theta_{u,d}^L \sin\theta_{u,d}^R - \frac{v}{\sqrt{2}} Y_{34}^{u,d} \sin\theta_{u,d}^L \cos\theta_{u,d}^R + M \cos\theta_{u,d}^L \cos\theta_{u,d}^R = m_{T,B},
\end{aligned} \tag{3.168}$$

where

$$\sin\theta_{u,d}^R = \frac{vM}{\sqrt{2}} \frac{Y_{43}^{u,d}}{\sqrt{\left(M^2 - m_{t,b}^2\right)^2 + \frac{v^2 M^2 |Y_{43}^{u,d}|^2}{2}}} \tag{3.169}$$

and

$$\tan\theta_{u,d}^L = \frac{m_{t,b}}{M_{T,B}} \tan\theta_{u,d}^R. \tag{3.170}$$

To obtain the couplings between T, B to the SM third generations and the EW

gauge bosons, we first write the fermion-gauge boson interaction in the EW basis

$$\begin{aligned}
&\left(\begin{array}{cc} \bar{t}'_L & \bar{b}'_L \end{array} \right) i\gamma^\mu \left(-igA^a_\mu \tau^a - ig' B_\mu Y\right) \left(\begin{array}{c} t'_L \\ b'_L \end{array} \right) \\
&+ \bar{t}'_R \, i\gamma^\mu \left(-ig' B_\mu Y\right) t'_R + \bar{b}'_R \, i\gamma^\mu \left(-ig' B_\mu Y\right) b'_R \\
&+ \left(\begin{array}{cc} \overline{T}'_L & \overline{B}'_L \end{array} \right) i\gamma^\mu \left(-igA^a_\mu \tau^a - ig' B_\mu Y\right) \left(\begin{array}{c} T'_L \\ B'_L \end{array} \right) \\
&+ \left(\begin{array}{cc} \overline{T}'_R & \overline{B}'_R \end{array} \right) i\gamma^\mu \left(-igA^a_\mu \tau^a - ig' B_\mu Y\right) \left(\begin{array}{c} T'_R \\ B'_R \end{array} \right), \qquad (3.171)
\end{aligned}$$

in the following we rewrite all interaction terms[1] in the vector mass eigenstates, to do this the following definitions will be considered

$$c^{u,d}_{L,R} \equiv \cos\theta^{L,R}_{u,d}, \qquad (3.172)$$

$$s^{u,d}_{L,R} \equiv \sin\theta^{L,R}_{u,d}, \qquad (3.173)$$

Now, we write in the mass eigenstate the Higgs interaction involving T, B and the SM third generations, which comes from the Yukawa couplings (3.162), by using (3.166), as follows

$$\begin{aligned}
&-\frac{gm_T}{2m_W}(s^u_R)^2 \overline{T}TH \\
&-\frac{gm_B}{2m_W}(s^d_R)^2 \overline{B}BH \\
&-\frac{gm_T}{2m_W}\overline{T}\left(\frac{m_t}{m_T}c^u_R s^u_R P_L + s^u_R c^u_R P_R\right) tH + \text{h.c.} \\
&-\frac{gm_B}{2m_W}\overline{B}\left(\frac{m_b}{m_B}c^d_R s^d_R P_L + s^d_R c^d_R P_R\right) bH + \text{h.c.} \\
&-\frac{gm_t}{2m_W}(c^u_R)^2 \bar{t}tH - \frac{gm_b}{2m_W}(c^d_R)^2 \bar{b}bH, \qquad (3.174)
\end{aligned}$$

Thus, we can identify from (B.1) the coupling to study the single production of

[1]The passing from the EW to the mass eigenstate can be seen in Appendix (B) by using the definitions given in (3.172) and (3.173).

T via W, that is given by

$$\frac{g}{\sqrt{2}}\sin\left(\theta_L^u-\theta_L^d\right)\overline{T}_L\not{W}^+b_L-\frac{g}{\sqrt{2}}\cos\theta_R^u\sin\theta_R^d\overline{T}_R\not{W}^+b_R+\text{h.c.} \tag{3.175}$$

Notice that the angle θ_L^d is negligible, because is suppressed by the m_b according to (3.170).

In the mass eigenstate basis we have also found terms as

$$-\frac{g}{2c_W}\bar{b}_L\not{Z}b_L+\frac{gs_W^2}{3c_W}\bar{b}\not{Z}b-\frac{g}{2c_W}(s_R^d)^2\bar{b}_R\not{Z}b_R, \tag{3.176}$$

and

$$\frac{g}{\sqrt{2}}\left(c_L^uc_L^d+s_L^us_L^d\right)\bar{t}_L\not{W}^+b_L+\text{h.c.} \tag{3.177}$$

respectively.

First, we can compute the s_R^d, by using the constraint associated to $Z\to b\bar{b}$, $R_b=0.21629\pm0.00066$ that is found in Ref. [41], the width is as follows

$$\begin{aligned}\Gamma(Z\to b\bar{b})=&\frac{e^2\left(m_Z^2\left(m_Z^2-4m_b^2\right)\right)^{1/2}}{288\pi c_W^2s_W^2m_Z^3}\times\left(-9c_W^4m_b^2-42c_W^2s_W^2m_b^2\right.\\&-54c_W^2(s_R^d)^2m_b^2-17s_W^4m_b^2-30s_W^2(s_R^d)^2m_b^2-9(s_R^d)^4m_b^2+9c_W^4m_Z^2\\&\left.+6c_W^2s_W^2m_Z^2+5s_W^4m_Z^2+12s_W^2(s_R^d)^2m_Z^2+9(s_R^d)^4m_Z^2\right)\end{aligned} \tag{3.178}$$

then we obtain,

$$0.09<s_R^d<0.16\text{ or }-0.16<s_R^d<-0.09. \tag{3.179}$$

Now, we used it jointly with (3.170) and $M_B=2250GeV$, obtaining

$$0.0002<s_L^d<0.0003\text{ or }-0.0003<s_R^d<-0.0002. \tag{3.180}$$

After that, we use (3.180) in (3.177), and applying the measurement of the V_{tb} (tbW coupling) given in Ref. [40],

and then we have

$$c_L^u>0.92, \tag{3.181}$$

which results in the constraint

$$s_L^u<0.4. \tag{3.182}$$

and for the QCD pair production of T, the following interaction is considered

$$\mathcal{L}_{gTT} \supset g_s \bar{T} \gamma_\mu \mathsf{T}^a g^{\mu,a} T, \tag{3.183}$$

and also we will consider the next interaction

$$\mathcal{L}_{GTt} \supset g_s \left(f_L \bar{t}_L \gamma_\mu \mathsf{T}^a G^{\mu,a} T_L + f_R \bar{t}_R \gamma_\mu \mathsf{T}^a G^{\mu,a} T_R + \text{h.c.} \right), \tag{3.184}$$

where $g_s f_{L,R}$ are the left- and right-handed couplings between T, t and G. Similarly for the QCD pair production of B, the following interaction is considered

$$\mathcal{L}_{gBB} \supset g_s \bar{B} \gamma_\mu \mathsf{T}^a g^{\mu,a} B, \tag{3.185}$$

and also we can consider the next interactions

$$\mathcal{L}_{GBb} \supset g_s \left(g_L \bar{b}_L \gamma_\mu \mathsf{T}^a G^{\mu,a} B_L + g_R \bar{b}_R \gamma_\mu \mathsf{T}^a G^{\mu,a} B_R + \text{h.c.} \right), \tag{3.186}$$

where $g_s g_L, R$ are the left- and right-handed couplings between B, b and G. Now that we have know the couplings associated for the single production of T, we will study the production and decay of this heavy state.

CHAPTER 4

Vector-Like Heavy Quarks at the LHC

In this chapter we will study the production and decay of vector-like quarks, motivated by extensions of the SM where the Higgs is a pNGB. We will focus on quiver theories as well as a model-independent effective Lagrangian approach. In particular, inspired by quiver theories we will add a possible decay mode of the heavy quark into a heavy gluon which has not been considered in the literature. It because the possibility of a first exited state of fermion as in quiver theories can be heavier than the first excited gluon as in Ref. [10]. We will first consider the phenomenology of the quiver theories and comment on the model-independent case, which only requires a rescaling of our results. We will focus on the phenomenology associated to single production of the first excited state of the top quark with left-handed zero mode (we denoted it by T_L) through the EW interactions because this mode of production becomes dominant over the pair production at higher masses [42], as saw in Table (3.3) the more relevant couplings were found in the third generation. Considering the following interactions involving T_L

$$\mathcal{L}_{gT_LT_L} \supset g_s \bar{T}_L \gamma_\mu \mathsf{T}^a g^{\mu,a} T_L, \tag{4.1}$$

$$\mathcal{L}_{GT_Lt} \supset g_s \bar{T}_L \gamma_\mu \mathsf{T}^a G^{\mu,a} (g^L_{T_LGt} P_L) t, \tag{4.2}$$

$$\begin{aligned} \mathcal{L}_{T_LEW} \supset & - c_{T_Lth} \bar{T}_L H P_R t + \text{h.c.} \\ & + c_{T_LbW} \frac{e}{\sqrt{2} s_W} \bar{T}_L \gamma_\mu W^{\mu,+} P_L b + \text{h.c.} \\ & + c_{T_LZt} \frac{e}{2 s_W c_W} \bar{T}_L \gamma_\mu Z^\mu P_L t + \text{h.c.}, \end{aligned} \tag{4.3}$$

where $g^L_{T_LGt}$ and c_{T_Lth} are inferred from Tables (3.2) e (3.3), respectively, $G^{\mu,a}$ is the first excited state of the gluon, H is the Higgs boson, $W^{\mu,+}$ and Z^μ are the massive EW gauge bosons. Now, to find a relation between c_{T_Lth}, c_{T_LbW}

and $c_{T_L Zt}$ we will use the equivalence theorem. Firstly, to obtain a the relation between $c_{T_L th}$ and $c_{T_L Zt}$, the widths of T_L to Higgs-top and Z-top will be assumed to be equal at high energies, for $m_T \gg m_t,\ m_h,\ m_Z$. The $T_L \to Zt$ partial width is given by

$$\begin{aligned}\Gamma_{Zt} =& \frac{1}{96\pi m_{T_L}^3}(m_t^4 - 2m_t^2 m_{T_L}^2 - 2m_t^2 m_Z^2 + m_{T_L}^4 - 2m_{T_L}^2 m_Z^2 + m_Z^4)^{1/2}\times \\ & \left[\frac{3e^2}{4m_Z^2 c_W^2 s_W^2} m_t^4 - \frac{3e^2}{2m_Z^2 c_W^2 s_W^2} m_t^2 m_{T_L}^2 + \frac{3e^2}{4c_W^2 s_W^2} m_t^2 + \frac{3e^2}{4m_Z^2 c_W^2 s_W^2} m_{T_L}^4 \right. \\ & \left. + \frac{3e^2}{4c_W^2 s_W^2} m_{T_L}^2 - \frac{3e^2}{2c_W^2 s_W^2} m_Z^2 \right] (c_{T_L Zt})^2 \end{aligned} \tag{4.4}$$

expanding in powers of $\frac{m_t}{m_{T_L}}$ or $\frac{m_Z}{m_{T_L}}$, we obtain

$$\begin{aligned}\Gamma_{Zt} =& \frac{m_{T_L}}{96\pi}\left\{1 + \mathcal{O}\left[\left(\frac{m_t}{m_{T_L}}\right)^2\right] + \mathcal{O}\left[\left(\frac{m_Z}{m_{T_L}}\right)^2\right]\right\}\left[\frac{3e^2}{4c_W^2 s_W^2}\left(\frac{m_t^2}{m_Z m_{T_L}}\right)^2 \right. \\ & - \frac{3e^2}{2c_W^2 s_W^2}\left(\frac{m_t}{m_Z}\right)^2 + \frac{3e^2}{4c_W^2 s_W^2}\left(\frac{m_t}{m_{T_L}}\right)^2 + \frac{3e^2}{4c_W^2 s_W^2}\left(\frac{m_{T_L}}{m_Z}\right)^2 \\ & \left. + \frac{3e^2}{4c_W^2 s_W^2} - \frac{3e^2}{2c_W^2 s_W^2}\left(\frac{m_Z}{m_{T_L}}\right)^2\right] (c_{T_L Zt})^2. \end{aligned} \tag{4.5}$$

The partial width corresponding to the decay mode of T_L into $h\ t$ is as follows

$$\begin{aligned}\Gamma_{ht} =& \frac{1}{96\pi m_{T_L}^3}(m_h^4 - 2m_h^2 m_t^2 - 2m_h^2 m_{T_L}^2 + m_t^4 - 2m_t^2 m_{T_L}^2 + m_{T_L}^4)^{1/2}\times \\ & \left[-3m_h^2 + 3m_t^2 + 3m_{T_L}^2\right] (c_{T_L th})^2, \end{aligned} \tag{4.6}$$

this can be expanded in powers of $\frac{m_h}{m_{T_L}}$ or $\frac{m_h}{m_{T_L}}$, we obtain

$$\begin{aligned}\Gamma_{ht} =& \frac{m_{T_L}}{96\pi}\left\{1 + \mathcal{O}\left[\left(\frac{m_h}{m_{T_L}}\right)^2\right] + \mathcal{O}\left[\left(\frac{m_t}{m_{T_L}}\right)^2\right]\right\}\times \\ & \left[-3\left(\frac{m_h}{m_{T_L}}\right)_h^2 + 3\left(\frac{m_t}{m_T}\right)^2 + 3\right] (c_{T_L th})^2. \end{aligned} \tag{4.7}$$

The Goldstone equivalence theorem as in Ref [42] implies that the ratios of the branching fractions of $T_L \to th$, tZ and $W^+ b$ are approximately 1:1:2. Then, for $m_{T_L} \gg m_h, m_t, m_W$ we have $\Gamma_{Zt} \simeq \Gamma_{ht}$, which results in a relation between

$c_{T_L Zt}$ and $c_{T_L th}$ as follows

$$\frac{e}{2c_W s_W}\left(\frac{m_{T_L}}{m_Z}\right) c_{T_L Zt} = c_{T_L th}. \tag{4.8}$$

In addition, to obtain the relation between $c_{T_L tZ}$ and $c_{T_L bW}$, we write the $T_L \to W^+ b$ partial width,

$$\begin{aligned}\Gamma_{W^+b} =& \frac{1}{96\pi m_{T_L}^3}(m_b^4 - 2m_b^2 m_{T_L}^2 - 2m_b^2 m_W^2 + m_{T_L}^4 - 2m_{T_L}^2 m_W^2 + m_W^4)^{1/2}\times \\ & \left[\frac{3e^2}{2s_W^2}m_b^4 + \frac{3e^2}{2s_W^2}m_{T_L}^2 + \frac{3e^2}{2s_W^2 m_W^2}m_b^4 - \frac{3e^2}{s_W^2 m_W^2}m_b^2 m_{T_L}^2 \right. \\ & \left. + \frac{3e^2}{2s_W^2 m_W^2}m_{T_L}^4 - \frac{3e^2}{s_W^2}m_W^2\right](c_{T_L bW})^2. \end{aligned} \tag{4.9}$$

In an analogous way to the previous expansion (4.6), but now expanding in powers of $\frac{m_W}{m_{T_L}}$ or $\frac{m_b}{m_{T_L}}$, we obtain

$$\begin{aligned}\Gamma_{W^+b} =& \frac{m_{T_L}}{96\pi}\left\{1 + \mathcal{O}\left[\left(\frac{m_b}{m_{T_L}}\right)^2\right] + \mathcal{O}\left[\left(\frac{m_W}{m_{T_L}}\right)^2\right]\right\}\left[\frac{3e^2}{2s_W^2}\left(\frac{m_b}{m_{T_L}}\right)^2 \right. \\ & + \frac{3e^2}{2s_W^2} + \frac{3e^2}{2s_W^2}\left(\frac{m_b^2}{m_W m_{T_L}}\right)^2 - \frac{3e^2}{s_W^2}\left(\frac{m_b}{m_W}\right)^2 \\ & \left. + \frac{3e^2}{2s_W^2}\left(\frac{m_{T_L}}{m_W}\right)^2 - \frac{3e^2}{2s_W^2}\left(\frac{m_W}{m_{T_L}}\right)^2\right](c_{T_L bW})^2. \end{aligned} \tag{4.10}$$

Again we use the equivalence theorem to establish the relation between $c_{T_L Zt}$ and $c_{T_L bW}$, imposing that $\Gamma_{Zt} \simeq \frac{1}{2}\Gamma_{W^+b}$, which results in

$$\frac{1}{c_W}\left(\frac{m_W}{m_Z}\right) c_{T_L tZ} = c_{T_L bW}. \tag{4.11}$$

Notice that the coupling $c_{T_L th} = Y_{T_L th}$, where $Y_{T_L th}/\sqrt{2}$ is inferred from the third column in Table (3.3). Using (4.7), (4.8), we can study the EW single T_L production for instance at the LHC. Figure (4.1) shows the single production of T_L through fusion of $W\ b$, i.e., involving $c_{T_L bW}$. We will consider both the model-independent case as well as the case of quiver theories. On the one hand we will consider the couplings given in Ref. [42], here we point out that $c_{T_L bW}$ is actually $\sin\theta_u^L$ mentioned in Subsection (3.2.1), for the study of the single production of the heavy fermion. On the other hand, from the quiver theory the couplings given in Table (3.3) will be also considered. According to quiver theories, once we fix

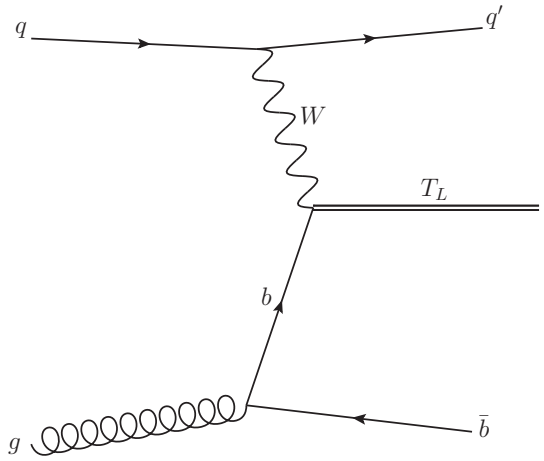

Figure 4.1. Production diagram for the process pp$\to T_L\bar{b}j$ with W, inferred from (4.3).

the parameters, e.g., N, v_1 and v_N, we are ready to compute all the couplings of the excited fermions, relevant for their production and decay at the LHC. In the next section we consider the pair production and the single production of T_L.

4.1 Heavy T_L Production at LHC

In this section, we consider T_L production. On the one hand, there is a heavy quark pair production via QCD, where these pairs come from quark-antiquark and gluon-gluon fusion [43, 44]. On the other hand, we consider the single production channel of T_L via the W b EW fusion. This production mode is shown in Figure (4.1).

We computed the pair and single T_L production cross section at the LHC with $s = \sqrt{13}$ by using MadGraph [45]. The first production mode is model-independent since is just QCD pair production. Figure (4.2) shows these production modes as a function of m_{T_L}. We considered the single production channel of T_L via the W exchange process pp$\to T_L\bar{b}j$ as can be seen in the top panel of Figure (4.2), the black line shows the pair production of T_L via QCD, whereas the other lines correspond to the single production for fixed values of the couplings $c_{T_LbW} \lesssim 0.4$ as considered in Ref. [42]. It shows that the single production dominates for m_{T_L} greater than 1 TeV.

Also, the T_L production as a function of the mass of T_L in quiver theories was computed. As shown in the bottom panel of Figure (4.2), the pair T_L pro-

duction is the same as in the top panel case. While, the single production cross section is given for the cases N=4 and N=15 by the medium turquoise and dark turquoise lines, respectively. It is shown that the pair production dominates for m_{T_L} masses below 1 TeV for both cases N=4 and N=15; however the single production dominates for m_{T_L} greater than 1 TeV and 3.9 Tev for N=15 and N=4 respectively.

4.2 Analysis Heavy T_L Decay Modes

Here, we examine the T_L decay to the Higgs sector and the additional way in which T_L can decay, i.e., the decay mode $T_L \to Gt$, where G the color-octet. To study the contribution of G to the signal, we will first compute the mass difference between T_L and G, i.e. Δm, for quiver models couplings. In order to have comparable branching ratios, the following condition is required

$$\Gamma_{W^+b} \lesssim \Gamma_{Gt}, \tag{4.12}$$

where Γ_{Gt}, is the $T_L \to Gt$ partial width and is given by

$$\begin{aligned}\Gamma_{Gt} =& \frac{1}{24\pi m_G^2 m_{T_L}^3}(m_G^4 - 2m_G^2 m_t^2 - 2m_G^2 m_{T_L}^2 + m_t^4 - 2m_t^2 m_{T_L}^2 + m_{T_L}^4)^{1/2}\times \\ & \left[m_{T_L}^4 + m_G^2 m_t^2 - 2m_G^4 + m_G^2 m_{T_L}^2 + m_t^4 - 2m_t^2 m_{T_L}^2\right](g_{T_L Gt})^2. \end{aligned} \tag{4.13}$$

We consider quiver models with $N = 4(15)$, with couplings $g_{T_L Gt} = 0.85(0.83)$ and $Y_{t_L Ht} = 0.028(0.352)$, respectively. Notice that the coupling $c_{T_L ht} = Y_{t_L Ht}/\sqrt{2}$. Now, we can substitute (4.9), (4.13) in (4.12) and considering G mass to be 2 TeV, and then, after solving for m_{T_L}, the mass differences are listed in Table (4.1).

N	m_G [GeV]	min m_{T_L} [GeV]	Δm
4	2000	2172	172
15	2000	2278	279

Table 4.1. Masses involved in the decay modes of T_L to the color-octet and EW sector for $N = 4, 15$.

From the information of the bottom panel of Figure (4.2) and Table (4.1), we conclude that to produce a heavy T_L decaying to G with reasonable branching ratio, we must consider the single production as the dominant channel for $N = 15$.

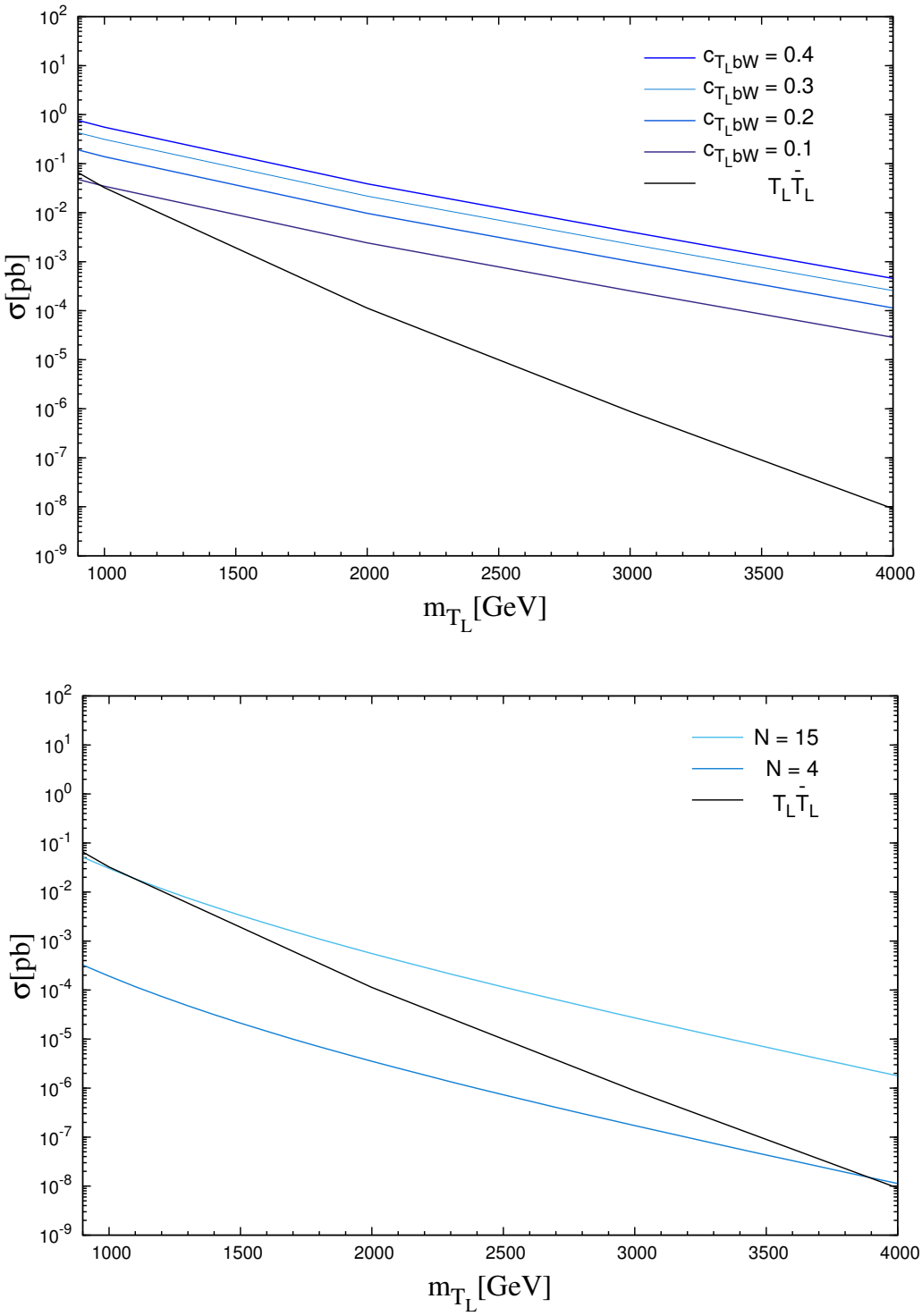

Figure 4.2. Cross sections for QCD pair and single production for T_L at LHC with $\sqrt{s} = 13$ TeV as a function of m_{T_L}. For fixed values of $c_{T_L bW}$ (top panel) and couplings from quiver theories with $N = 4, 15$ (bottom panel). In the later $c_{T_L ht}$ was inferred from the third column in Table (3.3) and $c_{T_L bW}$ vary according to (4.8) and (4.13) with respect to the T_L mass.

4.3 Prospects for the LHC

The previous section has shown that according the condition (4.12), is possible to study the case where both decay modes are comparable. The decay modes into the Higgs and EW gauge bosons were studied in the literature [37, 38, 42, 46]. Here, we will concentrate on the decay mode $T_L \to Gt$. We will consider both the $N = 15$ quiver theory as well as the model-independent case. We opted as signal process the production of that heavy top decaying into G, which afterwards decay into a pair of bottom quarks, i.e. pp$\to T_L bj \to Gtbj \to b\bar{b}bWbj$. To study the feasibility of detecting the signal we consider the example of single top production pp$\to tbj \to Wbbj$ as a background, this simple background was considered to estimate the required luminosity for the discovery of our signal. The couplings considered in for our signal were based on quiver theories with $N = 15$ and the masses were chosen to be m_T and m_G as 2.27 and 2 TeV, respectively. The cross sections both for signal and background were computed at $\sqrt{s} = 13$ TeV pp collider jointly with a cut given by $H_T > 500$ GeV (similar to Ref. [42]), where H_T is the total transverse hadronic energy and defined by

$$H_T = \sum_{hadronic\ particles} \|\vec{p}_T\|, \tag{4.14}$$

where $\vec{p}_T$ is the transverse momentum.

Thus, considering this cut we simulated 50K and 500K events for signal and background, respectively. To generate the events, the chain MadGraph [45]-Pythia [47]-Delphes [48] was used. After that, the comparison between the signal and background distributions was obtained by using Madanalysis (ma5) [49, 50, 51]. The baseline luminosity was assumed to be 1 ab^{-1}. Then, we implemented other kinematic cuts on the events as can be seen in Table (4.2). It shows a summary of the results of applying simple kinematic cuts, the selected cuts were inferred sequentially according to the kinematic distributions showed in Figures (4.3), (4.4), and (4.5). We considered the Fastjet algorithm anti-kt with $\Delta R = 0.6$ interfaced in ma5. For details of the recombination algorithm anti-kt see [52].

For the first selection after generating events, we took into account the number of jets distributions as shown in Figure (4.3). To compare the shapes of the curves related to both background and signal datasets, the events were normalized to unity. We select the following cut

$$N_j > 6, \tag{4.15}$$

	Signal	SM single top
Cross section	5.2×10^{-5} pb	0.2 pb
Events before cuts	50K a.u.	500K a.u.
$N_j > 6$	19952	51112
$H_T > 800$ GeV	18272	22290
$p_{T,j_1} > 400$ GeV	14231	7408
Reco. Eff.	0.28	1.48×10^{-2}

Table 4.2. Best cut-flow analysis obtained with ma5. Notice that a generator cut of $H_T > 500$ GeV was applied. Fastjet algorithm anti-kt with $\Delta R = 0.6$.

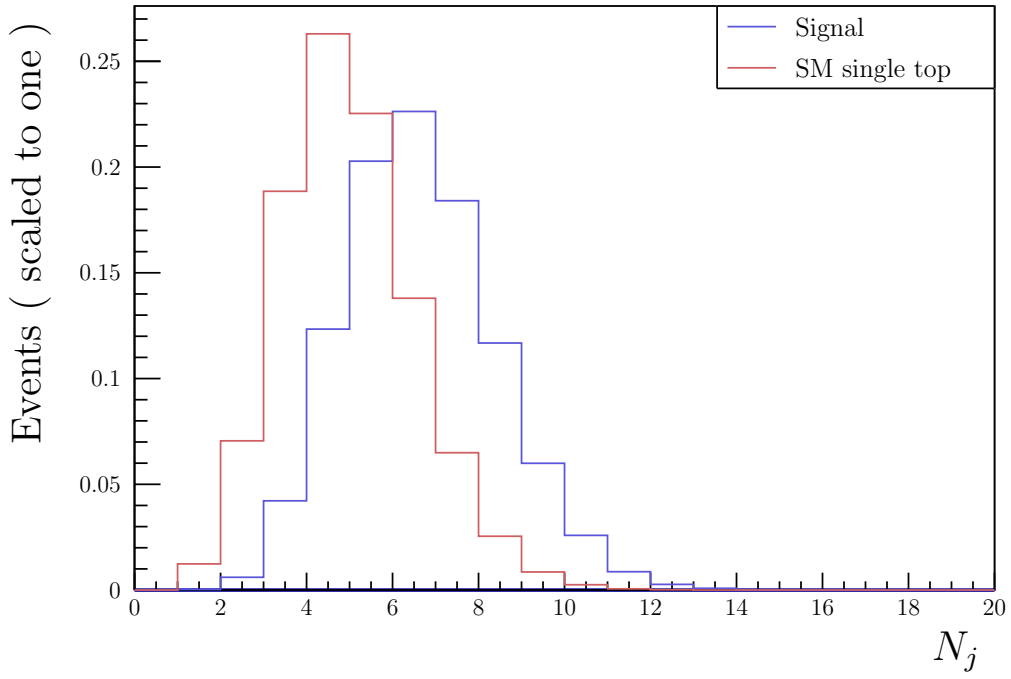

Figure 4.3. Number of jets distributions for events normalized to unity before any cuts.

where N_j, is the number of jets. Figure (4.4) shows the total transverse hadronic energy of jets distributions after the selection (4.15). To obtain this plot the events also were normalized to unity. So a good discrimination between signal and background can be obtained by using the following cut

$$H_T > 800 \text{ GeV}. \tag{4.16}$$

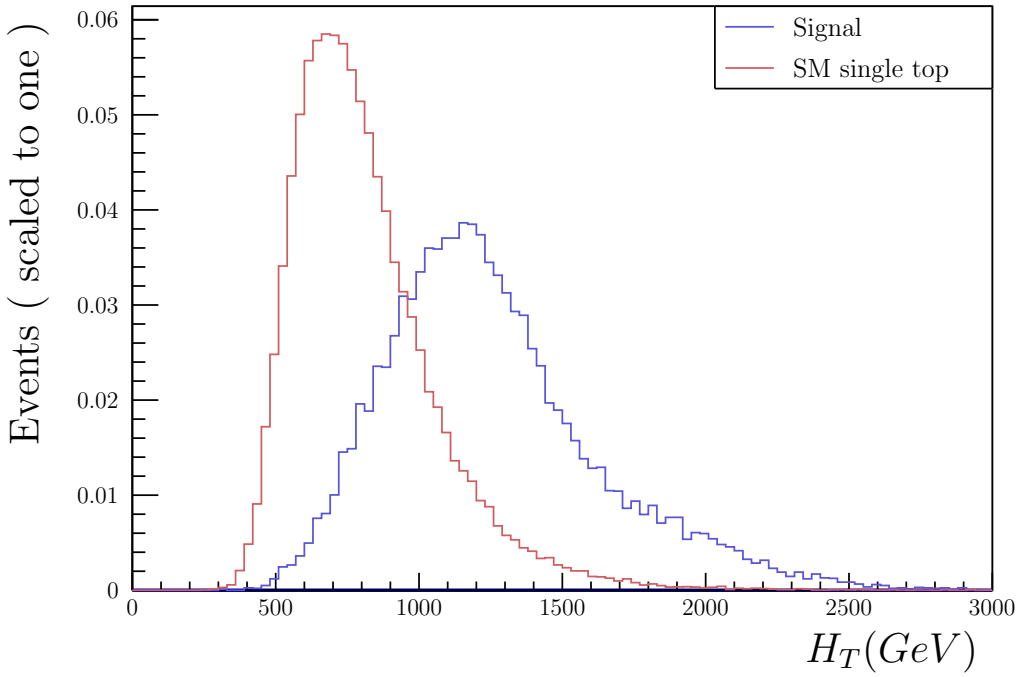

Figure 4.4. Total transverse hadronic energy of jets distributions for events normalized to unity after the selection $N_j > 6$.

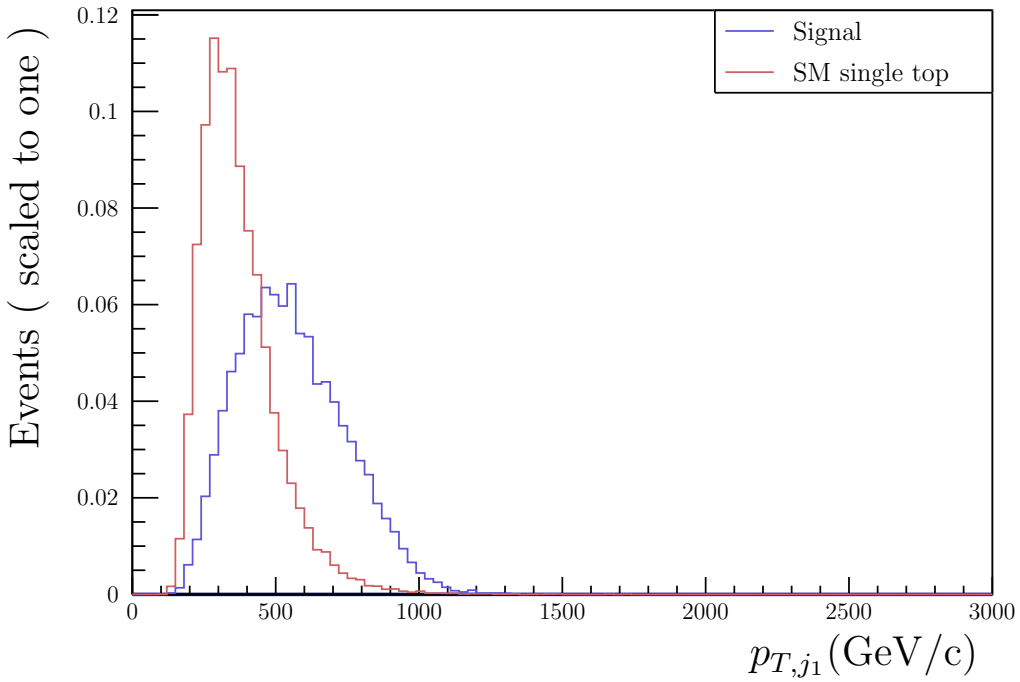

Figure 4.5. Transverse-momentum of the hardest jet distributions for events normalized to unity after the selection $H_T > 800$ GeV.

After these cuts, we also considered the transverse-momentum of the hardest jet distributions for events as shown in Figure (4.5), in such a way that to compare both signal and background distributions the events were also normalized to unity in this plot. Then, we select

$$p_{T,j_1} > 400 \text{ GeV}, \tag{4.17}$$

where p_{T,j_1} is the transverse-momentum of the hardest jet.

Now, from the values in Table (4.2), we are able to estimate the amount of luminosity that we need in order to have 5σ discovery. To estimate the required luminosity for 5σ we impose that $S/\sqrt{B} \geqslant 5$, where S and B are the number of events after cuts, which scale linearly with the luminosity. Then the previous requirement can be written as,

$$\mathcal{L} \geq 25 \frac{\sigma_B \times \epsilon_B}{(\sigma_S \times \epsilon_S)^2}, \tag{4.18}$$

where σ_B and σ_S are the background and signal cross sections, respectively. In (4.18) we also have that ϵ_B and ϵ_S are the efficiencies after cuts (these are given in the last row of Table (4.2)) for the background and signal, respectively. Then substituting the numerical values in (4.18), we have

$$\begin{aligned} &\geq 25 \frac{0.2 \times 1.48 \times 10^{-2}}{(5.2 \times 10^{-5} \times 0.28)^2} \times \frac{1}{1000} fb^{-1}, \\ &\geq \frac{7.4 \times 10^{-5}}{2.1 \times 10^{-10}} fb^{-1}, \\ &\geq 3.52 \times 10^5 fb^{-1} \ \left(352 ab^{-1}\right). \end{aligned} \tag{4.19}$$

Clearly, this number is too big to be achieved by the LHC, for these parameters the LHC will not be sensitive to quiver theories for high masses of the vector-like quarks.

On the other hand, we can estimate the reach of the model-independent scheme presented in Section (3.2). For instance, rescaling the calculations above, this is due to the main channel for the signal is proportional to $c^2_{T_L W b}$, so we have that

$$\mathcal{L} \geq 25 \frac{\sigma_B \times \epsilon_B}{(\sigma_S \times \epsilon_S)^2} \times \left(\frac{0.027}{c_{T_L W b}}\right)^4, \tag{4.20}$$

where 0.027 was the value of $c_{T_L W b}$ for $N = 15$. Now, we can see that a 5σ discovery can be achieved with the following values of the parameters: $c_{T_L W b} \geq 0.16$ for $300 fb^{-1}$, $c_{T_L W b} \geq 0.12$ for $1000 fb^{-1}$ and $c_{T_L W b} \geq 0.09$ for a High-Luminosity

Large Hadron Collider (HL-LHC) with $3000 fb^{-1}$.

The objects considered are too heavy, such that one possibility to study these kind of particles will be consider pp colliders, at high energies, for instance at $\sqrt{s}$ = 100 TeV.

CHAPTER 5

Vector-Like Heavy Quarks at High Energy Colliders

As we saw in chapter 4 the LHC will not be sensitive for vector-like quark masses $\gtrsim 2TeV$ in quiver theories. And after estimating the coupling between the heavy top, bottom quark with W gauge boson in a model-independent approach, we concluded that more energy was need in cases where couplings are smaller than 0.09 and with large vector-like quark masses (> 2 TeV). Here we look at a hypothetical pp collider with $\sqrt{s} = 100$ TeV. Other center-of-mass energies are being considered, such as 27 TeV at the LHC tunnel.

Just as in the previous chapter we use as benchmark the case of the Vector-like quark $SU(2)$-singlet up-type, T, in the case where it is coupled to a heavy gluon G, such that T can decay into Gt with subsequent decays of G into a pair of bottom or top quarks. The electroweak decays of T obey the approximate relations,

$$\Gamma(T \to Ht) \simeq \Gamma(T \to Zt) \simeq \frac{1}{2}\Gamma(T \to W^+ b), \tag{5.1}$$

as seen in [42].

Although extensive research has been carried out on the EW channels: $T \to (H, Z)t$ and $T \to (b_L, W^+)$, no study of the $T \to Gt$ channel was done, we will focus on it. We will take into account that the interactions between T, t and G as well as b and G are through the qcd coupling.

We considered as signal process the single T production, such that T decays into Gt with subsequent decays of G into a quark pair of b and the quark t decaying semi-leptonically. We took into account the couplings indicated in Section (3.2) and the masses were chosen for T and G as 2.3 and 2 TeV, respectively.

At this high energies it is still true that the single-T production is dominant over the pair production, as seen in Figure (5.1). Even for small values of $\sin\theta_u^L$ such

as 0.1, single-T production dominates for $m_T > 2.2$ TeV, at this point of m_T jointly with $\sin\theta_u^L = 0.1$, the corresponding value of the Yukawa coupling is

$$Y_{34}^u = 1.315, \tag{5.2}$$

it is obtained by using the relations (3.154) and (3.150). The maximum value of the coupling $\sin\theta_u^L$ comes from the relation (3.159), and the maximum Yukawa coupling is given in the second row of Table (5.1), this would still be perturbative. Table (5.1) shows the Yukawa couplings that were obtained by using the allowed values of $\sin\theta_u^L$ according to (3.159) as well as the relations given in (3.150), (3.154) and considering the same mass for T indicated above.

$\sin\theta_u^L$	Y_{34}^u
0.4	5.25
0.3	3.94
0.2	2.63
0.1	1.31

Table 5.1. Values of the Yukawa coupling Y_{34}^u for $m_T = 2.3$ TeV as a function of $\sin\theta_u^L$.

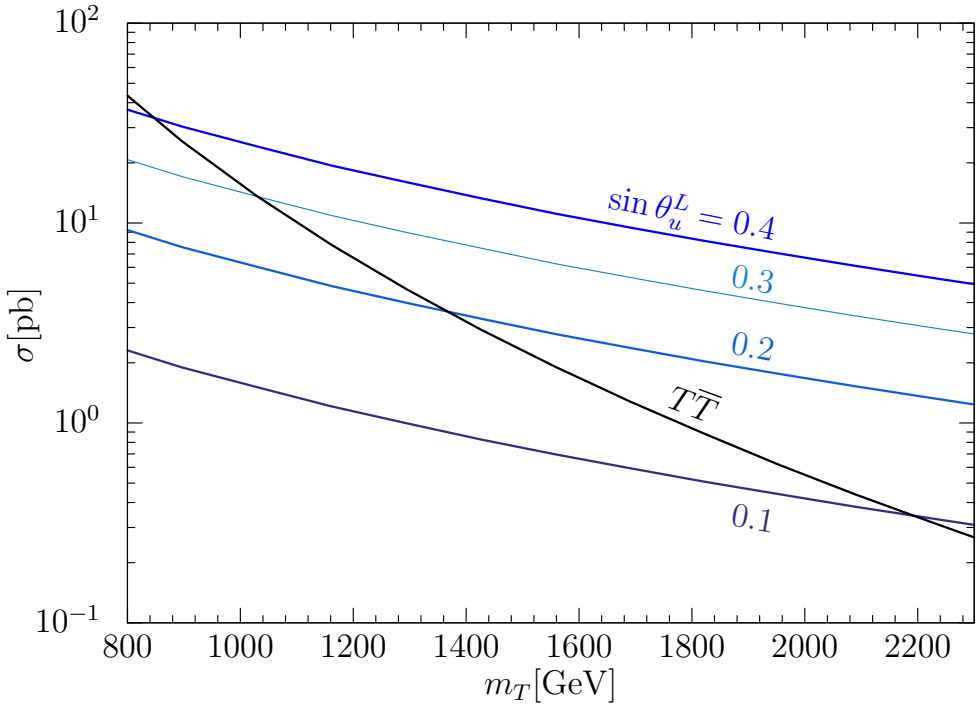

Figure 5.1. Cross section for single and pair T production at 100 TeV pp collider, as a function of the T mass.

The vector-like heavy quark pair production via QCD was considered, where these pairs come from quark-antiquark and gluon-gluon fusion. The pair production dominates for T masses below 0.8 TeV for T as a Vector-like $SU(2)$-singlet; however the single production dominates for m_T greater than 1 TeV, as shown in Figure (5.1).

The widths and branching ratios of T for the maximum value of $\sin\theta_u^L$ are shown in Table (5.2). The branching ratios of T to the EW sector are higher, of which the decay of T into a W^+ boson and a b quark provides easily the most proportion. Less than 1 percent of branching ratio consists of the heavy gluon mode.

$m_T = 2300$ [GeV]	Γ_T [GeV]	Br
$\Gamma(T \to W^+b)$	638.8	0.54
$\Gamma(T \to Ht)$	276.2	0.23
$\Gamma(T \to Zt)$	265.8	0.22
$\Gamma(T \to Gt)$	4.3	0.005

Table 5.2. Decays of T to the EW sector and the heavy gluon mode in units of GeV for $m_T = 2.3$ TeV, $\sin\theta_u^L = 0.4$ and $m_G = 2$ TeV.

We investigate whether the heavy gluon mode can be observed at this higher energies. Branching ratios are similar for other values of $\sin\theta_u^L$, as can be seen in Tables (5.3), (5.4) and (5.5). Similar results have been found for the branching ratios corresponding to the EW mode. However, for the heavy gluon mode its branching ratio increases with the decreases of $\sin\theta_u^L$. For instance, for $\sin\theta_u^L = 0.1$ the EW widths are lower when compared to the other cases, this is because the EW widths are increasing with $\sin\theta_u^L$.

$m_T = 2300$ [GeV]	Γ_T [GeV]	Br
$\Gamma(T \to W^+b)$	359.3	0.52
$\Gamma(T \to Ht)$	167.1	0.24
$\Gamma(T \to Zt)$	160.8	0.23
$\Gamma(T \to Gt)$	6.4	0.009

Table 5.3. Decays of T to the EW sector and the heavy gluon mode in units of GeV for $m_T = 2.3$ TeV, $\sin\theta_u^L = 0.3$ and $m_G = 2$ TeV.

$m_T = 2300$ [GeV]	Γ_T [GeV]	Br
$\Gamma(T \to W^+ b)$	159.7	0.50
$\Gamma(T \to Ht)$	78.3	0.25
$\Gamma(T \to Zt)$	75.4	0.24
$\Gamma(T \to Gt)$	6.4	0.02

Table 5.4. Decays of T to the EW sector and the heavy gluon mode in units of GeV for $m_T = 2.3$ TeV, $\sin\theta_u^L = 0.2$ and $m_G = 2$ TeV.

$m_T = 2300$ [GeV]	Γ_T [GeV]	Br
$\Gamma(T \to W^+ b)$	39.9	0.46
$\Gamma(T \to Ht)$	20.2	0.23
$\Gamma(T \to Zt)$	19.4	0.23
$\Gamma(T \to Gt)$	6.4	0.07

Table 5.5. Decays of T to the EW sector and the heavy gluon mode in units of GeV for $m_T = 2.3$ TeV, $\sin\theta_u^L = 0.1$ and $m_G = 2$ TeV.

5.1 Prospects for Future pp Colliders

In this section a different approach that showed in Section (4.3) will be considered, this due to the use of $\sqrt{s} = 100$ TeV pp collider and different relations to that considered in (4.12), for instance, as shown in Table (5.2), the widths of T to the EW sector are considerably higher than the heavy gluon mode. To study this latter mode of decay at $\sqrt{s} = 100$ TeV pp collider, the signal is pp$\to T\bar{b}j \to Gt\bar{b}j \to b\bar{b}W^+b\bar{b}j \to b\bar{b}l\nu_l b\bar{b}j$ and the backgrounds considered are pp$\to W^+bb\bar{b}\bar{b}j \to l\nu_l bb\bar{b}\bar{b}j$ and pp$\to t\bar{b}jb\bar{b} \to l\nu_l b\bar{b}jb\bar{b}$. We do not consider τ leptons in the final state because they are harder to identify. The cross sections for the signal and backgrounds were computed at $\sqrt{s} = 100$ TeV pp collider. We simulated 100K events for signal as well as backgrounds, these were obtained by using MadGraph. These events were analyzed in Madanalysis, and then the efficiencies were obtained. Simple cuts were applied as can be seen in Table (5.6), which shows a summary of the results. The events before cuts were normalized to 3000 fb^{-1} of luminosity.

Firstly, considering $\sin\theta_u^L = 0.4$, we implemented kinematic cuts on the events as can be seen in Table (5.6). It shows a summary of the results of applying simple kinematic cuts, inferred sequentially according to the kinematic distributions showed in Figures (5.2) and (5.3).

	Signal	$W^+b\bar{b}\bar{b}j$	$t\bar{b}jb\bar{b}$	Significance
σ[pb]	0.0219	13.69	5.528	$S/\sqrt{B}$
Events before cuts	65700	41070000	16584000	9
$M_{j_1j_2} > 1900.0$ GeV	56607.1	888344	459708	49
$H_T > 2200.0$ GeV	42641	31213	8623.7	214

Table 5.6. Sequence of cuts analyzed in ma5 for $\sin\theta_u^L$=0.4.

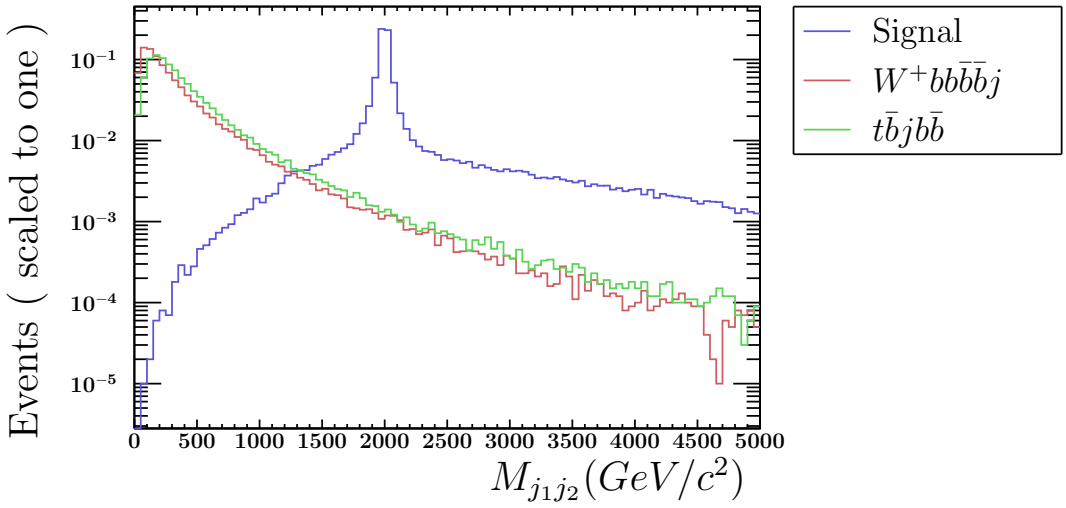

Figure 5.2. The invariant mass distribution for the two more energetic jets for the signal with $m_{T,G}$ = 2.3, 2 TeV, $\sin\theta_u^L$ = 0.4, and the $W^+b\bar{b}\bar{b}j$ and $t\bar{b}jb\bar{b}$ backgrounds before cuts.

For the first selection in Table (5.6) after generated events, we took into account the invariant mass distribution for the two more energetic jets as shown in Figure (5.2). To compare the shapes of the curves related to both background and signal datasets, the events were normalized to unity. We select the following cut

$$M_{j_1j_2} > 1900.0 \text{ GeV}, \tag{5.3}$$

where $M_{j_1j_2}$, is the invariant mass of the two more energetic jets. Figure (5.3) shows the distributions of the total transverse energy in jets, H_T after the selection (5.3). To obtained this plot the events also were normalized to unity. So a good discrimination between signal and background can be obtained by using the following cut

$$H_T > 2200.0 \text{ GeV}, \tag{5.4}$$

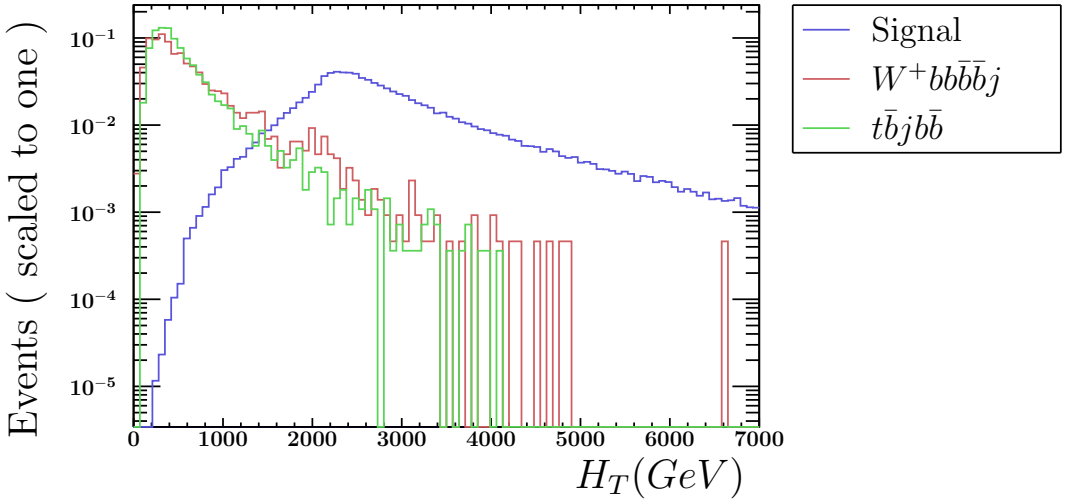

Figure 5.3. The transverse hadronic energy distribution for the signal with $m_{T,G} = 2.3$, 2 TeV, $\sin\theta_u^L = 0.4$, and the $W^+b\bar{b}\bar{b}\bar{b}j$ and $t\bar{b}jb\bar{b}$ backgrounds after the selection $M_{j_1j_2} > 1900.0$ GeV.

Now, assuming 70% b-tagging efficiency, and then considering 4 b tags the significance will be

$$\frac{S}{\sqrt{B}} \simeq 50. \tag{5.5}$$

Secondly, considering $\sin\theta_u^L = 0.3$, we implemented kinematic cuts on the events as can be seen in Table (5.7). It shows a summary of the results of apply simple kinematic cuts, the selected cuts were inferred sequentially according to the kinematic distributions showed in Figures (5.4) and (5.5).

	Signal	$W^+b\bar{b}\bar{b}\bar{b}j$	$t\bar{b}jb\bar{b}$	Significance
σ[pb]	0.01595	13.69	5.528	$S/\sqrt{B}$
Events before cuts	47850	41070000	16584000	6
$M_{j_1j_2} > 1800$ GeV	42706.6	1004161	518415	35
$H_T > 2000$ GeV	34090.7	50926	12935	135

Table 5.7. Sequence of cuts analyzed in ma5 for $\sin\theta_u^L$=0.3.

For the first selection in Table (5.6) after generated events, we took into account the invariant mass distribution for the two more energetic jets as shown in Figure (5.4). To compare the shapes of the curves related to both background and signal datasets, the events were normalized to unity. We select the following cut

$$M_{j_1j_2} > 1800.0 \text{ GeV}. \tag{5.6}$$

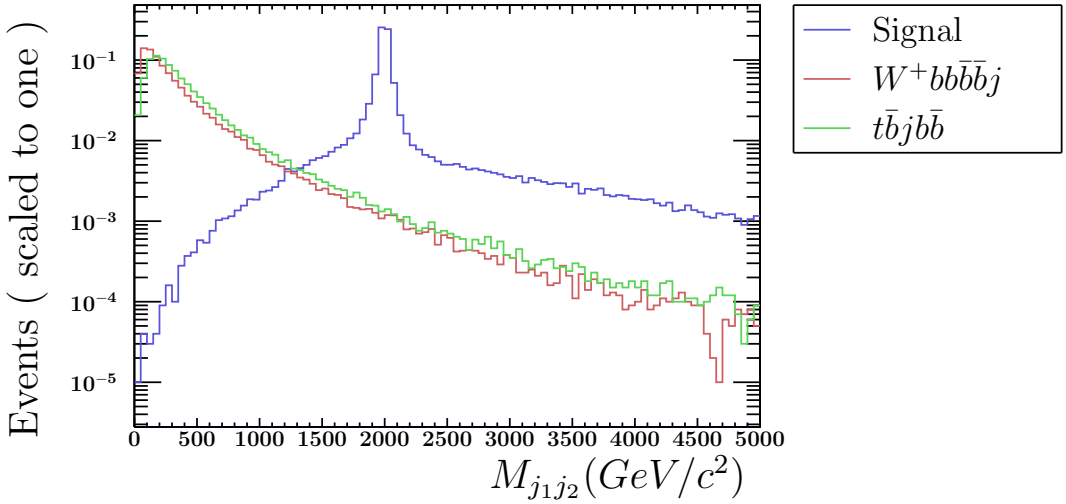

Figure 5.4. The mass distribution for the two more energetic jets for the signal with $m_{T,G} = 2.3$, 2 TeV, $\sin\theta_u^L = 0.3$, and the $W^+b\bar{b}\bar{b}\bar{b}j$ and $t\bar{b}jb\bar{b}$ backgrounds before cuts.

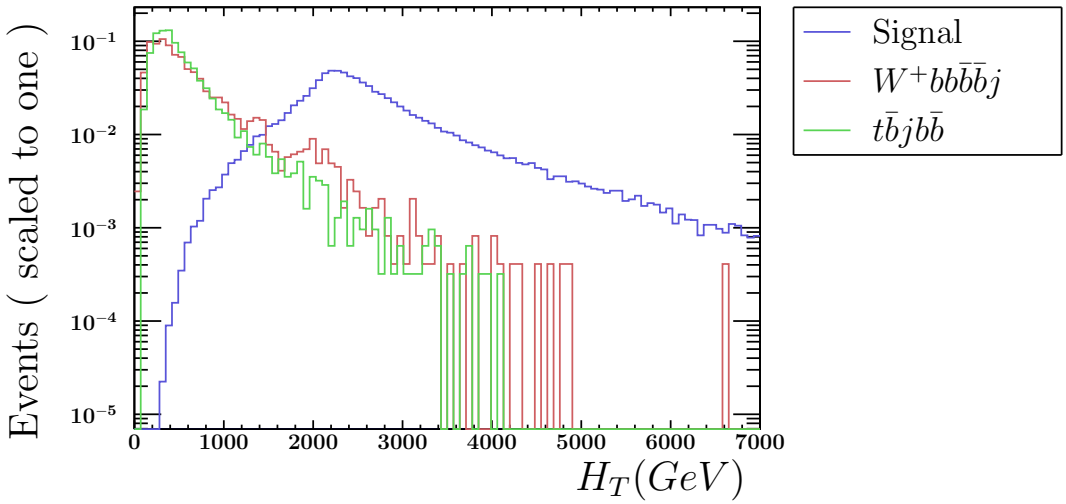

Figure 5.5. The transverse hadronic energy distribution for the signal with $m_{T,G} = 2.3$, 2 TeV, $\sin\theta_u^L = 0.3$, and the $W^+b\bar{b}\bar{b}\bar{b}j$ and $t\bar{b}jb\bar{b}$ backgrounds after the selection $M_{j_1 j_2} > 1800$ GeV.

Figure (5.5) shows the distributions of the total transverse energy in jets after the selection (5.6). To obtained this plot the events also were normalized to

unity. So a good discrimination between signal and background can be obtained by using the following cut

$$H_T > 2000.0 \text{ GeV}, \tag{5.7}$$

Now, assuming 70% b-tagging efficiency, and then considering 4 b tags the significance will be

$$\frac{S}{\sqrt{B}} \simeq 30. \tag{5.8}$$

Following this, considering $\sin\theta_u^L = 0.2$, we implemented kinematic cuts on the events as can be seen in Table (5.8). It shows a summary of the results of apply simple kinematic cuts, the selected cuts were inferred sequentially according to the kinematic distributions showed in Figures (5.6) and (5.7).

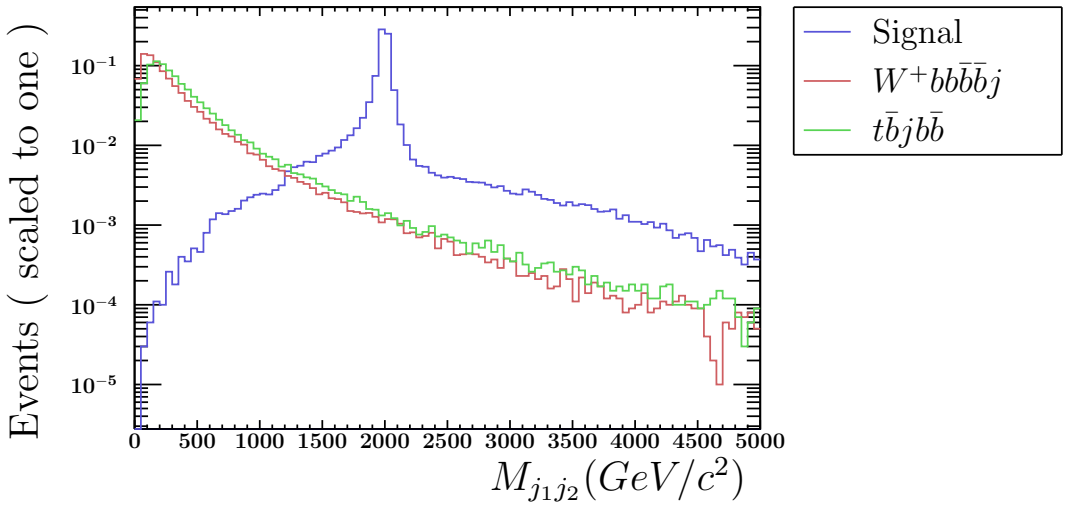

Figure 5.6. The mass distribution for the two more energetic jets for the signal with $m_{T,G} = 2.3$, 2 TeV, $\sin\theta_u^L = 0.2$, and the $W^+ b\bar{b}\bar{b}j$ and $t\bar{b}jb\bar{b}$ backgrounds before cuts.

	Signal	$W^+ b\bar{b}\bar{b}j$	$t\bar{b}jb\bar{b}$	Significance
σ[pb]	0.009938	13.69	5.528	$S/\sqrt{B}$
Events before cuts	29814	41070000	16584000	4
$M_{j_1 j_2} > 1800$ GeV	25922.4	1004161	518415	21
$H_T > 1800$ GeV	21132.2	70229	17744	71

Table 5.8. Sequence of cuts analyzed in ma5 for $\sin\theta_u^L$=0.2.

For the first selection in Table (5.8) after generated events, we took into account the invariant mass distribution for the two more energetic jets as shown in Figure (5.6). To compare the shapes of the curves related to both background and signal datasets, the events were normalized to unity. We select the following cut

$$M_{j_1 j_2} > 1800.0 \text{ GeV}. \tag{5.9}$$

Figure (5.7) shows the distributions of the total transverse energy in jets after the selection (5.9). To obtained this plot the events also were normalized to unity. So a good discrimination between signal and background can be obtained by using the following cut

$$H_T > 1800.0 \text{ GeV}, \tag{5.10}$$

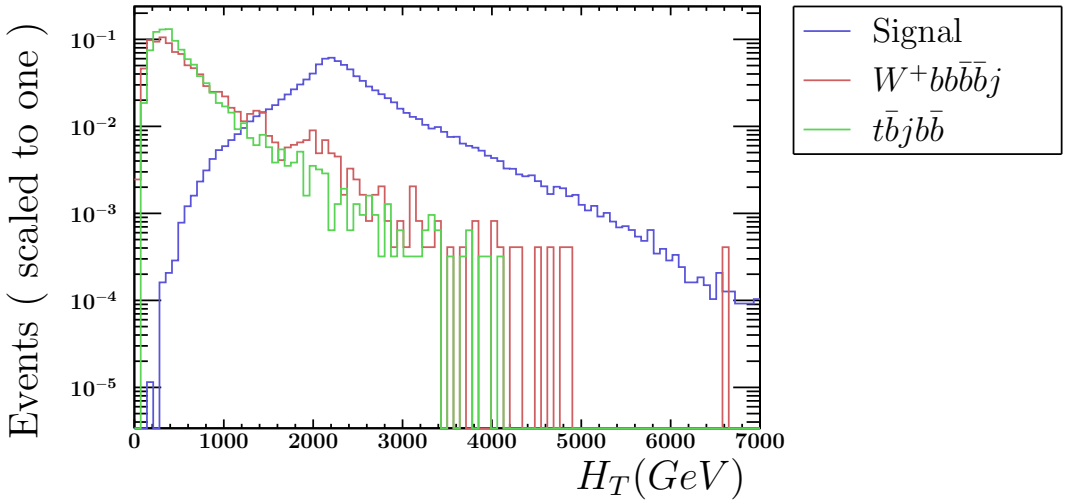

Figure 5.7. The transverse hadronic energy distribution for the signal with $m_{T,G} = 2.3$, 2 TeV, $\sin\theta_u^L = 0.2$, and the $W^+b\bar{b}\bar{b}\bar{b}j$ and $t\bar{b}jb\bar{b}$ backgrounds after the selection $M_{j_1 j_2} > 1800$ GeV.

Now, assuming 70% b-tagging efficiency, and then considering 4 b tags the significance will be

$$\frac{S}{\sqrt{B}} \simeq 17. \tag{5.11}$$

Finally, considering $\sin\theta_u^L = 0.1$, we implemented kinematic cuts on the events as can be seen in Table (5.9). It shows a summary of the results of apply sim-

ple kinematic cuts, the selected cuts were inferred sequentially according to the kinematic distributions showed in Figures (5.8) and (5.9).

	Signal	$W^+b\bar{b}\bar{b}j$	$t\bar{b}jb\bar{b}$	Significance
σ[pb]	0.005148	13.69	5.528	$S/\sqrt{B}$
Events before cuts	15443	41070000	16584000	2
$M_{j_1j_2} > 1850$ GeV	12313.5	946663	486076	10
$H_T > 1700$ GeV	9455.1	75979	19734	31

Table 5.9. Sequence of cuts analyzed in ma5 for $\sin\theta_u^L$=0.1.

For the first selection in Table (5.9) after generated events, we took into account the invariant mass distribution for the two more energetic jets as shown in Figure (5.8). To compare the shapes of the curves related to both background and signal datasets, the events were normalized to unity. We select the following cut

$$M_{j_1j_2} > 1850.0 \text{ GeV}. \tag{5.12}$$

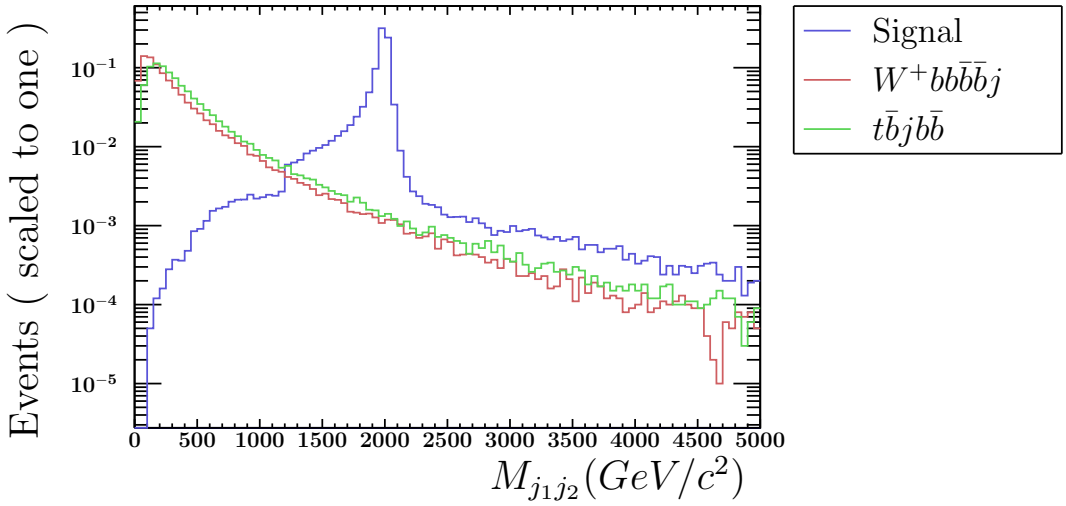

Figure 5.8. The mass distribution for the two more energetic jets for the signal with $m_{T,G} = 2.3$, 2 TeV, $\sin\theta_u^L = 0.1$, and the $W^+b\bar{b}\bar{b}j$ and $t\bar{b}jb\bar{b}$ backgrounds before cuts.

Figure (5.9) shows the distributions of the total transverse energy in jets after the selection (5.12). To obtained this plot the events also were normalized to unity. So a good discrimination between signal and background can be obtained

by using the following cut

$$H_T > 1700.0 \text{ GeV}, \tag{5.13}$$

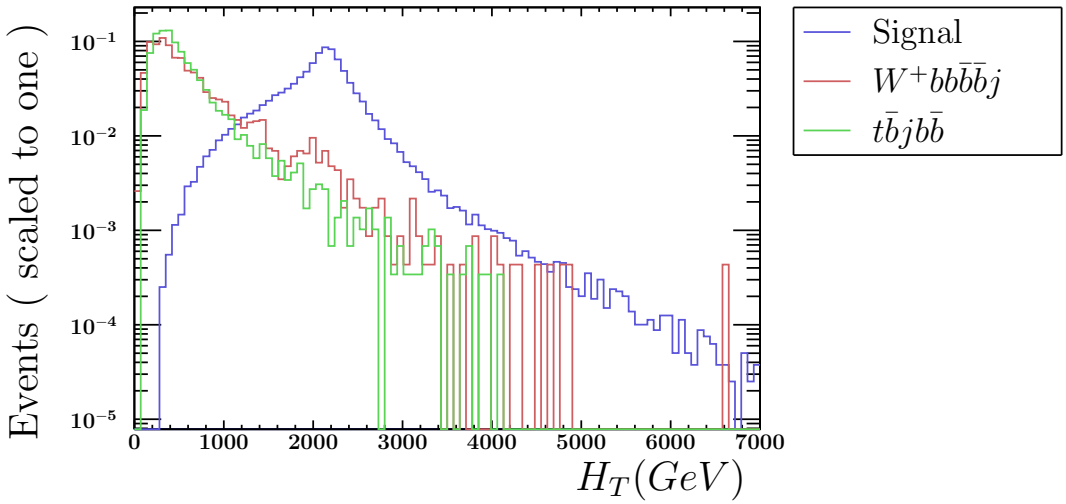

Figure 5.9. The transverse hadronic energy distribution for the signal with $m_{T,G} = 2.3$, 2 TeV, $\sin\theta_u^L = 0.1$, and the $W^+b\bar{b}\bar{b}\bar{b}j$ and $t\bar{b}jb\bar{b}$ backgrounds after the selection $M_{j_1j_2} > 1850$ GeV.

Now, assuming 70% b-tagging efficiency, and then considering 4 b tags the significance will be

$$\frac{S}{\sqrt{B}} \simeq 7. \tag{5.14}$$

For more realistic simulation we would like to consider as background the case where the involving final state has 5 jets jointly with $e^-\nu$ or $\mu^-\nu$. In addition that, for futures studies we can consider the EW decay modes to study the phenomenology at high energy colliders.

We do not have different kinematic cuts for each different values of $\sin\theta_u^L$, that is the sequence of cuts implemented as in Table (5.9) should be more than adequate. The ratio $\frac{S}{\sqrt{B}}$ is large enough for $\sin\theta_u^L = 0.1$ to be promising for larger m_T and smaller values of $\sin\theta_u^L$, this work is in progress.

For more realistic study, we need to simulate more backgrounds. But looks promising.

Also, we need to add pile-up effect, it is still unknown for future machine, we do not know machine parameters, but can guess that pile-up is large.

Ultimately, it looks like $\sqrt{s} = 100$ TeV pp collider is how we will be able to study a new sector of vector-like quarks with large masses in detail.

CHAPTER 6

Conclusions and Outlook

Extensions of the SM that solve the hierarchy problem by having the Higgs as a pNGB typically must contain new vector-like quarks. In this thesis are studied the phenomenology of vector-like quarks in two such theories: quiver theories and a model-independent effective theory of vector-like quarks. In the case of quiver theories we computed the spectrum and couplings of vector-like quarks as well as excited gauge bosons to SM states, particularly $W^{\pm}$, Z and the Higgs. In the last case we needed to formulate the Higgs as a pNGB in the quiver theory. Once we obtained the spectrum and its couplings we started studying the phenomenology of vector-like quarks at the LHC. We saw that for quiver theories the production cross section are dominated by the single T channel, is too small even for the HL-LHC. The reason was a combination of the small TWb coupling and the large value of m_T. the vector-like quark mass.

For the model-independent approach we concluded that the LHC could discover the $T \to Gt$ decay channel with 300 fb^{-1} if $c_{TWb} > 0.16$, and for 3000 fb^{-1} (the ultimate HL-LHC luminosity) if $c_{TWb} > 0.09$. Thus is clear that for $m_T \gtrsim$ 2TeV, quiver theories uses $c_{TWb} \simeq 0.03$, are out of reach of the LHC.

The results of chapter 4 indicated that in order to study the $T \to Gt$ in quiver theories for $m_T > 2$TeV higher center-of-mass energies are needed. In chapter 5 we started a study of this channel for a hypothetical pp collider with $\sqrt{s} =$ 100 TeV. We studied the signal to background significance after cuts for various values of the coupling responsible for single T production. As a first pass, we used pp$\to W^+ b\bar{b}\bar{b}j \to l\nu_l b\bar{b}\bar{b}j$, and pp$\to t\bar{b}jb\bar{b} \to l\nu_l b\bar{b}jb\bar{b}$ as background.

We conclude that for $\sqrt{s} = 100$ TeV 5σ discoveries will be accessible for couplings well below 0.1, other possible.

In the future a more complete background study will be needed. Furthermore,

there is a need to include the effects of pile-up which were not considered here. We can see that if the discoveries of the LHC point to the possibility of heavy vector-like quarks, high energy pp colliders could study these sector in detail.

Appendices

Appendix A

Wave-Function of Excited States

An specific example for hypothetical fermion with left-handed zero mode and localization parameter $c_L = 0.2$, in this case the left-handed zero mode is localized toward the N-th site, we show their Wave-Functions in Figures A.1, A.2 and A.3 for $N = 4$, $N = 9$ and $N = 15$ respectively.

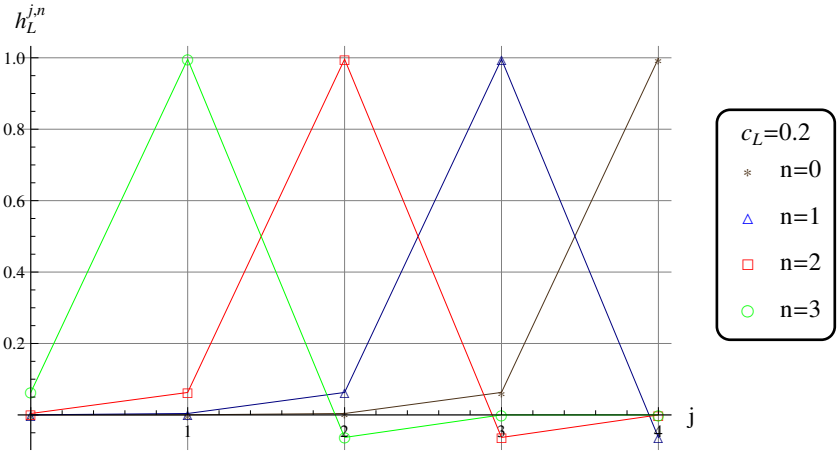

Figure A.1: Wave-Functions of hypothetical fermion with left-handed zero mode and localization parameter $c_L = 0.2$, where j is a index of site and n is a index of Kaluza-Klein mode. In this case $N = 4$ and some allowed n are shown. For the visualization, we choose by the opposite signs of $h_L^{j,1}$ and $h_L^{j,2}$.

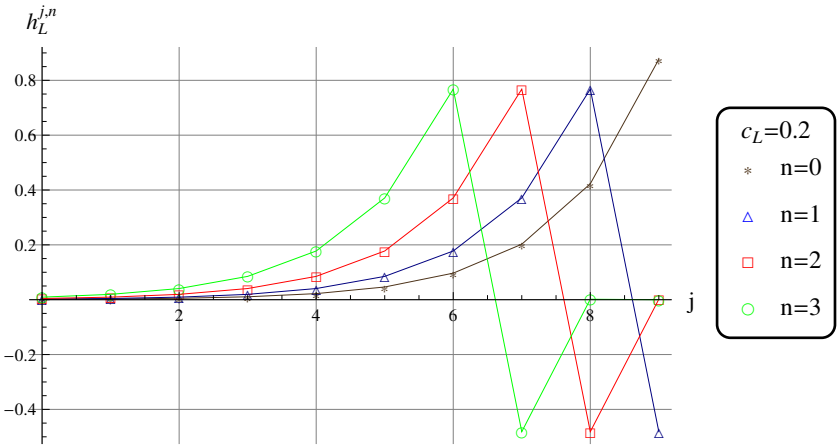

Figure A.2: Wave-Functions of hypothetical fermion with left-handed zero mode and localization parameter $c_L = 0.2$, where j is a index of site and n is a index of Kaluza-Klein mode. In this case $N = 9$ and some allowed n are shown. For the visualization, we choose by the opposite sign of $h_L^{j,3}$.

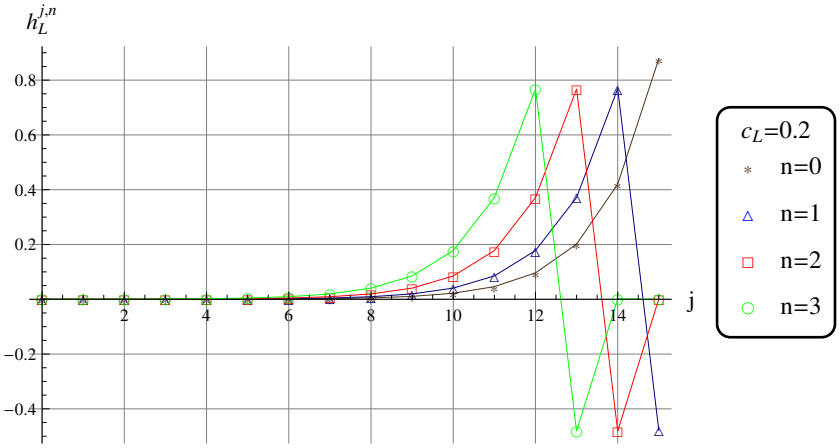

Figure A.3: Wave-Functions of hypothetical fermion with left-handed zero mode and localization parameter $c_L = 0.2$, where j is a index of site and n is a index of Kaluza-Klein mode. In this case $N = 15$ and some allowed n are shown.

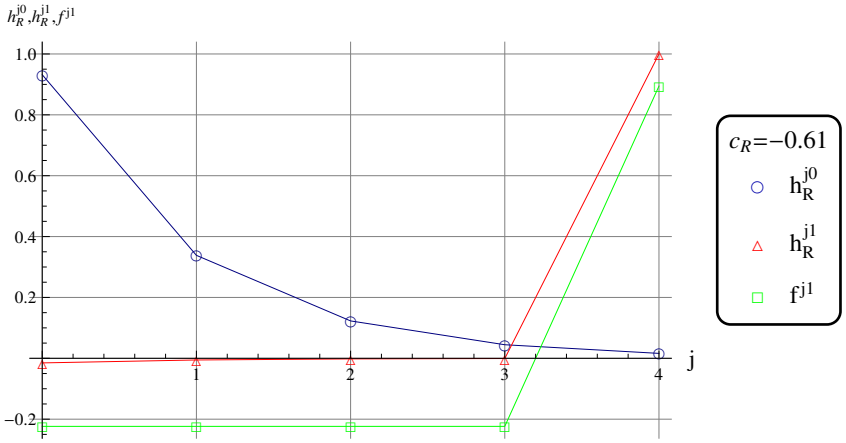

Figure A.4: Wave-Functions zero mode $h_R^{j,0}$, first mode $h_R^{j,1}$ of bottom fermion with right-handed zero mode and localization parameter $c_R = -0.61$, and Wave-Function first mode of gauge boson $f^{j,1}$ where j is a index of site and n is a index of Kaluza-Klein mode. In this case $N = 4$ and some allowed n are shown. For the visualization, we choose by the opposite sign of $h_R^{j,0}$.

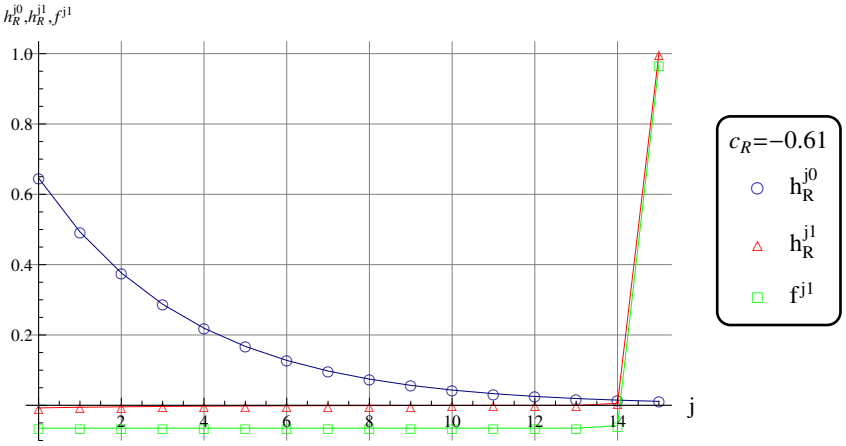

Figure A.5: Wave-Functions zero mode $h_R^{j,0}$, first mode $h_R^{j,1}$ of bottom fermion with right-handed zero mode and localization parameter $c_R = -0.61$, and Wave-Function first mode of gauge boson $f^{j,1}$ where j is a index of site and n is a index of Kaluza-Klein mode. In this case $N = 15$ and some allowed n are shown.

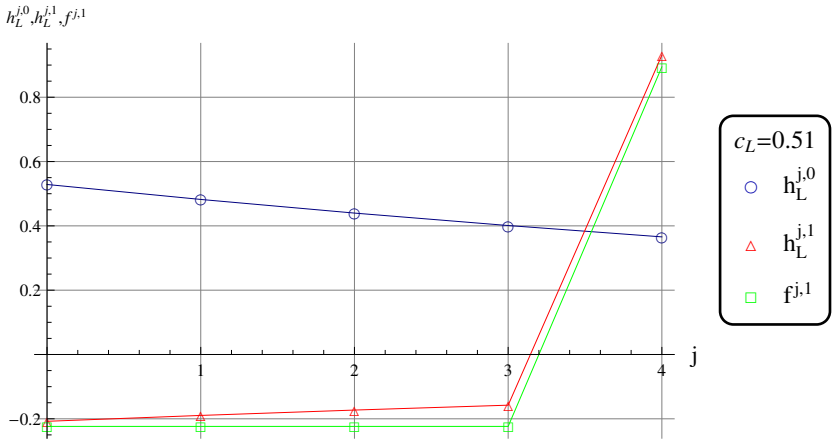

Figure A.6: Wave-Functions zero mode $h_L^{j,0}$, first mode $h_L^{j,1}$ of top fermion with left-handed zero mode and localization parameter $c_L = 0.51$, and Wave-Function first mode of gauge boson $f^{j,1}$ where j is a index of site and n is a index of Kaluza-Klein mode. In this case $N = 4$ and some allowed n are shown. For the visualization, we choose by the opposite sign of $h_L^{j,0}$.

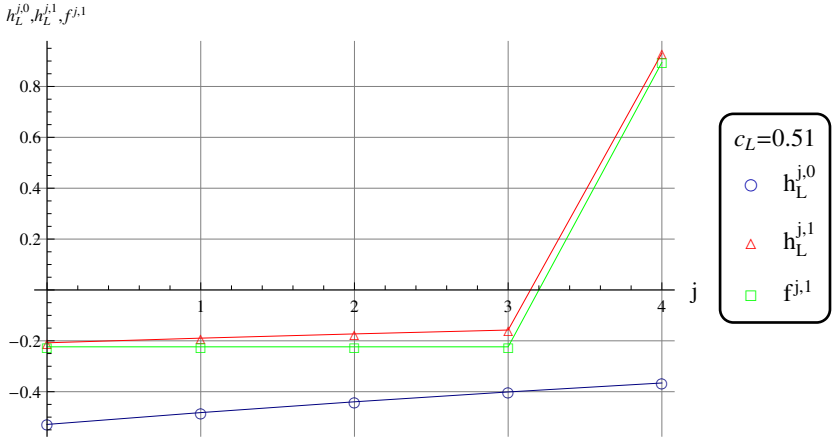

Figure A.7: Wave-Functions zero mode $h_L^{j,0}$, first mode $h_L^{j,1}$ of top fermion with left-handed zero mode and localization parameter $c_L = 0.51$, and Wave-Function first mode of gauge boson $f^{j,1}$ where j is a index of site and n is a index of Kaluza-Klein mode. In this case $N = 15$ and some allowed n are shown.

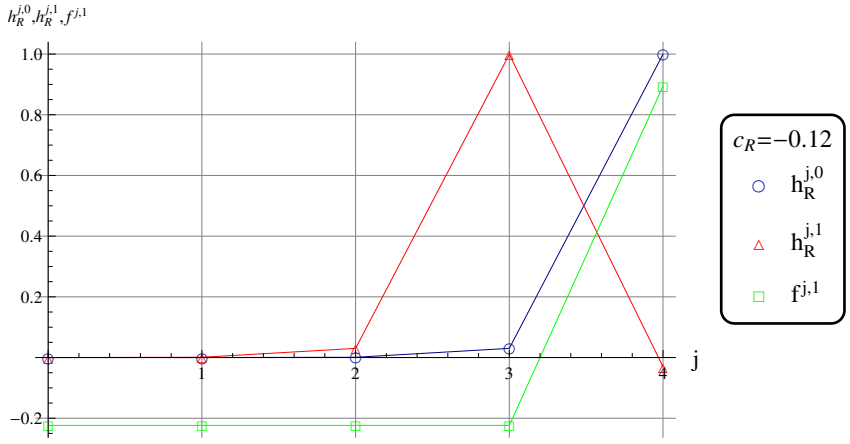

Figure A.8: Wave-Functions zero mode $h_R^{j,0}$, first mode $h_R^{j,1}$ of top fermion with right-handed zero mode and localization parameter $c_R = -0.12$, and Wave-Function first mode of gauge boson $f^{j,1}$ where j is a index of site and n is a index of Kaluza-Klein mode. In this case $N = 4$ and some allowed n are shown. For the visualization, we choose by the opposite sign of $h_R^{j,1}$.

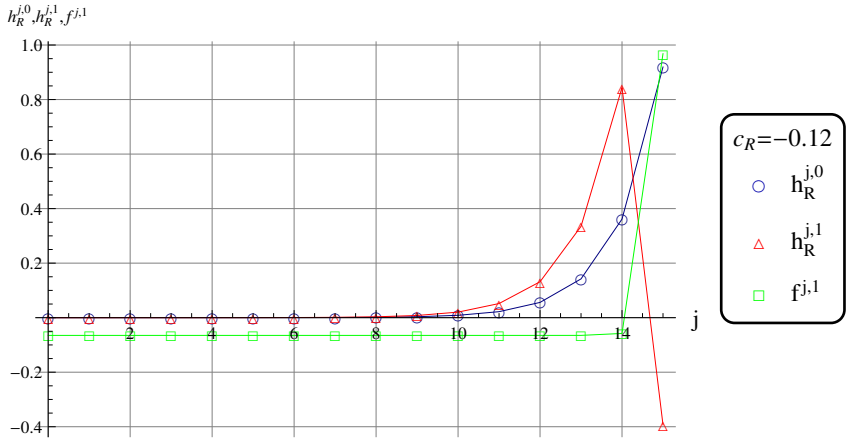

Figure A.9: Wave-Functions zero mode $h_R^{j,0}$, first mode $h_R^{j,1}$ of top fermion with right-handed zero mode and localization parameter $c_R = -0.12$, and Wave-Function first mode of gauge boson $f^{j,1}$ where j is a index of site and n is a index of Kaluza-Klein mode. In this case $N = 15$ and some allowed n are shown.

Appendix B

For the vector-like quark SM SU(2)-doublet, we pass the interactions between T', B' the SM third generations and the EW gauge bosons from the EW to the mass eigenstate,

$$
\begin{aligned}
&\frac{g}{\sqrt{2}}\bar{t}'_L \not{W}^+ b'_L + \frac{g}{\sqrt{2}}\bar{b}'_L \not{W}^- t'_L \\
&+ \frac{g}{c_W}\bar{t}'_L \not{Z} \left(\frac{1}{2} - \frac{2}{3}s_W^2\right) t'_L + \frac{g}{c_W}\bar{b}'_L \not{Z} \left(-\frac{1}{2} + \frac{1}{3}s_W^2\right) b'_L \\
&+ \frac{2gs_W}{3}\bar{t}'_L \not{A} t'_L - \frac{gs_W}{3}\bar{b}'_L \not{A} b'_L \\
&+ \frac{g}{c_W}\bar{t}'_R \not{Z} \left(-\frac{2}{3}s_W^2\right) t'_R + \frac{g}{c_W}\bar{b}'_R \not{Z} \left(\frac{1}{3}s_W^2\right) b'_R \\
&+ \frac{2gs_W}{3}\bar{t}'_R \not{A} t'_R - \frac{gs_W}{3}\bar{b}'_R \not{A} b'_R \\
&+ \frac{g}{\sqrt{2}}\overline{T}'_L \not{W}^+ B'_L + \frac{g}{\sqrt{2}}\overline{B}'_L \not{W}^- T'_L \\
&+ \frac{g}{c_W}\overline{T}'_L \not{Z} \left(\frac{1}{2} - \frac{2}{3}s_W^2\right) T'_L + \frac{g}{c_W}\overline{B}'_L \not{Z} \left(-\frac{1}{2} + \frac{1}{3}s_W^2\right) B'_L \\
&+ \frac{2gs_W}{3}\overline{T}'_L \not{A} T'_L - \frac{gs_W}{3}\overline{B}'_L \not{A} B'_L \\
&+ \frac{g}{\sqrt{2}}\overline{T}'_R \not{W}^+ B'_R + \frac{g}{\sqrt{2}}\overline{B}'_R \not{W}^- T'_R \\
&+ \frac{g}{c_W}\overline{T}'_R \not{Z} \left(\frac{1}{2} - \frac{2}{3}s_W^2\right) T'_R + \frac{g}{c_W}\overline{B}'_R \not{Z} \left(-\frac{1}{2} + \frac{1}{3}s_W^2\right) B'_R \\
&+ \frac{2gs_W}{3}\overline{T}'_R \not{A} T'_R - \frac{gs_W}{3}\overline{B}'_R \not{A} B'_R,
\end{aligned}
\tag{B.1}
$$

and then with the rotations defined by (3.166) into (B.1) we find that

$$
\begin{aligned}
&\frac{g}{\sqrt{2}}\left(c_L^u c_L^d \bar{t}_L \not{W}^+ b_L + c_L^u s_L^d \bar{t}_L \not{W}^+ B_L + s_L^u c_L^d \overline{T}_L \not{W}^+ b_L + s_L^u s_L^d \overline{T}_L \not{W}^+ B_L + \text{h.c.}\right)\\
&+\frac{g}{c_W}\left(\frac{1}{2}-\frac{2}{3}s_W^2\right)\left((c_L^u)^2 \bar{t}_L \not{Z} t_L + c_L^u s_L^u \bar{t}_L \not{Z} T_L + s_L^u c_L^u \overline{T}_L \not{Z} t_L + (s_L^u)^2 \overline{T}_L \not{Z} T_L\right)\\
&+\frac{g}{c_W}\left(-\frac{1}{2}+\frac{1}{3}s_W^2\right)\left((c_L^d)^2 \bar{b}_L \not{Z} b_L + c_L^d s_L^d \bar{b}_L \not{Z} B_L + s_L^d c_L^d \overline{B}_L \not{Z} b_L + (s_L^d)^2 \overline{B}_L \not{Z} B_L\right)\\
&+\frac{2gs_W}{3}\left((c_L^u)^2 \bar{t}_L \not{A} t_L + c_L^u s_L^u \bar{t}_L \not{A} T_L + s_L^u c_L^u \overline{T}_L \not{A} t_L + (s_L^u)^2 \overline{T}_L \not{A} T_L\right)\\
&-\frac{gs_W}{3}\left((c_L^d)^2 \bar{b}_L \not{A} b_L + c_L^d s_L^d \bar{b}_L \not{A} B_L + s_L^d c_L^d \overline{B}_L \not{A} b_L + (s_L^d)^2 \overline{B}_L \not{A} B_L\right)\\
&-\frac{2gs_W^2}{3c_W}\left((c_R^u)^2 \bar{t}_R \not{Z} t_R + c_R^u s_R^u \bar{t}_R \not{Z} T_R + s_R^u c_R^u \overline{T}_R \not{Z} t_R + (s_R^u)^2 \overline{T}_R \not{Z} T_R\right)\\
&+\frac{gs_W^2}{3c_W}\left((c_R^d)^2 \bar{b}_R \not{Z} b_R + c_R^d s_R^d \bar{b}_R \not{Z} B_R + s_R^d c_R^d \overline{B}_R \not{Z} b_R + (s_R^d)^2 \overline{B}_R \not{Z} B_R\right)\\
&+\frac{2gs_W}{3}\left((c_R^u)^2 \bar{t}_R \not{A} t_R + c_R^u s_R^u \bar{t}_R \not{A} T_R + s_R^u c_R^u \overline{T}_R \not{A} t_R + (s_R^u)^2 \overline{T}_R \not{A} T_R\right)\\
&-\frac{gs_W}{3}\left((c_R^d)^2 \bar{b}_R \not{A} b_R + c_R^d s_R^d \bar{b}_R \not{A} B_R + s_R^d c_R^d \overline{B}_R \not{A} b_R + (s_R^d)^2 \overline{B}_R \not{A} B_R\right)\\
&+\frac{g}{\sqrt{2}}\left(s_L^u s_L^d \bar{t}_L \not{W}^+ b_L - s_L^u c_L^d \bar{t}_L \not{W}^+ B_L - c_L^u s_L^d \overline{T}_L \not{W}^+ b_L + c_L^u c_L^d \overline{T}_L \not{W}^+ B_L + \text{h.c.}\right)\\
&+\frac{g}{c_W}\left(\frac{1}{2}-\frac{2}{3}s_W^2\right)\left((s_L^u)^2 \bar{t}_L \not{Z} t_L - s_L^u c_L^u \bar{t}_L \not{Z} T_L - c_L^u s_L^u \overline{T}_L \not{Z} t_L + (c_L^u)^2 \overline{T}_L \not{Z} T_L\right)\\
&+\frac{g}{c_W}\left(-\frac{1}{2}+\frac{1}{3}s_W^2\right)\left((s_L^d)^2 \bar{b}_L \not{Z} b_L - s_L^d c_L^d \bar{b}_L \not{Z} B_L - c_L^d s_L^d \overline{B}_L \not{Z} b_L + (c_L^d)^2 \overline{B}_L \not{Z} B_L\right)\\
&+\frac{2gs_W}{3}\left((s_L^u)^2 \bar{t}_L \not{A} t_L - s_L^u c_L^u \bar{t}_L \not{A} T_L - c_L^u s_L^u \overline{T}_L \not{A} t_L + (c_L^u)^2 \overline{T}_L \not{A} T_L\right)\\
&-\frac{gs_W}{3}\left((s_L^d)^2 \bar{b}_L \not{A} b_L - s_L^d c_L^d \bar{b}_L \not{A} B_L - c_L^d s_L^d \overline{B}_L \not{A} b_L + (c_L^d)^2 \overline{B}_L \not{A} B_L\right)\\
&+\frac{g}{\sqrt{2}}\left(s_R^u s_R^d \bar{t}_R \not{W}^+ b_R - s_R^u c_R^d \bar{t}_R \not{W}^+ B_R - c_R^u s_R^d \overline{T}_R \not{W}^+ b_R + c_R^u c_R^d \overline{T}_R \not{W}^+ B_R + \text{h.c.}\right)\\
&+\frac{g}{c_W}\left(\frac{1}{2}-\frac{2}{3}s_W^2\right)\left((s_R^u)^2 \bar{t}_R \not{Z} t_R - s_R^u c_R^u \bar{t}_R \not{Z} T_R - c_R^u s_R^u \overline{T}_R \not{Z} t_R + (c_R^u)^2 \overline{T}_R \not{Z} T_R\right)\\
&+\frac{g}{c_W}\left(-\frac{1}{2}+\frac{1}{3}s_W^2\right)\left((s_R^d)^2 \bar{b}_R \not{Z} b_R - s_R^d c_R^d \bar{b}_R \not{Z} B_R - c_R^d s_R^d \overline{B}_R \not{Z} b_R + (c_R^d)^2 \overline{B}_R \not{Z} B_R\right)\\
&+\frac{2gs_W}{3}\left((s_R^u)^2 \bar{t}_R \not{A} t_R - s_R^u c_R^u \bar{t}_R \not{A} T_R - c_R^u s_R^u \overline{T}_R \not{A} t_R + (c_R^u)^2 \overline{T}_R \not{A} T_R\right)\\
&-\frac{gs_W}{3}\left((s_R^d)^2 \bar{b}_R \not{A} b_R - s_R^d c_R^d \bar{b}_R \not{A} B_R - c_R^d s_R^d \overline{B}_R \not{A} b_R + (c_R^d)^2 \overline{B}_R \not{A} B_R\right), \qquad \text{(B.2)}
\end{aligned}
$$

Bibliography

[1] Georges Aad et al. Observation of a new particle in the search for the Standard Model Higgs boson with the ATLAS detector at the LHC. *Phys.Lett.*, B716:1–29, 2012.

[2] Serguei Chatrchyan et al. Observation of a new boson at a mass of 125 GeV with the CMS experiment at the LHC. *Phys.Lett.*, B716:30–61, 2012.

[3] J. Beringer et al. Review of Particle Physics (RPP). *Phys.Rev.*, D86:010001, 2012.

[4] L. Montanet et al. Review of particle properties. Particle Data Group. *Phys.Rev.*, D50:1173–1823, 1994.

[5] Gustavo Burdman. New solutions to the hierarchy problem. *Braz.J.Phys.*, 37:506–513, 2007.

[6] Gustavo Marques Tavares, Martin Schmaltz, and Witold Skiba. Higgs mass naturalness and scale invariance in the UV. *Phys.Rev.*, D89:015009, 2014.

[7] Yang Bai, Gustavo Burdman, and Christopher T. Hill. Topological Interactions in Warped Extra Dimensions. *JHEP*, 1002:049, 2010.

[8] Gustavo Burdman, Nayara Fonseca, and Leonardo de Lima. Full-hierarchy Quiver Theories of Electroweak Symmetry Breaking and Fermion Masses. *JHEP*, 1301:094, 2013.

[9] Gustavo Burdman, Nayara Fonseca, and Gabriela Lichtenstein. Resonances from Quiver Theories at the LHC. *Phys.Rev.*, D88:116006, 2013.

[10] Gustavo Burdman, Pedro Ormonde, and Victor Peralta. Fermion Resonances in Quiver Theories with a pNGB Higgs. *JHEP*, 1411:045, 2014.

[11] N. F. de Sá. Desconstrução Dimensional e Violação de Sabor, Universidade de são Paulo . 2011.

[12] Leonardo de Lima. Novos Modelos na Escala TeV para a Hierarquia de Gauge e das Massas dos Férmions, Universidade de são Paulo . 2013.

[13] Tony Gherghetta and Alex Pomarol. Bulk fields and supersymmetry in a slice of AdS. *Nucl.Phys.*, B586:141–162, 2000.

[14] Ben Lillie, Lisa Randall, and Lian-Tao Wang. The Bulk RS KK-gluon at the LHC. *JHEP*, 0709:074, 2007.

[15] Martin Schmaltz and David Tucker-Smith. Little Higgs review. *Ann. Rev. Nucl. Part. Sci.*, 55:229–270, 2005.

[16] E. Golowich J. F. Donoghue and B. Holstein. *Dynamics of the Standard Model*. Cambridge University Press, 1994.

[17] M. E. Peskin and D. V. Schroeder. *Introduction to Quantum Field Theory*. Addison-Wesley, 1995.

[18] W.M. Yao et al. Review of Particle Physics. *J.Phys.*, G33:1–1232, 2006.

[19] Guido ALTARELLI. The Standard model of particle physics. 2005.

[20] Csaba Csáki and Philip Tanedo. Beyond the Standard Model. In *Proceedings, 2013 European School of High-Energy Physics (ESHEP 2013): Paradfurdo, Hungary, June 5-18, 2013*, pages 169–268, 2015.

[21] Stephen P. Martin. A Supersymmetry primer. 1997. [Adv. Ser. Direct. High Energy Phys.18,1(1998)].

[22] Maxim Perelstein. Little Higgs models and their phenomenology. *Prog.Part.Nucl.Phys.*, 58:247–291, 2007.

[23] Roberto Contino. The Higgs as a Composite Nambu-Goldstone Boson. 2010.

[24] Giuliano Panico and Andrea Wulzer. The Composite Nambu-Goldstone Higgs. *Lect. Notes Phys.*, 913:pp.1–316, 2016.

[25] Marcela Carena, Leandro Da Rold, and Eduardo Pontón. Minimal Composite Higgs Models at the LHC. *JHEP*, 06:159, 2014.

[26] Maxim Perelstein, Michael E. Peskin, and Aaron Pierce. Top quarks and electroweak symmetry breaking in little Higgs models. *Phys. Rev.*, D69:075002, 2004.

[27] Victor Peralta. O dílaton em teorias quiver de hierarquia completa, Universidade de são Paulo . 2012.

[28] Jorge de Blas, Adam Falkowski, Manuel Perez-Victoria, and Stefan Pokorski. Tools for deconstructing gauge theories in AdS(5). *JHEP*, 0608:061, 2006.

[29] R. F. Swarttouw. Deconstruction and gauge theories in AdS_5, thesis, Delft Technical University. 1992.

[30] Lisa Randall and Raman Sundrum. A Large mass hierarchy from a small extra dimension. *Phys.Rev.Lett.*, 83:3370–3373, 1999.

[31] Walter D. Goldberger and Mark B. Wise. Modulus stabilization with bulk fields. *Phys.Rev.Lett.*, 83:4922–4925, 1999.

[32] Walter D. Goldberger and Mark B. Wise. Phenomenology of a stabilized modulus. *Phys.Lett.*, B475:275–279, 2000.

[33] Roberto Contino, Yasunori Nomura, and Alex Pomarol. Higgs as a holographic pseudoGoldstone boson. *Nucl.Phys.*, B671:148–174, 2003.

[34] Kaustubh Agashe, Roberto Contino, and Alex Pomarol. The Minimal composite Higgs model. *Nucl.Phys.*, B719:165–187, 2005.

[35] Brando Bellazzini, Csaba Csáki, and Javi Serra. Composite Higgses. *Eur.Phys.J.*, C74(5):2766, 2014.

[36] Gabriela Lichtenstein. Fenomenologia de Teorias Quiver da Quebra da Simetria Eletrofraca, Universidade de são Paulo . 2014.

[37] J. A. Aguilar-Saavedra. Identifying top partners at LHC. *JHEP*, 11:030, 2009.

[38] Giacomo Cacciapaglia, Aldo Deandrea, Daisuke Harada, and Yasuhiro Okada. Bounds and Decays of New Heavy Vector-like Top Partners. *JHEP*, 11:159, 2010.

[39] Yasuhiro Okada and Luca Panizzi. LHC signatures of vector-like quarks. *Adv. High Energy Phys.*, 2013:364936, 2013.

[40] Serguei Chatrchyan et al. Measurement of the single-top-quark t-channel cross section in pp collisions at $\sqrt{s} = 7$ TeV. *JHEP*, 12:035, 2012.

[41] C. Patrignani et al. Review of Particle Physics. *Chin. Phys.*, C40(10):100001, 2016.

[42] Mihailo Backovic, Thomas Flacke, Jeong Han Kim, and Seung J. Lee. Search Strategies for TeV Scale Fermionic Top Partners with Charge 2/3. *JHEP*, 04:014, 2016.

[43] K.A. Olive et al. Review of Particle Physics. *Chin.Phys.*, C38:090001, 2014.

[44] Vernon D. Barger and Roger J. N. Phillips. *Collider Physics (Frontiers in Physics)*. Addison Wesley Publishing Company, 1997.

[45] Johan Alwall, Michel Herquet, Fabio Maltoni, Olivier Mattelaer, and Tim Stelzer. MadGraph 5 : Going Beyond. *JHEP*, 1106:128, 2011.

[46] J. A. Aguilar-Saavedra, R. Benbrik, S. Heinemeyer, and M. Pérez-Victoria. Handbook of vectorlike quarks: Mixing and single production. *Phys. Rev.*, D88(9):094010, 2013.

[47] Torbjörn Sjöstrand, Stefan Ask, Jesper R. Christiansen, Richard Corke, Nishita Desai, Philip Ilten, Stephen Mrenna, Stefan Prestel, Christine O. Rasmussen, and Peter Z. Skands. An Introduction to PYTHIA 8.2. *Comput. Phys. Commun.*, 191:159–177, 2015.

[48] J. de Favereau, C. Delaere, P. Demin, A. Giammanco, V. Lemaître, A. Mertens, and M. Selvaggi. DELPHES 3, A modular framework for fast simulation of a generic collider experiment. *JHEP*, 02:057, 2014.

[49] Eric Conte, Benjamin Fuks, and Guillaume Serret. MadAnalysis 5, A User-Friendly Framework for Collider Phenomenology. *Comput. Phys. Commun.*, 184:222–256, 2013.

[50] Eric Conte, Béranger Dumont, Benjamin Fuks, and Chris Wymant. Designing and recasting LHC analyses with MadAnalysis 5. *Eur. Phys. J.*, C74(10):3103, 2014.

[51] B. Dumont, B. Fuks, S. Kraml, S. Bein, G. Chalons, E. Conte, S. Kulkarni, D. Sengupta, and C. Wymant. Toward a public analysis database for LHC new physics searches using MADANALYSIS 5. *Eur. Phys. J.*, C75(2):56, 2015.

[52] Matteo Cacciari, Gavin P. Salam, and Gregory Soyez. The Anti-k(t) jet clustering algorithm. *JHEP*, 04:063, 2008.